Doublet deployment strategies for geothermal Hot Sedimentary Aquifer exploitation

Application to the Lower Cretaceous Nieuwerkerk Formation in the West Netherlands Basin

Willems, Cees

DOI
10.4233/uuid:2149da75-ca29-4804-8672-549efb004048

Publication date
2017

Document Version
Final published version

Citation (APA)
Willems, C. (2017). *Doublet deployment strategies for geothermal Hot Sedimentary Aquifer exploitation: Application to the Lower Cretaceous Nieuwerkerk Formation in the West Netherlands Basin*. [Dissertation (TU Delft), Delft University of Technology]. https://doi.org/10.4233/uuid:2149da75-ca29-4804-8672-549efb004048

Doublet deployment strategies for geothermal Hot Sedimentary Aquifer exploitation:

Application to the Lower Cretaceous Nieuwerkerk Formation, West Netherlands Basin

Doublet deployment strategies for geothermal Hot Sedimentary Aquifer exploitation:

Application to the Lower Cretaceous Nieuwerkerk Formation, West Netherlands Basin

Proefschrift

ter verkrijging van de graad van doctor
aan de Technische Universiteit Delft,
op gezag van de Rector Magnificus prof. ir. K.C.A.M. Luyben,
voorzitter van het College voor Promoties,
in het openbaar te verdedigen op woensdag 3 mei 2017 om 10:00 uur

door

Cees WILLEMS

Master of Science in Applied Earth Science,
Technische Universiteit Delft, Nederland,
geboren te Amsterdam, Nederland.

Dit proefschrift is goedgekeurd door de promotors:
Prof. dr. D.F. Bruhn and Prof. dr. G.J. Weltje
copromotor: Dr. M.E. Donselaar

Samenstelling promotiecommissie:

Rector Magnificus	voorzitter
Prof. dr. D.F. Bruhn	Technische Universiteit Delft, promotor
Prof. dr. G.J. Weltje	Katholieke Universiteit Leuven, promotor
Dr. M.E. Donselaar	Technische Universiteit Delft, copromotor
Onafhankelijke leden:	
Prof. dr. ir. J.D. Jansen	Technische Universiteit Delft
Prof. dr. R.J. Schotting	Universiteit Utrecht
Prof. dr. J.D. van Wees	Universiteit Utrecht
Dr. M. Antics	GPC-IP Geofluid
Prof. dr. ir. T.J. Heimovaara	Technische Universiteit Delft, reserve lid

Dr. H.M. Nick heeft in belangrijke mate aan de totstandkoming van het proefschrift bijgedragen.

Keywords: Geothermal Field Development, Direct-use geothermal, Low enthalpy geothermal, sustainable energy.
Printed by: Drukkerij raddraaier b.v.
Cover design: R.J.G. Charton & C.J.L. Willems

ISBN 978-94-92516-49-7

An electronic version of this dissertation will be available at
http://repository.tudelft.nl/.

Contents

Summary

Coordinated doublet deployment strategies based on detailed geological modelling are crucial to enhance heat production from sedimentary aquifers. Detailed geological modelling is required for optimisation of doublet design which aims to maximise energy production while minimising pump energy losses and investment costs. A regional doublet deployment approach will increase the possible number of doublets exploiting a resource while reducing the risk for negative interference. In this thesis, several main parameters of a doublet deployment strategy are studied and in addition, the advantages of a regional deployment approach are shown.

The first requirement for the development of a coordinated doublet deployment strategy is a regional geological model. Such a model should describe regional sandstone distribution and sandstone architecture. These are fundamental parameters for doublet design as they are related to the net aquifer volume and flow path formation in the aquifer. In chapter 2 of this thesis, an improved regional model of the Lower Cretaceous, fluvial Nieuwerkerk Formation was described. Previous correlation studies were based on the interpretation of facies trends. Because sandstone-rich intervals were correlated between wells, the continuity of aquifers was overestimated and facies heterogeneity oversimplified. Utilising a combination of palynological age dating of drill cuttings, seismic interpretation and Gamma-Ray log correlation, we were able to correlate fluvial successions based on age, while their facies distribution varied laterally. With this approach, a better understanding of (1) the lateral continuity of sandstone-rich successions and (2) thickness variations of these successions throughout the WNB was obtained. Furthermore, this study formed the basis of the aquifer modelling that was used to derive deployment strategy parameters such as doublet orientation, well spacing and doublet distance in following chapters of this thesis.

In chapter 3 and 4, the impact of fluvial architecture on the life time of doublet systems and net energy production was studied. This was required to determine preferred doublet orientation with respect to geological trends and evaluate well spacing design. Based on the study of a core from a West Netherlands Basin hydrocarbon well, combined with the results of chapter 2, detailed fluvial architecture realisations were generated utilising a process-based facies modelling approach. Hundreds of realisations were generated while varying net sandstone volume in these realisations. These realisations were used in finite element heat flow simulations. In chapter 3 we compared production simulations with flow parallel and perpendicular to the paleoflow direction of the fluvial system that formed the Nieuwerkerk Formation. In this chapter, it was shown that approximately 10% less pump energy losses can be expected if doublets are oriented parallel to the paleoflow

direction. This is a result of the reduced probability that flow is blocked or diverted by impermeable claystone bodies compared to when doublets are oriented perpendicular to the paleoflow direction. In chapter 4 it was shown that these impermeable bodies can have a positive effect on heat exploitation as they provide thermal recharge to the cold water plume. This reduces the speed of temperature reduction after thermal breakthrough and increases doublet life time. In contrast, impermeable claystone bodies can also reduce doublet life time by separating permeable sandstone bodies into isolated clusters, reducing the net aquifer volume and bringing the moment of thermal breakthrough forward. The results of chapter 3 and 4 highlight the importance of geological modelling for HSA exploitation. This is because ranges of doublet life time and pump energy losses were larger when detailed facies architecture models were used in our simulations, compared to when homogeneous models were used. Homogenous models might overestimate net sandstone volume in the aquifer volume and therefore doublet life time and its uncertainty. In addition they underestimate pump energy losses.

Subsequently, well spacing design was evaluated in chapter 5. In addition, a discussion was introduced on the minimal required production temperature and its relation to life time and well spacing. Well spacing is an attractive parameter for optimisation of doublet design, because it is strongly related to drilling costs which form the main barrier of geothermal development. The results of this chapter indicate that a reduction of the current well spacing standard could improve the financial competiveness of Hot Sedimentary Aquifer exploitation. By reducing doublet well spacing by several hundred meters below the current WNB standards, the Net Present Value of a doublet could be increased by some 10%. Importantly, it was also shown in this chapter that such a reduction in well spacing could still result in sufficient doublet life time. In our study thermal recharge from over- and underburden was taken into account, as well as thermal recharge from impermeable claystone bodies within the aquifer (chapter 4). This increased the life time compared to previous studies. Moreover, in these previous studies doublet life time estimations were conservative because often the first thermal breakthrough moment was used as a life time estimate. Current WNB doublets are designed such that the expected thermal breakthrough occurs after 30-50 years. In this chapter ,however, it is assumed that a 10% production temperature is a better estimation of the minimal required production temperature. Firstly this is because heat use efficiency is likely to improve in the next decades like it did in the past decades, which will reduce the heat requirement. Secondly, production temperature only reduces by several degrees per decade after thermal breakthrough. Therefore it could take a significant amount of years for the production temperature to drop below economic values in current WNB doublets. Furthermore I showed that, the effect of well spacing reduction on NPV becomes more significant in more marginal economic doublets.

Finally the effect of production rate contrasts of adjacent geothermal doublet systems on the required doublet distance is analysed in chapter 6. In this chapter interference is expressed in terms of life time, net-energy production and Net Present Value. Two extreme doublet layout configurations were compared, checkboard and

tramline configuration. In the checkboard configuration, injection and production wells of adjacent doublets are alternated. In contrast, in the tramline configuration injectors and producers are aligned. The results of this study indicate that doublet interference is most significant in terms of life time. Dimensionless relations between production rate contrast and required doublet spacing were derived from a multi-parameter analysis. These relations indicate that the required doublet distance is a function of doublet configuration, minimal required production temperature and production rate contrasts between adjacent doublets. In the tramline configuration, required doublet distance is larger compared to when doublets are placed in checkboard configuration. In tramline configuration, negative interference was still recognised even when the doublet distance was multiple times larger than the spacing between injector and producer of the individual doublets. In contrast, checkboard configuration could result in positive life time interference when the doublet distance is larger or equal to the well spacing in the individual doublets. Moreover, optima in positive life time interference are described in this chapter. Finally, the results underline the importance of a coordinated approach to doublet deployment as this could avoid negative interference, and increase the possible number of doublets exploiting the same aquifer.

With this thesis, I hope to convince the reader that a regional coordinated approach to doublet deployment is required to disclose the full potential of hot sedimentary aquifers.

Samenvatting

Een strategie voor doubletplaatsing op regionaal niveau is cruciaal om warmtewinning uit sedimentaire aquifers zo efficiënt mogelijk toe te passen. Hiervoor zijn gedetailleerde modellen nodig die de geologische heterogeniteit en geologische onzekerheden beschrijven. Op basis van zulke modellen kan het ontwerp en de plaatsing van doubletten worden geoptimaliseerd met als doel maximale regionale energieproductie en minimale investeringskosten. Een regionale aanpak kan ervoor zorgen dat meer doubletsystemen warmte kunnen produceren uit hetzelfde aquifer omdat het risico op negatieve interferentie kan worden verkleind. In dit proefschrift worden de voordelen van een dergelijke strategie beschreven en parameters die een dergelijke strategie beschrijven onderzocht voor warmtewinning uit de Onder Krijt aquifers in het West Nederlands Bekken.

Voor de ontwikkeling van een gecoördineerde strategie voor doubletplaatsing is een geologisch model vereist dat de regionale architectuur en dikte van het aquifer beschrijft. In hoofdstuk 2 van dit proefschrift is een dergelijk model bestudeerd van de Nieuwerkerk Formatie. Hiervoor is gebruik gemaakt van palynologische analyse van boorgruis, regionale Gamma-Ray log correlatie en seismische interpretatie. Door deze gecombineerde aanpak was het mogelijk zandsteenrijke, fluviatiele intervallen in verschillende geothermieputten te correleren op basis van ouderdom in plaats van lithofacies. Volgens de correlatie op basis van lithofacies werd voorheen aangenomen dat de huidige geothermiedoubletten water produceren uit één enkel zandsteenrijk interval dat in dikte varieert in verschillende delen van het bekken. De nieuwe correlatiemethode op basis van de palynologische analyse toonde aan dat de huidige doubletten ten minste twee zandsteenrijke zones hebben aangeboord op verschillende stratigrafische niveaus. Overlap van zandsteenrijke zones op beide intervallen resulteert in sommige doubletten tot meer dikte van het aquifer. Regionale Gamma-Ray log correlatie en seismische interpretatie suggereren dat de laterale continuïteit van deze zandsteenrijke zones het gevolg zijn van tektonische bewegingen tijdens sedimentatie. Op basis van deze analyse zijn prognoses gemaakt van de verspreiding van deze zones in verschillende breukblokken in het bekken om daarmee de dikte en diepte van het aquifer voor nieuwe doubletten beter te kunnen voorspellen. Dat vormde de basis voor de gedetailleerde geologische modellen die gebruikt zijn voor productiesimulaties die beschreven zijn in de volgende hoofdstukken van dit proefschrift.

In hoofdstuk 3 en 4 van dit proefschrift is de impact van de fluviatiele architectuur van een aquifer onderzocht op pompverlies en de levensduur van doubletten. Deze factoren zijn van belang om te bepalen welke richting (vanaf nu: oriëntatie) van een doublet ten opzichte van geologische trends en de benodigde afstand tussen de injectie- en productieput. Op basis van boorkernanalyse is een inschatting gemaakt

van de dimensies van het fluviatiele systeem van de Nieuwerkerk Formatie. Deze dimensies zijn gebruikt voor het maken van gedetailleerde modellen van de fluviatiele architectuur met een 'process-based' modelleermethode. Honderden modellen zijn gegenereerd, waarin het volume van het netto zandsteen varieerde van 10 tot 90%. Al deze modellen zijn gebruikt in eindige-elementenmethode simulaties van water- en warmtestroming. Stroming die parallel loopt met en stroming die haaks staat op de paleo-stromingsrichting van het fluviatiele systeem van het aquifer zijn met elkaar vergeleken (hoofdstuk 3). De vergelijking toonde aan dat ongeveer 10% minder pompverlies kan worden verwacht wanneer de oriëntatie van een doublet parallel loopt met de paleo-stromingsrichting. Dit komt doordat er een verhoogde kans is dat impermeabele kleisteenlichamen stromingsblokkades of barrières vormen haaks op de paleo-stromingsrichting. Deze blokkades en barrières beïnvloeden de lengte van de stroombanen tussen putten en de kans dat deze worden gevormd. Daarmee beïnvloedt faciesarchitectuur de benodigde pompdruk. Hoofdstuk 4 laat zien dat de impermeabele kleisteenlichamen ook een positief effect kunnen hebben op warmte-exploitatie omdat ze door geleiding het afgekoelde, geïnjecteerde water opwarmen. Daarentegen kunnen de kleisteenlichamen ook de connectiviteit van zandsteenlichamen verkleinen, en daarmee ook het netto aquifervolume verlagen. Dit heeft als gevolg dat de doorbraaktijd van het koude geïnjecteerde water vervroegd wordt en de levensduur van het doublet omlaag gaat. Onze resultaten laten zien dat de faciesarchitectuur in acht moet worden genomen bij de inschatting van de levensduur en het pompenergieverlies van doubletten. Het gebruik van homogene aquifermodellen zou kunnen leiden tot een minder nauwkeurige inschatting van de onzekerheid mbt levensduur en pompverlies.

Vervolgens is de putafstand tussen de injectie- en productieput van een doublet geëvalueerd in hoofdstuk 5. Deze putafstand beïnvloedt de boorkosten omdat de putten gedevieerd geboord worden vanaf een enkele boorlocatie. De hoge boorkosten vormen een belangrijke barrière voor de ontwikkeling van geothermie. Desalniettemin is verkleining van de putafstand niet ter discussie gesteld in voorgaande studies als mogelijke maatregel om deze barrière te verlagen. In hoofdstuk 5 van dit proefschrift wordt aangetoond dat de netto contante waarde van een typisch doublet in het West Nederland Bekken tot 10% kan toenemen wanneer de momenteel gangbare putafstand van 1500 m met enkele honderden meters afneemt. Daarbij is ook onderzocht of een dergelijke afname nog steeds tot voldoende levensduur van het doublet kan leiden. Voor deze studie zijn productiesimulaties gebruikt met aquifermodellen die zijn ontwikkeld in de voorgaande hoofdstukken. Deze simulaties tonen aan dat zelfs bij een aquifer van 50 m dikte en een netto zandsteenvolume variërend van 15% tot 70%, voldoende levensduur van het doublet kan worden verwacht bij een putafstand van 800 m, ondanks het conservatief geschatte netto volume zandsteen in onze modellen. Onze simulaties laten een relatief lange levensduur zien vergeleken met eerdere studies. Dit komt omdat in onze studie de voorheen verwaarloosde warmtetoevoer vanuit impermeabel boven- en onderliggend gesteente naar het aquifer in beschouwing is genomen. Daarnaast heb ik dit berekend met de aanname dat de warmteproductie niet hoeft te stoppen zodra de productietemperatuur begint te dalen, maar pas wanneer de productietemperatuur met 10%

is gedaald. Vaak wordt het eerste moment van temperatuurdaling beschouwd als het einde van de levensduur van het doublet. Dit is een te conservatieve aanname omdat de productietemperatuur dan niet direct afneemt naar een oneconomische waarde. Bovendien is het waarschijnlijk dat er per gebruiker minder warmte nodig is in de toekomst, aangezien de efficiëntie van energieverbruik alleen maar zal toenemen. Daarom concludeer ik dat verkleining van de putafstand standaard voor geothermische warmte-exploitatie in aanmerking moet worden genomen als een mogelijke stimulans voor de groei daarvan. Tot slot is in dit hoofdstuk aangetoond dat deze maatregel extra relevant is voor doubletsystemen die economisch marginaler zijn.

In het hoofdstuk 6 is tenslotte de invloed van debietcontrasten tussen naastgelegen doubletten onderzocht met het oog op de benodigde doubletafstand. De benodigde doubletafstand heeft tot doel om negatieve interferentie te voorkomen. Interferentie is in dit hoofdstuk uitgedrukt in termen van netto energieproductie, levensduur en netto contante waarde. De resultaten van dit hoofdstuk laten zien dat interferentie tussen warmte porducerende doubletten met name de levensduur beïnvloedt en verwaarloosbare impact heeft op de netto contante waarde en netto energieproductie. Op basis van anlayses van productiesimulaties waarin doubletafstand, putafstand, debiet en reservoirdikte zijn gevarieerd, heb ik dimensieloze relaties afgeleid tussen de benodigde doubletafstand en het verschillen in productiedebiet. Twee extreme doubletconfiguraties zijn vergeleken: de checkboard en tramline configuratie. In de checkboard configuratie heeft de dichtsbijzijnde naastgelegen put een tegenovergestelde functie, in de tramline configuratie liggen injectie- en productieputten op een lijn. Bij de tramline configuratie kan negatieve interferentie alleen worden voorkomen wanneer de doubletafstand meederde malen de afstand tussen de injectie en productieput van hetzelfde doublet bedraagt. Daarentegen is er positieve interferentie mogelijk bij de checkboard configuratie. In onze studie zijn optima in positieve interferentie herkend bij checkboard configuratie wanneer de doubletafstand groter is dan de afstand tussen de injectie- en productieput van hetzelfde doublet. De resultaten van dit hoofdstuk laten zien dat gecoördineerde doubletplaatsing de efficiëntie van exploitatie kan verhogen, waarmee rekening moet worden gehouden bij voorbereiding van HSA exploitatie.

Met dit proefschrift hoop ik de lezer te overtuigen dat een regionale benadering in doublet plaatsing nodig is om de de potentie van geothermische warmtewinnig optimaal te benutten.

1 Introduction

1.1. Hot Sedimentary Aquifers

Huge amounts of heat are stored in sedimentary rocks. These resources, often referred to as Hot Sedimentary Aquifers (HSA), can be found away from tectonic plate boundaries and conventional geothermal resources usually connected with volcanically active regions, in areas with average thermal gradients of approximately 30°/km. Because of the high required minimal temperatures for economic geothermal electricity production(Shengjun et al., 2011), HSA are especially suitable for heat production applications. Nevertheless, they should be considered as an important energy source since half of the total energy consumption in countries with moderate to cold climates is for heat generation (Sanner et al., 2011). In the Netherlands, for example, it is estimated that the total recoverable heat from sedimentary aquifers is 55 times larger than the Dutch annual heat consumption (Kramers et al., 2012; EU-Commission, 2016; Schoots et al., 2016). Next to the large potential, another advantage of HSA is that they are often located in regions with hydrocarbon production history. Examples are the Idaho thrust Belt (Welhan, 2016), the West Netherlands Basin, The Netherlands (Van Heekeren and Bakema, 2013), the Paris Basin, France (Lopez et al., 2010) and the Perth Basin, Australia (Pujol et al., 2015). The extensive knowledge about the nature of subsurface sedimentary rocks, and the experience from oil and gas production, significantly reduce the risks of HSA exploration. Nevertheless, a large gap exists between potential and actual exploitation. Currently, the main barrier for HSA development is the competition with a relatively cheap and existing fossil-fuel-based heating network (Sanner et al., 2011). Initial investment costs for HSA operators are very high because of a combination of large well completion and drilling costs, as well as costs associated with the installation of new heat distribution grids. This distinguishes HSA exploitation from more conventional geothermal electricity production and other sustainable energy sources, because electricity is easier to distribute and connect to existing energy networks. Geological uncertainties form another barrier for the growth of HSA exploitation. Large geological uncertainties make it complicated to justify large investment costs. Similar geological uncertainties also form a barrier in hydrocarbon production. However, the larger revenues from hydrocarbon production compensate the risks of drilling unsuccessful wells. In addition, hydrocarbon exploitation uses well placement strategies that involve many wells. The impact of

failure of individual wells is therefore reduced. In contrast, geothermal resources are often exploited by different independent operators with a single or a few doublets (e.g. Van Heekeren and Bakema, 2013; Jaxa-rozen et al., 2015).Therefore the impact of well failure is significantly higher. The small-scale approach to HSA exploitation focusses on individual interests. This could negatively affect collective interests because it increases the risk of interference between operators and suboptimal exploitation (e.g. Jaxa-rozen et al., 2015; Tureyen et al., 2015). Therefore this thesis aims to develop regional doublet deployment strategies for HSA exploitation that will reduce geological risks, minimise negative interference and enhance heat recovery.

1.2. HSA in the West Netherlands Basin

An example of a promising HSA region is the West Netherlands Basin (WNB) which is the current epicentre of geothermal energy exploitation in the Netherlands. In 2016, nine geothermal doublets have been realised in this basin for-direct use applications. This is almost 70% of all doublets in the Netherlands. In addition, 40% of all granted exploration licences are located in this basin (Figure 1.1). Currently, the main target is the fluvial Delft Sandstone Member, part of the Cretaceous Nieuwerkerk Formation (e.g. Van Adrichem Boogaert and Kouwe, 1993). Seven out of nine doublets and most of the 30 exploration licences where no doublet is drilled yet target this aquifer. The focus on this fluvial sandstone results from a combination of high productivity in several current doublets as well as publically available well data from surrounding oil and gas fields. The depth of the Nieuwerkerk Formation aquifers range from 2 to 3 km. In the current doublets, water of 70 to 90°C water is produced and water of 30°C to 40°C water is re-injected. In most doublets, a well spacing of 1 to 1.5 km is chosen which should guarrantee a life time of at least 30 years. The flow rates in these doublets vary between some 100 to 200 m^3/h and the associated doublet capacity ranges from 5 to 20 MW_{th}. According to Kramers et al. (2012), 9492 PJ of recoverable heat could be produced from the Nieuwerkerk Formation alone, which is six times the total annual heat consumption of the Netherlands (Schoots et al., 2016). However, because of the current doublet deployment strategy which is based on a 'first come, first served' approach it is unlikely that this will be actually recovered. Even if doublets will be realised in all 30 licences, with an average net energy production of 10 MW_{th} and expected life time of 50 years, only 45% of the total available heat will be recovered from this aquifer. Unfortunately, this is still a very optimistic estimate because it neglected down time of the doublet systems and the risk that some doublets could have more disappointing or no production at al. Moreover, the current increase in geothermal doublets is low. Approximately two new doublets are realised each year. In this way, it will therefore take decades to reach full capacity. The use of the large well spacing standard and the irregular layout of the doublets limits the available space for the realisation of new doublets which will slow down the overall growth of the geothermal heat provision. In this thesis I try to show that a regional doublet deployment strategy could stimulate HSA exploitation. The derivation of the strategy is based on detailed geological modelling of the Nieuwerkerk Fm. aquifers.

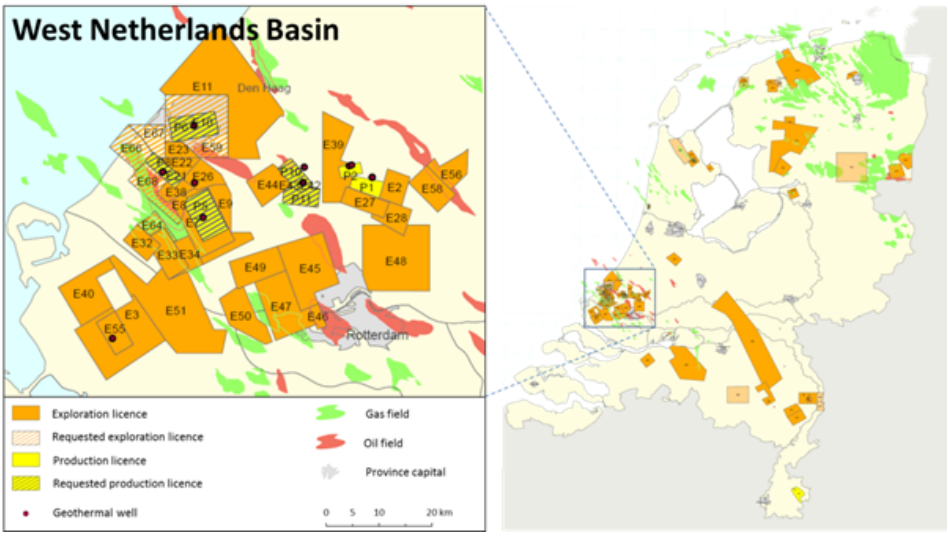

Figure 1.1: Overview of the current geothermal exploration and production licence layout, modified from www.nlog.nl.

1.3. Regional geological model of the Nieuwerkerk Formation

The Nieuwerkerk Formation sandstones were one of the main reservoir targets for hydrocarbon exploitation in the West Netherlands Basin in the past 50 years (e.g. Herngreen and Wong, 2007; Kombrink et al., 2012). The Formation was formed during the Late Jurassic to Early Cretaceous and is characterised by fluvial, syn-rift sediments (e.g. Van Adrichem Boogaert and Kouwe, 1993; Den Hartog Jager, 1996; Devault and Jeremiah, 2002; Jeremiah et al., 2010; Donselaar et al., 2015). This origin is reflected by large thickness differences of the total Nieuwerkerk Formation interval. In some graben fault blocks the formation has a thickness of more than a kilometre while it is less than 100 m on some horst and pop-up structures. Within the Formation sandstone-rich zones occur but their lateral extent is debated because of (1) large thickness variations of the sandstone successions that were encountered in wells and (2) discontinuous seismic reflectors (e.g. Den Hartog Jager, 1996). Van Adrichem Boogaert and Kouwe (1993) recognised a continuous sandstone rich layer in the top of the interval that extends throughout most of the onshore part of the basin which is referred to as the Delft Sandstone Member. This model is generally used for geothermal exploitation in the basin. However, in a more recent study by Devault and Jeremiah (2002) this Member was not acknowledged. Devault and Jeremiah (2002) state that sandstone-rich zones with limited lateral extent occur at different stratigraphic levels,and do not necessarily form a continuous interval. These different views have significant implications for doublet deployment in the region because it affects expected aquifer thickness and occurrence in areas without well coverage. Because aquifer thickness is one of the main

parameters that influence injectivity and doublet life time, the coexistence of the two models leads to uncertainty in the potential of new geothermal doublets. As a result, conservative large well spacing distances are used in current WNB doublets to prevent the risk of early cold-water breakthrough. This measure increases the drilling costs because deviated wells must bedrilled from one surface location. The combination of high costs as well as the uncertainties in life time and net energy production makes it complicated to justify large investments. The high costs also result in limited data acquisition in the geothermal wells because of investment cutbacks. This lack of data limits our knowledge and therefore does not contribute to risk reduction. To prevent this negative spiral, a better understanding is required of the sandstone distribution in the Nieuwerkerk Formation. Based on an improved geological model that describes sandstone distribution in the Nieuwerkerk Formation, doublet deployment can be optimised which will reduce geological risks for new geothermal doublets.

1.4. Fluvial reservoir architecture

Geological modelling of fluvial aquifers is complex because of their heterogeneity in sediment bodies. Spatial distribution of these bodies can be a result of both autogenic as well as allogenic controls (Hajek et al., 2010; Flood and Hampson, 2015) which make it difficult to identify laterally persistent trends on well logs. These type of aquifers are composed of impermeable floodplain fines and permeable sandstone bodies. The distribution of these sedimentary bodies is referred to as the fluvial architecture in this thesis. The sandstone bodies can form one big network or, in contrast, smaller sandstone compartments separated by impermeable claystone bodies. In hydrocarbon related recovery studies of fluvial reservoirs it has been shown that the recovery efficiency is governed by the degree of compartmentalisation of permeable sandstone bodies in the impermeable claystone matrix (Jones and Doyle, 1995; Larue and Friedmann, 2005; Larue and Hovadik, 2006, 2008). Previous work on this topic identified the net-sandstone volume or net-to-gross (N/G), the sand-body width-thickness ratio and the range in paleoflow direction as main factors that control compartmentalization (King, 1990; Larue and Hovadik, 2006; Geel and Donselaar, 2007; Hovadik and Larue, 2007; Ainsworth, 2005; Pranter and Sommer, 2011). However, these previously mentioned studies focussed on hydrocarbon production. In this type of exploitation, the main objective is to intersect as many sandstone bodies as possible to maximise drainable volume (e.g. Geel and Donselaar, 2007). Often a hydrocarbon well deployment strategy is a well grid (e.g. Pranter and Sommer, 2011). In contrast, in HSA exploitation geothermal well pairs are used in the exploitation. A primary requirement for a doublet system is that flow paths are formed through the reservoir between the injection and production wells of the pair. This requires a new directional component to connectivity analyses. The orientation of the doublet well pairs with respect to paleo fluvial trends affects the probability that flow paths exist between the wells. The claystone bodies not only influence flow paths between the wells, but can also supply heat to the cold water plume and thereby influence lifetime (Hamm and Lopez, 2012). Poulsen et al. (2015) showed the significance of thermal recharge from the over- and un-

derburden of an aquifer. Internal claystone bodies can have a similar effect on life time that is currently not taken into account in doublet design and deployment strategies. Therefore, in this study the impact of fluvial architecture on heat flow is evaluated, utilising detailed facies architecture models which are derived from well log and core data. This evaluation is used to support well spacing design and doublet orientation design.

1.5. Objectives

The overarching goal of this thesis is to show that a coordinated, science-based approach to geothermal doublet planning is a prerequisite for efficient exploitation of HSA. A first requirement for coordinated doublet planning is a regional geological model that describes fluvial aquifer architecture and sandstone distribution (objective1). The Lower Cretaceous Nieuwerkerk Formation (WNB) has been used as a case study. Based on the geological model, a number of pertinent research questions are be addressed: The preferred doublet orientation with respect to geological trends (objective 2), the inferred impact of geological heterogeneity on doublet life time (objective 3), the preferred well spacing in individual doublets (objective 4), and the required distance between doublets and allowed production rate contrasts between doublets (objective 5).

The objectives corresponding to these research questions are:

1. Model the regional sandstone distribution of the Nieuwerkerk Formation for aquifer thickness and continuity prediction.
2. Derive preferred doublet orientation with respect to geological trends.
3. Evaluate the impact of geological heterogeneities on doublet life time.
4. Evaluate the impact of reduction of doublet well spacing on the Net Present Value and the life time of doublets.
5. Analyse effect of layout and production rates contrasts on required doublet distance.

These objectives will be discussed in different chapters of this thesis. In the final chapter, a synthesis of all results and their implications for improved exploitation efficiency will be presented and evaluated in order to address the overarching goal of the thesis.

References

Ainsworth, R. B. (2005). Sequence stratigraphic-based analysis of reservoir connectivity: influence of sealing faults - a case study from a marginal marine depositional setting. *Petroleum Geoscience*, 12(2):127–141.

Den Hartog Jager, D. G. (1996). Fluviomarine sequences in the Lower Cretaceous of West Netherlands Basin: correlation and seismic expression. In Rondeel, H., Batjes, D., and Nieuwenhuijs, W., editors, *Geology of gas and oil under the Netherlands*, pages 229–241. Kluwer Academic Publishers.

Devault, B. and Jeremiah, J. (2002). Tectonostratigraphy of the Nieuwerkerk Formation (Delfland Subgroup) West Netherlands Basin. *AAPG Bulletin*, 86(10):1679–1707.

Donselaar, M. E., Groenenberg, R. M., and Gilding, D. T. (2015). Reservoir Geology and Geothermal Potential of the Delft Sandstone Member in the West Netherlands Basin. In *World Geothermal Congress 2015*, Melbourne, Australia.

EU-Commission (2016). Communication from the commission to the European Parlaiment, the council, the European Economic and Social Committee and the Committee of the regions. Technical report.

Flood, Y. S. and Hampson, G. J. (2015). Quantitative analysis of the dimensions and distribution of channelized fluvial sandbodies within a large outcrop dataset: Upper Cretaceous Blackhawk Formation, Wasatch plateau, Central Utah, U.S.A. *Journal of Sedimentary Research*, 85:315–336.

Geel, C. R. and Donselaar, M. E. (2007). Reservoir modelling of heterolithic tidal deposits: Sensitivity analysis of an object-based stochastic model. *Netherlands Journal of Geosciences*, 86(4):403–411.

Hajek, E. A., Heller, P. L., and Sheets, B. A. (2010). Significance of channel-belt clustering in alluvial basins. *Geology*, 38(6):535–538.

Hamm, V. and Lopez, S. (2012). Impact of Fluvial Sedimentary Heterogeneities on Heat Transfer at a Geothermal Doublet Scale. In *Thirty-Seventh Workshop on Geothermal Reservoir Engineering*, Stanford, California.

Herngreen, G. and Wong, T. E. (2007). Cretaceous. In Wong, T. E., Batjes, D., and De Jager, J., editors, *Geology of the Netherlands*, chapter Cretaceous, pages 127–150. Edita-the Publishing House of the Royal.

Hovadik, J. M. and Larue, D. K. (2007). Static characterizations of reservoirs: refining the concepts of connectivity and continuity. *Petroleum Geoscience*, 13:195–211.

Jaxa-rozen, M., Kwakkel, J., and Bloemendal, M. (2015). The Adoption and Diffusion of Common-Pool Resource-Dependent Technologies : The Case of Aquifer Thermal Energy Storage Systems. In *Proceedings of PICMET '15: Management of the Technology Age*, pages 2390–2408, Portland, Oregon.

Jeremiah, J. M., Duxbury, S., Rawson, P., E, S. I., Ashford, N. D., and Tx, H. (2010). Lower Cretaceous of the southern North Sea Basins : reservoir distribution within a sequence stratigraphic framework. *Netherlands Journal of Geosciences*, 89(3/4):203–237.

Jones, A. and Doyle, J. (1995). Which sub-seismic heterogeneities influence waterflood performance ? A case study of a low net-to-gross fluvial reservoir. In De Haan, H., editor, *New Developments in Improved Oil Recovery*, number 84, pages 5–18. Geological Society Special Publication, Bath, 84 edition.

King, P. R. (1990). The connectivity and conductivity of overlapping sand bodies. In Buller, A., Berg, E., Hjelmeland, O., Kleppe, J., Torsaeter, O., and Aasen, J. O., editors, *North sea oil and gas reservoirs - II*, pages 353–362. Graham and Trotman, London.

Kombrink, H., Doornenbal, J. C., Duin, E. J. T., Dulk, M. D., Gessel, S. F. V., Veen, J. H., and Witmans, N. (2012). New insights into the geological structure of the Netherlands ; results of a detailed mapping project. *Netherlands Journal of Geosciences*, 91(4):419–446.

Kramers, L., Wees, J. V., Pluymaekers, M. P. D., Kronimus, A., and Boxem, T. (2012). Direct heat resource assessment and subsurface information systems for geothermal aquifers ; the Dutch perspective. *Netherlands Journal of Geosciences*, 91(4):637–649.

Larue, D. K. and Friedmann, F. (2005). The controversy concerning stratigraphic architecture of channelized reservoirs and recovery by waterflooding. *Petroleum Geoscience*, 11(2):131–146.

Larue, D. K. and Hovadik, J. (2006). Connectivity of channelized reservoirs: a modelling approach. *Petroleum Geoscience*, 12(4):291–308.

Larue, D. K. and Hovadik, J. (2008). Why is reservoir architecture an insignificant uncertainty in many appraisal and development studies of clastic channelized reservoirs? *Journal of Petroleum Geology*, 31(4):337–366.

Lopez, S., Hamm, V., Le Brun, M., Schaper, L., Boissier, F., Cotiche, C., and Giuglaris, E. (2010). 40 years of Dogger aquifer management in Ile-de-France, Paris Basin, France. *Geothermics*, 39(4):339–356.

Poulsen, S. E., Balling, N., and Nielsen, S. B. (2015). A parametric study of the thermal recharge of low enthalpy geothermal reservoirs. *Geothermics*, 53:464–478.

Pranter, M. J. and Sommer, N. K. (2011). Static connectivity of fluvial sandstones in a lower coastal-plain setting: An example from the Upper Cretaceous lower Williams Fork Formation, Piceance Basin, Colorado. *AAPG Bulletin*, 95(6):899–923.

Pujol, M., Ricard, L. P., and Bolton, G. (2015). 20 years of exploitation of the Yarragadee aquifer in the Perth Basin of Western Australia for direct-use of geothermal heat. *Geothermics*, 57(2015):39–55.

Sanner, B., Ria, K., Land, A., Mutka, K., Papillon, P., Stryi-Hipp, G., and Weiss, W. (2011). Common Vision for the Renewable Heating & Cooling sector in Europe. Technical report, European Commission.

Schoots, K., Hekkenberg, M., and Hammingh, P. (2016). Nationale Energieverkenning 2016. Technical report, Energieonderzoek Centrum Nederland (ECN), Amsterdam/Petten.

Shengjun, Z., Huaixin, W., and Tao, G. (2011). Performance comparison and parametric optimization of subcritical Organic Rankine Cycle (ORC) and transcritical power cycle system for low-temperature geothermal power generation. *Applied Energy*, 88(8):2740–2754.

Tureyen, O. I., Sarak, H., Altun, G., and Satman, A. (2015). A modeling analysis of unitized production : Understanding sustainable management of single-phase geothermal resources with multiple lease owners. *Geothermics*, 55:159–170.

Van Adrichem Boogaert, H. and Kouwe, W. (1993). Stratigraphic nomenclature of the Netherlands, revision and update by Rijks Geologische Dienst (RGD) and Netherlands Oil and Gas Exploration and Production Association (NOGEPA). *Mededelingen Rijks Geologische Dienst*, 50:1—180.

Van Heekeren, V. and Bakema, G. (2013). Geothermal Energy Use, Country Update forthe Netherlands. In *European Geothermal Congress*, pages 2013–2016, Pisa.

Welhan, J. A. (2016). Gigawatt-Scale Power Potential of a Magma-Supported Geothermal System in the Fold and Thrust Belt of Southeast Idaho. In *41st Workshop on Geothermal Reservoir Engineering*, Stanford, California.

2

Fluvial sequence stratigraphy of Lower Cretaceous geothermal aquifers derived from palynological cutting analysis

Abstract
Sandstone-rich fluvial successions of the Nieuwerkerk Formation are the main target for geothermal heat exploitation in the West Netherlands Basin. Primary challenge for efficient doublet design and deployment is the adequate prediction of the size, shape, lateral extent and thickness (or: aquifer architecture) of the geothermal aquifers. Large variations in the thickness of sandstone-rich successions are recognised in current West Netherlands Basin doublet systems. These variations cannot be explained by the currently applied lithostratigraphic framework. Uncertainty in the aquifer architecture increases the uncertainty in doublet lifetime as it has an impact on net aquifer volume. The goal of this study was to improve our understanding of the regional aquifer architecture by identifying a sequence stratigraphic framework in the Nieuwerkerk Formation aquifers. For this purpose we evaluated new palynological data with the aim to place the geothermal aquifers in a well-defined sequence stratigraphic framework. The palynological analyses enabled regional well-log correlation based on age of intervals and regional sequence stratigraphic markers. We subdivided the fluvial interval in a Late Ryazanian to Early Valanginian succession and a Valanginian succession and identified trends in sandstone content within these successions. In combination with seismic interpretation, maps were constructed that predict aquifer thickness and their lateral extent in the basin. The study emphasises the value of palynological analyses to reduce the uncertainty of fluvial Hot Sedimentary Aquifer exploitation.

This chapter is based on: Willems, C.J.L., Vondrak, A.,Munsterman, D.K., Donselaar, M.E., Mijnlieff, H.F., *Fluvial sequence stratigraphy of Lower Cretaceous geothermal aquifers derived from palynological cuttings analysis*, **Submitted**.

2.1. Introduction

In geothermal exploitation of sedimentary rocks, it is crucial to adequately predict the regional aquifer distribution. Often geological data is sparse and property extrapolation is required over large distances. This is especially challenging for fluvial aquifers, which are notorious for lateral variation in lithofacies and aquifer properties. The prediction of the regional sandstone distribution (henceforth fluvial architecture) from well logs in fluvial aquifers is often ambiguous because lithofacies distribution could be affected by both allogenic and autogenic processes (e.g. Hajek et al., 2010; Donselaar et al., 2013; Flood and Hampson, 2015; Toorenenburg et al., 2016). This is reflected by large aquifer thickness variations that are recognised in currently active geothermal doublet wells in the West Netherlands Basin (WNB). The fluvial, sandstone-rich successions that form the aquifer of the geothermal HON-GT doublet, range in thickness from 50 to 150 m in approximately 1.5 km spaced wells (Figure 2.1). In addition, the depth of this aquifer below the top of the marginally marine Rodenrijs Claystone Member (e.g. Van Adrichem Boogaert and Kouwe, 1993) ranges from almost 100 m to more than 200 m in different geothermal wells. These variations cannot be explained by lithostratigraphic well-log correlation and create uncertainty in the prediction of lifetime and drilling costs of future doublet systems in the WNB.

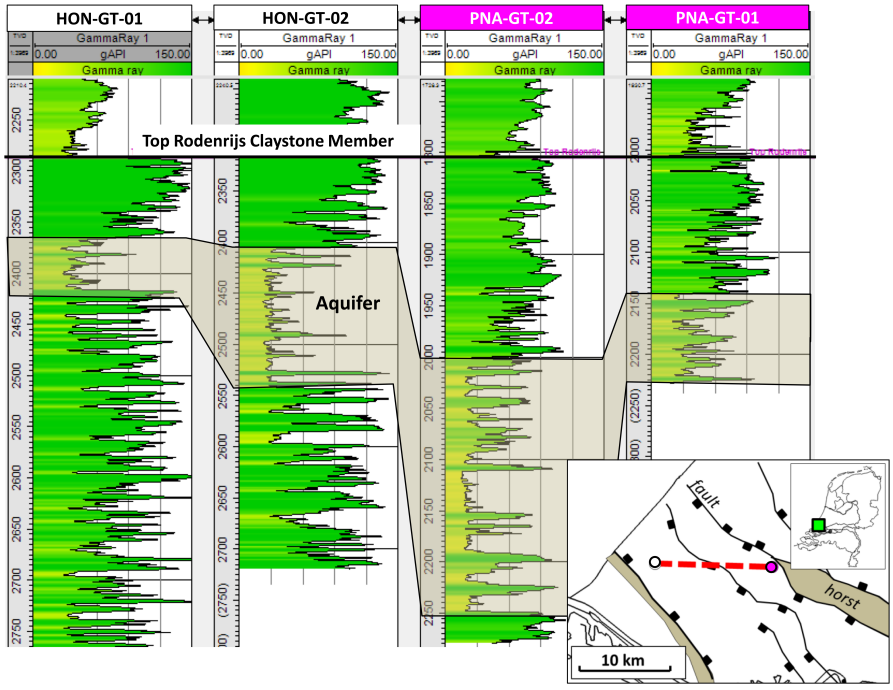

Figure 2.1: Gamma-Ray logs of two doublet well pairs. Fault interpretation on the map is derived from Duin et al. (2006).

The aquifer in the geothermal wells of Figure 2.1 is interpreted as the Delft Sandstone Member which is part of the Lower Cretaceous Nieuwerkerk Formation (e.g. Van Adrichem Boogaert and Kouwe, 1993; Den Hartog Jager, 1996; Herngreen and Wong, 2007; Donselaar et al., 2015). This member is characterised as a syn-rift, sandstone-rich interval ranging in age from Valanginian to Early Hauterivian, deposited in a meandering fluvial environment. Regional transgression and subsidence resulted in increasingly marine character of the overlying sediments ranging from the restricted marine Rodenrijs Claystone Member to the marine Rijnland Group (Figure 2.2).

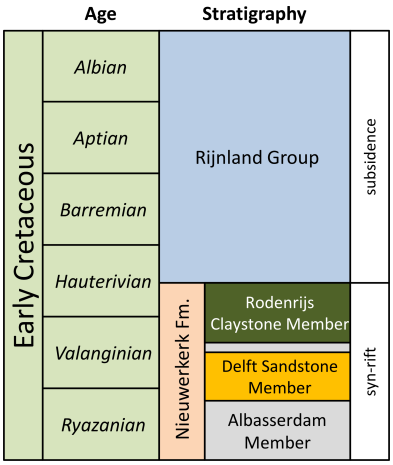

Figure 2.2: Stratigraphic column for the Early Cretaceous section in the WNB.

The interpretation of the Delft Sandstone Member as a single sandstone-rich interval in the upper section of the Nieuwerkerk Formation Figure 2.3-A) is derived from lithostratigraphic regional well-log correlation from numerous hydrocarbon wells in the WNB (e.g. Racero-Baena and Drake, 1996; Herngreen and Wong, 2007). This model is commonly used in geothermal exploitation in the basin for doublet design and deployment. However, recent regional stratigraphic studies based on sequence stratigraphic principles did not acknowledge the Delft Sandstone Member (Devault and Jeremiah, 2002; Jeremiah et al., 2010). Devault and Jeremiah (2002) state that because of the syn-rift origin of the Nieuwerkerk Formation, clusters of amalgamated sandstone-rich zones can exist throughout the Nieuwerkerk Formation that not necessarily form one single, continuous sandstone-rich interval (Figure 2.3-B). The existence of two geological models that describe sandstone distribution in the Nieuwerkerk Formation creates uncertainty for geothermal exploitation because both models have a different impact on possible interference and aquifer thickness prediction. If the aquifer is formed by a single continuous sandstone-rich interval, pressure communication could affect injectivity and productivity of adjacent doublets, as is illustrated in Figure 2.3-A. In contrast, pressure communication is less straightforward if different sandstone-rich zones occur with limited lateral extent. In the example of Figure 2.3-B, claystone-dominated zones

can form flow barriers or baffles between doublets 1 and 2. Furthermore, when the aquifer is not formed by a single sandstone-rich zone, the aquifer thickness depends on the lateral extent of the sandstone-rich zones that the doublets can encounter as is illustrated for doublet 2 in Figure 2.3-B. Furthermore, the model in Figure 3-B suggests that multiple aquifer targets can be present at deeper and hotter stratigraphic intervals affecting the geothermal potential in the region.

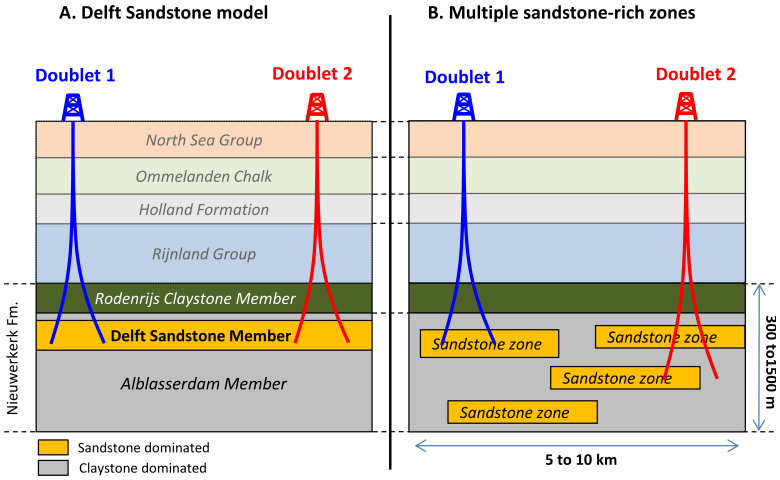

Figure 2.3: (A) Cartoons illustrating the difference in sandstone distribution in the Nieuwerkerk Formation in strike sections on graben scale according to (A) the Delft Sandstone model and (B) the multiple sandstone-rich zone model.

The goal of this study is to place the fluvial aquifers in a sequence stratigraphic framework. The results should decrease the uncertainty in the prediction of aquifer thickness for new doublet systems in the WNB and contribute to optimised doublet design. To reach this goal, drill cuttings are analysed in three geothermal wells: HON-GT-01, PNA-GT-02 and VDB-GT-04. Utilising the age interpretation of fluvial intervals and identification of regional Maximum Flooding Surfaces (MFS), aquifer are placed in a sequence stratigraphic-based correlation framework. This framework is used to interpret regional aquifer architecture in different fault blocks. With our approach, we were able to show the added value of palynological cuttings analysis to improve the understanding of the regional fluvial aquifer architecture in the WNB and reduce exploitation risks of future doublet systems.

2.2. Data and Methods

2.2.1. Overview

This study was based on a combination of seismic interpretation, Gamma-Ray (GR) log correlation, and palynological analysis of cuttings. In the seismic interpretation, faults were identified in our study area, which were active during deposition of the Nieuwerkerk Formation. In combination with a regional structural interpretation by Duin et al. (2006) the lateral extent of these faults was identified. Secondly, a fluvial intervals were placed in a sequence stratigraphic framework, utilising palynological analyses of cuttings. These analyses were used to interpret the age of intervals and Maximum Flooding Surfaces, forming the basis of the framework. GR logs of eleven geothermal wells in our study area were used to compare fluvial architecture in different fault blocks. All results were finally combined in maps that predict the lateral extent of the sandstone-rich successions in the basin. An overview of the data that was used in our study is presented in Figure 2.4.

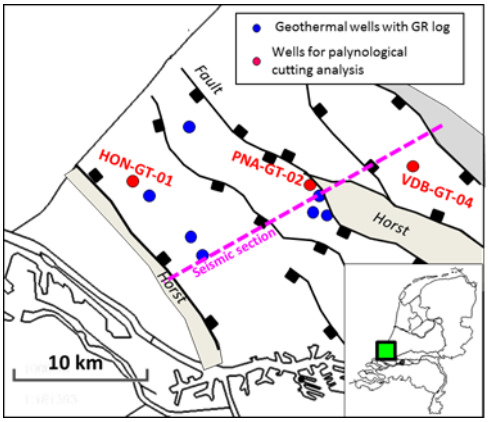

Figure 2.4: Location of the geothermal wells for the GR well-log correlation, cutting analysis, the outline of the seismic cross-section and the regional structural interpretation by Duin et al. (2006).

2.2.2. Structural setting of the Nieuwerkerk Formation

The surveys were merged to a basin-wide seismic cross-section perpendicular to the regional fault trend (Figure 2.4, Vondrak, 2016). On the seismic section, major faults were interpreted as well as two seismic horizons: the top and base of the Nieuwerkerk Formation (Kombrink et al., 2012). Thickness differences on the section reveal which faults were active when the formation was formed. Fault blocks were identified that experienced different tectonic movement affecting fluvial architecture of the Nieuwerkerk Formation. The regional outline of these faults was derived from structural interpretation by Duin et al. (2006) in the WNB. This result was used as the basis for regional well-log correlations and generation of maps that describe the distribution of sandstone-rich successions.

2.2.3. Palynological analysis

A total of 42 cuttings samples from well PNA-GT-02 and 40 samples from HON-GT-01 was analysed. Two additional samples from well VDB-GT-04 (at depth 1890 m and 1910 m) complemented the palynological analysis of Munsterman (2012). The samples were processed at the TNO laboratory using the standard sample processing procedures (e.g. Janssen, 2008), which involved HCl and HF treatment, and sieving over an 18 µm mesh sieve. The well selection was based on the well location in different graben blocks and the total thickness of the Nieuwerkerk Formation that these wells encountered. Larger total thickness could potentially reveal more information from the fluvial interval. The location of the wells in different fault blocks allowed relating differences in fluvial architecture to the syn-tectonic origin of the interval. The palynological analysis consisted of age dating and identification of the Elegans Maximum Flooding Surface (MFS) and the Paratollia MFS (e.g. Jeremiah et al., 2010), which formed the framework of our regional correlation scheme.

2.2.4. Age dating

The age interpretation was based on the Last Occurrence Date (LOD) of palynomorphs, in particular dinoflagellate cysts (dinocysts), and pollen and spores (sporomorphs). Key-references concerning the palynostratigraphy of Early Cretaceous from the North Sea region were: Abbink (1998), Costa and Davey (1992), Davey (1979, 1982), Duxbury et al. (1999), Duxbury (2001), Heilmann-Clausen (1987), Herngreen et al. (2000), Partington et al. (1993) and Riding and Thomas (1992). The international geological time scale of Gradstein et al. (2012) was followed.

2.2.5. Sporomorph Eco-Grouping (SEG) method

The SEG method (Abbink, 1998; Abbink et al., 2004). Abbink (1998) and Abbink et al. (2004) were used to identify the Paratollia MFS in the fluvial aquifer interval of HON-GT-01 and PNA-GT-02. With this method, sporomorph types were related to vegetation eco-groups. Abbink et al. (2004) classified Jurassic to Lower Cretaceous sporomorphs into six eco-groups. (1) Upland vegetation grows on higher terrain well above ground water level, which is never submerged by water. (2) Lowland vegetation is found on plains with or without fresh water swamps. It is not influenced by salt water. When periodically submerged it is referred to as 'Wet-Lowland' otherwise 'Dry-Lowland'. (3) River vegetation is found on riverbanks and could be periodically submerged. (4) Pioneering vegetation occupies recently developed eco-space that has been previously submerged by seawater. (5) Coastal vegetation is found along the coast. (6) Tidally influenced vegetation is daily influenced by tidal changes and regularly submerged in a salt-water regime. Quantitative analysis of sporomorphs indicated percentages of eco-groups that were represented in the cuttings samples. In the SEG method it was assumed that the relative share in lowland vegetation and the area where it accumulates decrease during a transgression (Figure 2.5-A) and show minimal presence on the moment of maximum transgression when a MFS is formed (Figure 2.5-B). Based on this assumption, trends in relative representation of eco-groups were related to sea-level fluctuation. MFS were as-

signed to samples where the relative share of 'Upland' sporomorphs peaked with respect to the 'Lowland' eco-group while the marine influenced eco-groups were poorly represented or absent. Cuttings samples with 10 m intervals were analysed in the 2560 to 2810 m (MD) interval in HON-GT-01 and 2440-2850 m (MD) in PNA-GT-02.

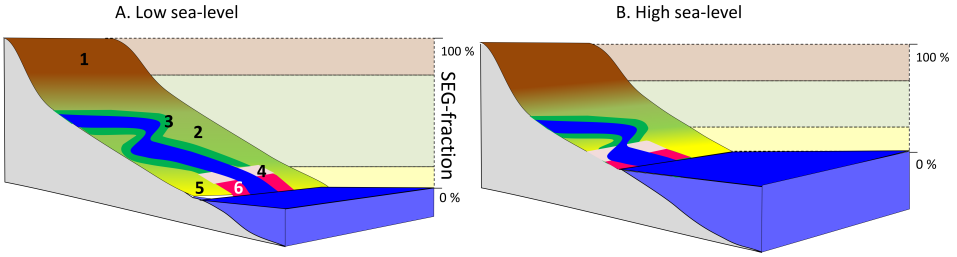

Figure 2.5: Schematic representation of the impact of (A) low sea-level and (B) high sea-level on the relative occurrence of eco-groups; 1= Upland, 2= Lowland, 3=River, 4 =Pioneer, 5=Coastal, 6= Tidally influenced. Edited after Abbink et al. (2004).

2.3. Results

2.3.1. Seismic interpretation

Three half grabens and one horst block were recognised in the seismic cross-section (Figure 2.6-1). The grabens were referred to as 'Westland fault block', 'Pijnacker/Delft fault block' and 'VDB fault block'. The interpretation of the top and base of the Nieuwerkerk formation indicated a lateral thickness variation of the Nieuwerkerk Formation in these grabens. Horizon flattening of the Top Nieuwerkerk Formation horizon was applied to highlight syn-depositional fault movement (Figure 2.6-2). The associated faults that were active during deposition of the Formation are highlighted in red. The regional extent of these faults was derived from the structural interpretation by Duin et al. (2006). These results were used for the comparison of fluvial reservoir architecture in these three fault blocks.

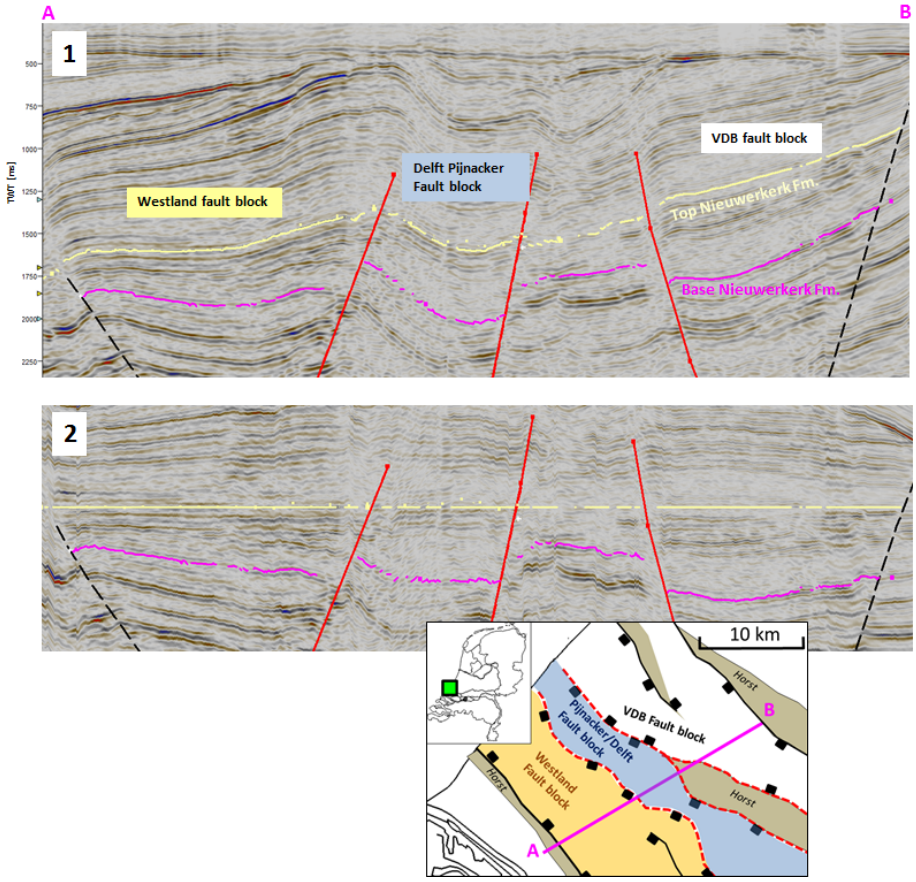

Figure 2.6: (1) seismic section with interpretation of faults as well as top (yellow) and base (pink) of the Nieuwerkerk Formation horizons. (2) Horizon flattening on top Nieuwerkerk Fm. The outline of the seismic section as wells as the outline of the interpreted fault are indicated on the map.

2.3.2. Palynological analysis

Palynological age dating of intervals in the three wells formed the basis of the sequence stratigraphic correlation scheme. An overview of the results is presented in table 2.1 and a detailed description of the analysis of all samples is presented in **AppendixA**.

Depth (m)	PNA-GT-02
2120-2175	Late Barremian
2195-2215	late Early Barremian, ***Elegans Ammonite Zone*** or older
2235-2275	earliest Barremian variabilis Ammonite Zone or older
2440-2590	Valanginian
2600-2850	Late Ryazanian - Early Valanginian
	HON-GT-01
2320	Late Barremian
2340-2360	early Late Barremian
2380-2420	late Early Barremian,***Elegans Ammonite Zone*** or older
2560-2730	Valanginian
2740	Early/earliest Valanginian
2750-2810	Late Ryazanian, post-*kochi* Ammonite Zone
	VDB-GT-04
1320-1530	Barremian (Munsterman (2012)
1530-1625	Barremian-Hauterivian (Munsterman (2012)
1625-1890	Valanginian (Munsterman (2012)
1890-1910	Late Ryazanian - Early Valanginian

Table 2.1: Palynological age dating in well PNA-GT-02, HON-GT-01 and VDB-GT-04. Depth is 'Measured Depth along hole.

Several MFS were identified in the Valanginian to Late Ryazanian intervals of PNA-GT-02 and HON-GT-01 with the SEG method. This method was applied to cutting samples at 2440-2850 m Measured Depth (MD) in PNA-GT-01 and 2560-2810 m MD in HON-GT-01. SEG graphs in Figure 2.7 show the relative occurrence of sporomorph association in the samples. MFS were related to the reduced occurrences in the "Lowland" sporomorph Eco Group in combination with relative increase of the "Upland" sporomorph Eco Group (Figure 2.7). The "Pioneer", "Coastal" and "Tidally-influenced" vegetation showed minimal values. Four MFS were identified in PNA-GT-02 and two in HON-GT-01. The Paratollia MFS was associated with 'MFS 2' in both wells. In well PNA-GT-02, this was based on the LOD of *Stiphrosphaeridium dictyophorum* (Sdi) at 2600 m and the LOD of *Canningia compta* (Cco) at depth 2620 m (Figure 2.7). In HON-GT-01, the Paratollia MFS was interpreted at depth 2730 m based on the LODs of *Canningia compta* (and a morphologically closely related Escharisphaeridia spp. at 2730 m) and *Perisseiasphaeridium insolitum* at depth 2740 m MD. In VDB-GT-04, the interpretation of the Paratollia Ammonite Zone was based on the presence of *Perisseiasphaeridium insolitum, Stiphrosphaeridium dictyophorum, Canningia compta, Hystrichosphaeridium scoriaceum* and *Oligosphaeridium diluculum* in the samples at 1890 m and 1910 m MD. A marine origin of the sample at 1890 was recognised and therefore it may most likely be associated with the Paratollia MFS. Please note that this is not based on the SEG analysis in this well. The well-log correlation (Figure 2.7) indicates that the aquifers in these wells are not part of a single sandstone-rich succession. At least two sandstone-rich zones are encountered of Valanginian and Late Ryazanian age with limited lateral extent. The Valanginian sandstone-rich zone in HON-GT-01 relates to the upper

section of the sandstone-rich zone in PNA-GT-02 with the same age. In contrast, the Valanginian succession in VDB-GT-04 is claystone-dominated. In this well the aquifer is formed by a Late Ryazanian sandstone rich-zone that relates to the Late Ryazanian sandstone-rich zone in PNA-GT-02. In HON-GT-01 the Late Ryazanian succession is claystone-dominated. Stacking of both sandstone-rich zones accounts for the increased aquifer thickness in well PNA-GT-02. In contrast, lower aquifer thickness could be explained by the presence of a single sandstone-rich zone in HON-GT-01 and VDB-GT-04.

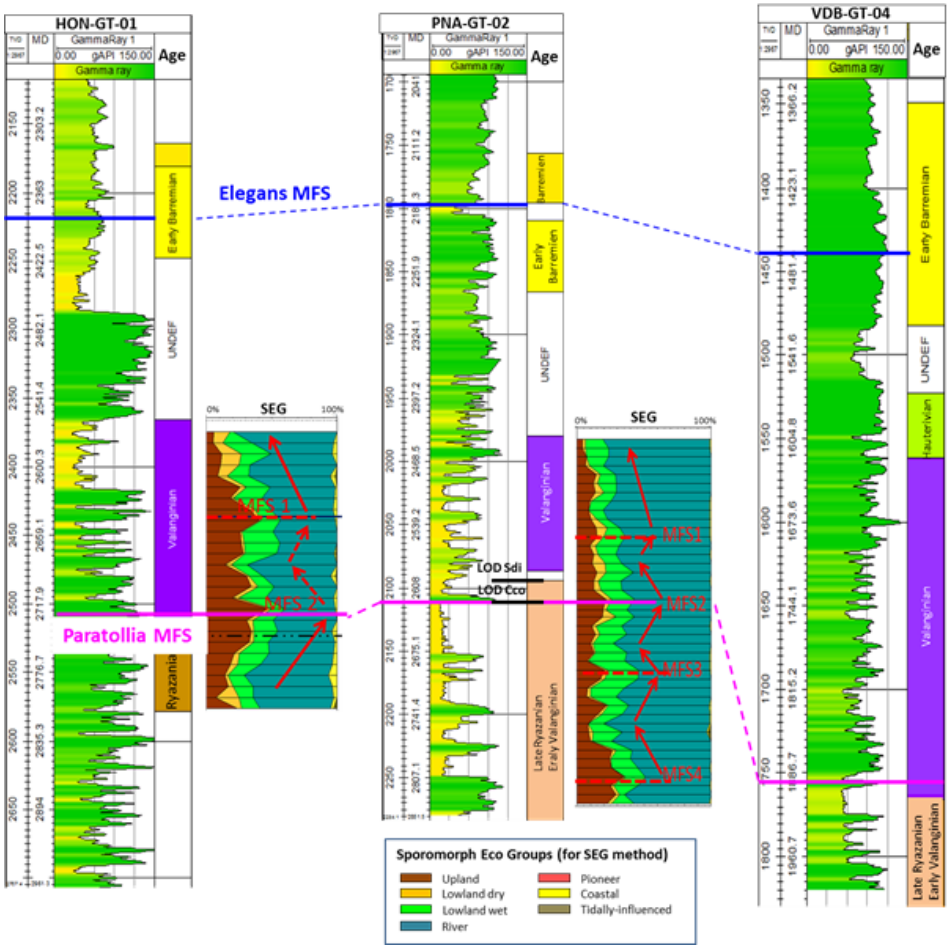

Figure 2.7: Combination GR logs, Palynological age dating of intervals, MFS interpretation from the SEG analysis in the fluvial interval of HON-G-01 and PNA-GT-02. Age interpretation in VDB-GT-04 is based on Munsterman (2012). Please note differences in GR log scale.

2.3.3. Regional well-log correlation

Regional well-log correlation based on interpretation of the Elegans MFS indicates that the Valanginian succession is sandstone-rich in both the Westland and Pijnacker/Delft fault blocks (Figure 2.8). Following the GR log pattern in these wells, the top of this succession is selected in the other wells in the absence of palynological age dating. In most wells, the sandstone content of the Valanginian succession is even larger than in HON-GT-01 and PNA-GT-02. The lateral extent of this sandstone-rich zone is limited because the Valanginian succession has low sandstone content in the VDB fault block (Figure 2.8). The Ryazanian succession has a low sandstone content in the Westland fault block, but high sandstone content in the Pijnacker/Delft and VDB fault blocks. The top of the Ryazanian succession is related to the Paratollia MFS. In the three wells with palynological analysis, the Paratollia MFS was recognised at approximately 300 m True Vertical Depth (TVD) below the Elegans MFS. This trend is used to approximate the depth of the Paratollia MFS in all wells as not all wells reached sufficient depth to compare GR log patterns of the deeper Ryazanian succession. Our correlation scheme suggests that the prevailing position of the meander belts in which sand was deposited during these periods, shifted from the east to the west side of the basin from the Late Ryazanian to the Valanginian.

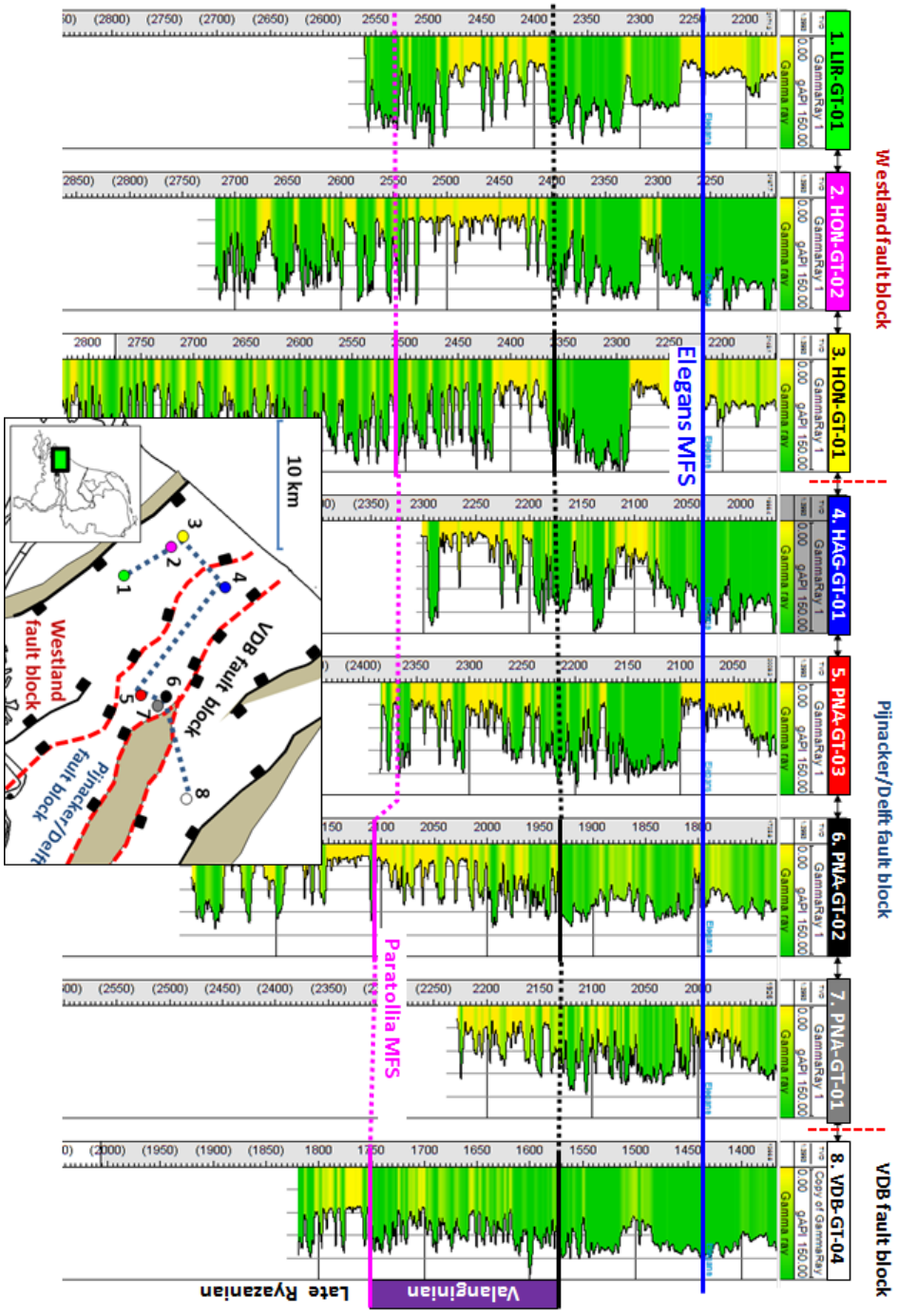

Figure 2.8: Well-log correlation of geothermal wells in three different fault blocks in the WNB.

2.4. Discussion

The results of this study show a regional westward shift of sandstone-dominated facies during the Valanginian Figure 2.8). Based on the unidirectional shift and the recognition of syn-depositional fault movement (Figure 2.6), we propose a tectonic origin for this shift. In contrast, a more random distribution of sandstone-rich zones in the three fault blocks would be expected if only avulsion controlled sandstone distribution in the basin (e.g. Hajek et al., 2010; Donselaar et al., 2013; Flood and Hampson, 2015; Toorenenburg et al., 2016). Based on this conclusion maps are generated that predict the lateral extent of the Late Ryazanian/Early Valanginian sandstone-rich zone (Figure 2.9A) and the Valanginian sandstone-rich zone (Figure 2.9B). These maps confirm the prediction of a westward shift of sandstone-dominated facies during the Valanginian by Den Hartog Jager (1996) which was based on seismic facies interpretation. This trend was not recognised in previous correlation studies because of the use of hydrocarbon wells on structural highs in the basin that experienced different tectonic movement during deposition compared to the graben fault blocks (Devault and Jeremiah, 2002; Jeremiah et al., 2010).

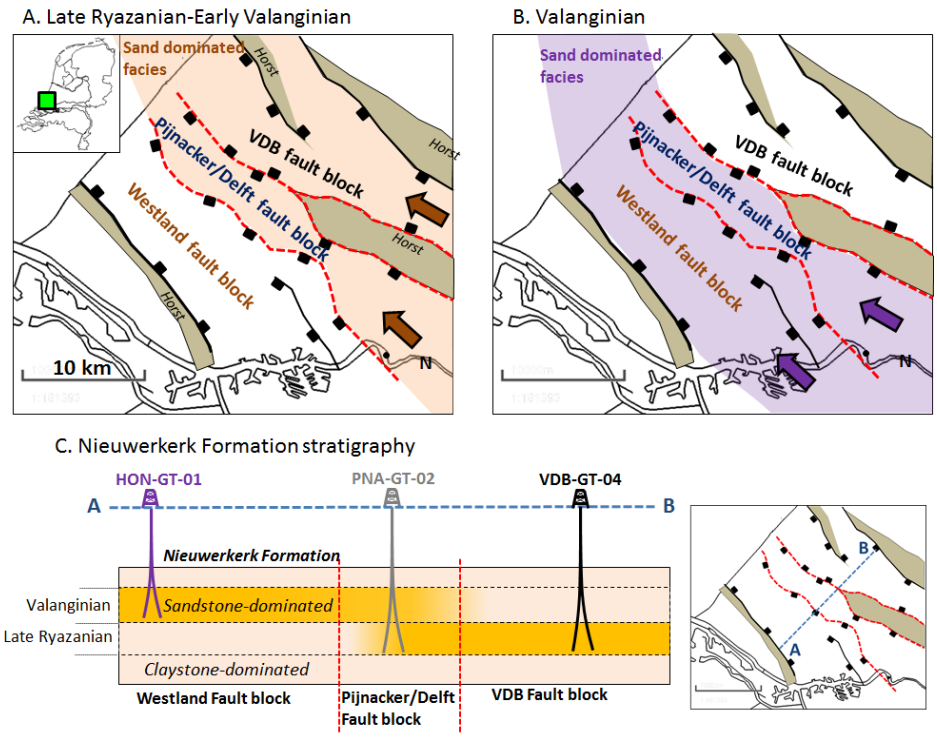

Figure 2.9: Series of maps indicating the location of sandstone-dominated sedimentation during the (A) Ryazanian/Early Valanginian and (B) Valanginian. Arrows indicate fluvial paleoflow direction. (C) Cartoon illustrating facies distribution in the fluvial interval of the Nieuwerkerk Formation on a cross-section perpendicular to the fault trend.

The revised fluvial architecture of the Delft Sandstone has an impact on expected aquifer thickness in different fault blocks. Larger aquifer thickness could be expected in the Pijnacker/Delft fault block where sandstone-dominated zones in both succession overlap. Furthermore, it affects expected aquifer depth and therefore drilling costs.The aquifer is found at larger depth in the VDB fault block compared to the other two fault blocks (Figure 2.9C). In current WNB doublets, productivity and injectivity vary considerably (van Wees et al., 2012). The variability could be a result of different porosity and permeability distributions in stratigraphically different sandstone successions. In that case, the expected injectivity and productivity of future doublets should be based on values which are measured in geothermal doublets in the same fault block. However, because of limited data acquisition and monitoring, it is not possible to identify a single cause of this variability (Wees et al., 2012). Because of the limited number of wells with palynological cutting analysis in our study, uncertainty remains about the continuity of the sandstone-rich zones between the wells. The Nieuwerkerk Formation is deposited by a relatively small meandering fluvial system with a paleoflow depth of approximately 4 m (e.g. Devault and Jeremiah, 2002). The associated paleochannel width and channel belt width are therefore estimated to be approximately 40 m and 1 to 2 km, respectively (e.g. Gibling, 2006; Bridge, 2006). Lateral continuity of individual sandstone bodies during deposition is limited to the channel belt widths (e.g. Donselaar and Overeem, 2008). Through amalgamation sandstone body width might extend further. However, claystone bodies are likely to form flow baffles or barriers perpendicular to the paleoflow direction. This should be taken into account in doublet placement. Our results underline the importance of palynological analysis for fluvial well-log correlation. These analyses enabled the identification of markers within fluvial claystone-dominated as well as sandstone-dominated successions in the HON-GT-01 and PNA-GT-02 wells, respectively Figure 2.7). This would not have been possible based on GR log interpretation alone.

2.5. Conclusions

Based on the results of this study we can conclude that:

- Current WNB geothermal doublets encounter sandstone-rich zones in at least two stratigraphic intervals of Late Ryazanian-Early Valanginian and Valanginian age.
- Sandstone-rich zones in both intervals can overlap which accounts for aquifer thickness variations.
- During the Valanginian, tectonic movement induced a unidirectional shift of the deposition of sandstone-dominated facies from the east to the west of the basin.
- This shift has an impact on expected aquifer thickness and aquifer depth in different fault blocks in the basin.

References

Abbink, O. A. (1998). *Palynological investigations in the Jurassic of the North Sea region.* Phd thesis, Utrecht University.

Abbink, O. A., Van Konijnenburg-Van Cittert, J., Van der Zwan, C., and Visscher, H. (2004). A sporomorph ecogroup model for the Northwest European Jurassic - Lower Cretaceous II: Application to an exploration well from the Dutch North Sea. *Netherlands Journal of Geosciences*, 83(2):81–92.

Bridge, J. (2006). Fluvial facies models: Recent developments. In Posamentier, H. and Walker, R., editors, *Facies Models Revised*, pages 85–170. SEPM Special Publication volume 84.

Costa, L. I. and Davey, R. J. (1992). Dinoflagellate cysts of the Cretaceous System. In Powell, A., editor, *A stratigraphic index of dinoflagellate cysts*, pages 99–131. British Micropalaeontological Society.

Davey, R. J. (1979). The stratigraphic distribution of dinocysts in the Portlandian (latest Jurassic) to Barremian (Early Cretaceous) of northwest Europe. *American Association of Stratigraphic Palynologists Contributions Series*, 58:49–81.

Davey, R. J. (1982). Dinocyst stratigraphy of the latest Jurassic to Early Cretaceous of the Haldager No. 1 borehole, Denmark. *Danmarks Geologiske Undersøgelse Serie B*, 6:1–57.

Den Hartog Jager, D. G. (1996). Fluviomarine sequences in the Lower Cretaceous of West Netherlands Basin: correlation and seismic expression. In Rondeel, H., Batjes, D., and Nieuwenhuijs, W., editors, *Geology of gas and oil under the Netherlands*, pages 229–241. Kluwer Academic Publishers.

Devault, B. and Jeremiah, J. (2002). Tectonostratigraphy of the Nieuwerkerk Formation (Delfland Subgroup) West Netherlands Basin. *AAPG Bulletin*, 86(10):1679–1707.

Donselaar, M. E., Gozalo, M. C. C., and Moyano, S. (2013). Avulsion processes at the terminus of low-gradient semi-arid fl uvial systems : Lessons from the Río Colorado , Altiplano endorheic basin , Bolivia. *Sedimentary Geology*, 283:1–14.

Donselaar, M. E., Groenenberg, R. M., and Gilding, D. T. (2015). Reservoir Geology and Geothermal Potential of the Delft Sandstone Member in the West Netherlands Basin. In *World Geothermal Congress 2015*, Melbourne, Australia.

Donselaar, M. E. and Overeem, I. (2008). Connectivity of fluvial point-bar deposits: An example from the Miocene Huesca fluvial fan, Ebro Basin, Spain. *AAPG Bulletin*, 92(9):1109–1129.

Duin, E. J. T., Doornenbal, J. C., Rijkers, R. H. B., Verbeek, J. W., and Wong, T. E. (2006). Subsurface structure of the Netherlands – results of recent onshore and offshore mapping. *Netherlands Journal of Geosciences*, 85(4):245–276.

Duxbury, S. (2001). A palynological zonation scheme for the lower cretaceous-united kingdom sector, central north sea. *Neues Jahrbuch fur Geologie und Palaontologie-Abhandlungen*, 219:95–137.

Duxbury, S., Kadolsy, D., and Johansen, S. (1999). Sequence stratigraphic subdivision of the Humber Group in the Outer Moray Firth area (UKCS, North Sea). In Jones, R. and Simmons, M., editors, *Biostratigraphy in Production and Development Geology*, number 152, pages 23–54. Geological Society, London, Special Publications.

Flood, Y. S. and Hampson, G. J. (2015). Quantitative analysis of the dimensions and distribution of channelized fluvial sandbodies within a large outcrop dataset: Upper Cretaceous Blackhawk Formation, Wasatch plateau, Central Utah, U.S.A. *Journal of Sedimentary Research*, 85:315–336.

Gibling, M. R. (2006). Width and Thickness of Fluvial Channel Bodies and Valley Fills in the Geological Record: A Literature Compilation and Classification. *Journal of Sedimentary Research*, 76:731–770.

Gradstein, F. M., Ogg, J. G., and Hilgen, F. J. (2012). On The Geologic Time Scale. *Newsletters on Stratigraphy*, 45(2):171–188.

Hajek, E. A., Heller, P. L., and Sheets, B. A. (2010). Significance of channel-belt clustering in alluvial basins. *Geology*, 38(6):535–538.

Heilmann-Clausen, C. (1987). Lower Cretaceous dinoflagellate biostratigraphy in the Danish Central Trough. *Danmarks Geologiske Undersøgelse*, 17:1–90.

Herngreen, G. and Wong, T. E. (2007). Cretaceous. In Wong, T. E., Batjes, D., and De Jager, J., editors, *Geology of the Netherlands*, chapter Cretaceous, pages 127–150. Edita-the Publishing House of the Royal.

Herngreen, G. F. W., Munsterman, D., and Kerstholt, S. (2000). *Callovian-Ryazanian ('Upper Jurassic') Palynostratigraphy of the Central North Sea Graben and Vlieland Basin, the Netherlands*. Mededelingen Nederlands Instituut voor Toegepaste Geowetenschappen TNO 63.

Janssen, N, D. G. (2008). Sample processing for pre-Quaternary palynology. Internal report TNO Built Environment and Geosciences. Technical report, TNO, Utrecht.

Jeremiah, J. M., Duxbury, S., Rawson, P., E, S. I., Ashford, N. D., and Tx, H. (2010). Lower Cretaceous of the southern North Sea Basins : reservoir distribution within a sequence stratigraphic framework. *Netherlands Journal of Geosciences*, 89(3/4):203–237.

Kombrink, H., Doornenbal, J. C., Duin, E. J. T., Dulk, M. D., Gessel, S. F. V., Veen, J. H., and Witmans, N. (2012). New insights into the geological structure of the Netherlands ; results of a detailed mapping project. *Netherlands Journal of Geosciences*, 91(4):419–446.

Partington, M., Copestake, P., Mitchener, B., and Underhill, J. (1993). In Parker, J., editor, *Petroleum Geology of North-West Europe*, volume 4, pages 371–386. Graham and Trotman, London.

Racero-Baena, A. and Drake, S. J. (1996). Structural style and reservoir development in the West Netherlands oil province. In Rondeel, H. E. and Batjes, D. A. J.and Nieuwenhuijs, W. H., editors, *Geology of Gas and Oil under the Netherlands*, pages 211–227. Springer Netherlands, Dordrecht.

Riding, J. B. and Thomas, J. E. (1992). Dinoflagellate cysts of the Jurassic System. In Powell, A., editor, *A stratigraphic index of dinoflagellate cysts*, pages 7–98. luwer Academic Publishers, Dordrecht.

Toorenenburg, K. A. V., Donselaar, M. E., Noordijk, N. A., and Weltje, G. J. (2016). On the origin of crevasse-splay amalgamation in the Huesca fl uvial fan (Ebro Basin , Spain): Implications for connectivity in low net-to-gross fl uvial deposits. *Sedimentary Geology*, 343:156–164.

Van Adrichem Boogaert, H. and Kouwe, W. (1993). Stratigraphic nomenclature of the Netherlands, revision and update by Rijks Geologische Dienst (RGD) and Netherlands Oil and Gas Exploration and Production Association (NOGEPA). *Mededelingen Rijks Geologische Dienst*, 50:1—180.

Vondrak, A. (2016). (Bio-) stratigraphic correlation of geothermal aquifers in the West Netherlands Basin (Bio-) stratigraphic correlation of geothermal aquifers in the West Netherlands Basin. Technical report, PanTerra Geoconsultants B.V., Leiderdorp.

Wees, J. V., Kronimus, A., Putten, M. V., Pluymaekers, M. P. D., Mijnlieff, H., Hooff, P. V., Obdam, A., and Kramers, L. (2012). Geothermal aquifer performance assessment for direct heat production – Methodology and application to Rotliegend aquifers. *Netherlands Journal of Geosciences*, 91(4):651–665.

3

On the connectivity anisotropy in fluvial Hot Sedimentary Aquifers and its influence on geothermal doublet performance

Abstract
Geothermal doublet layout with respect to the paleoflow direction in fluvial sedimentary reservoirs could significantly affect pump energy losses. These losses can be reduced by up to 10% if a doublet well pair is oriented parallel to the paleoflow trend compared to perpendicular. The chance that flow paths are formed perpendicular to this trend strongly depends on the net sandstone volume in the reservoir. Detailed fluvial facies architecture realisations which are used in this study, are generated with a process-based approach utilising geological data from the Lower Cretaceous Nieuwerkerk Formation in the West Netherlands Basin. Finally, this study emphasizes the importance of detailed facies architecture modelling for the assessment of both risks and production strategies in Hot Sedimentary Aquifers.

This chapter is based on: Willems, C.J.L., Nick, H.M., Donselaar, M.E., Weltje, G.J., Bruhn, D.F., *On the connectivity anisotropy in fluvial Hot Sedimentary Aquifersand its influence on geothermal doublet performance*. Geothermics **65**, 222-233, (2017).

3.1. Introduction

Hot Sedimentary Aquifers (HSA) are commonly exploited by a doublet system, consisting of a hot-water production and a cold-water reinjection well. Downhole well distance typically is 1000 to 2000 m, and both wells target the same aquifer to maintain pressure support in the reservoir. In fluvial reservoir rocks the doublet connectivity is via a network of permeable fluvial channel sandstone bodies embedded in non-permeable floodplain mudstone. Detailed knowledge of the size, shape, spatial distribution and connectivity of the fluvial sandstone bodies (or: fluvial reservoir architecture) is required to assess the risk of pressure communication loss between the wells and the inherent (Figure 3.1).

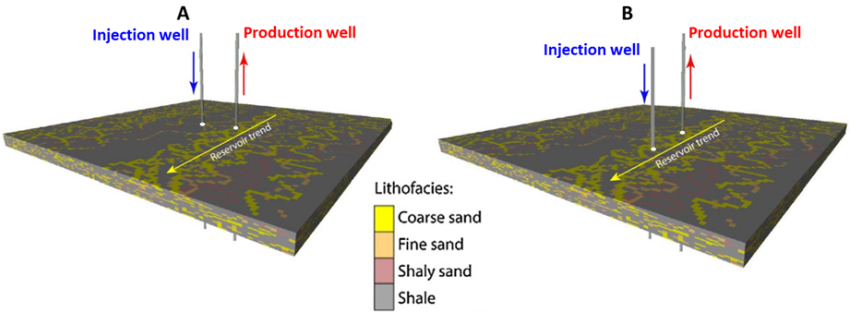

Figure 3.1: Example of the effect of doublet layout with respect to the orientation of sandstone bodies in the reservoir. Example (A) shows a perpendicular layout and (B) a parallel layout.

The effect of the fluvial reservoir architecture on the recovery of hydrocarbons has extensively been studied (e.g. Jones and Doyle, 1995; Larue and Friedmann, 2005; Larue and Hovadik, 2006; Pranter et al., 2007; Larue and Hovadik, 2008; de Jager et al., 2009). To a much more limited extent, this topic is addressed for geothermal energy production (e.g. Hamm and Lopez, 2012; Crooijmans et al., 2016) and for CO_2 sequestration (e.g. Issautier et al., 2014). Larue and Hovadik (2008) identified 'connectivity' as one of the main parameters that control the recovery efficiency of hydrocarbon reservoirs. Connectivity could be defined as the ratio of the volume of the largest sandstone body cluster and the total sandstone body volume (e.g. Larue and Hovadik, 2006). If the connectivity is high, less isolated clusters occur and therefore fewer wells are required to drain the reservoir (e.g. Geel and Donselaar, 2007). Previous work on connectivity in sedimentary reservoirs identified several main factors that control the chance that sandstone bodies connect: (1) the net-sandstone volume or net-to-gross (N/G); (2) the sandstone body geometry, and (3) the range in paleo- flow direction, which determines the reservoir trend (King, 1990; Larue and Hovadik, 2006; Geel and Donselaar, 2007; Larue and Hovadik, 2008; Ainsworth, 2005; Pranter and Sommer, 2011). Connectivity of reservoir bodies is also influenced by post-depositional faulting (Bailey et al., 2002), by diagenetic processes, and by depositional permeability heterogeneity within in the sandstone bodies (Willis and Tang, 2010; Henares et al., 2014). To date, studies into the risk assessment of connectivity are dominantly focused on the

optimization of hydrocarbon recovery efficiency. A main goal of connectivity analyses was to identify a N/G threshold below which isolated bodies start to occur. In meandering fluvial reservoirs, this N/G threshold is often recognized between 20 to 30% N/G, depending on the sandstone body geometries (e.g. Larue and Hovadik, 2006). Because in geothermal exploitation well pairs are used, a new directional component in connectivity analyses is required. This can assist engineers to design geothermal doublet systems with the largest possible exchange surface between two wells in order to minimize pump energy losses and to delay cold water breakthrough. A conceptual fluvial reservoir model illustrates the difference between the hydrocarbon and geothermal exploitation objectives (Figure 3.2). The model contains five wells in an L-pattern with a 500 m spacing and an alignment parallel and perpendicular to the paleo-flow direction. In terms of drainable volume, these wells are efficiently placed and intersect most of the sandstone bodies in the reservoir. However, if the wells included geothermal doublets, the distance and orientation of the well pair layout would significantly influence the chance that flow paths are formed between well pairs. Please note that the well spacing in the model is a third to one half of the 1.5 km spacing commonly used in HSA doublets (Lopez et al., 2010; Mottaghy et al., 2011). A larger well spacing would increase the risk of connectivity loss. The chance that sandstone bodies form flow paths parallel and perpendicular to the paleoflow direction (i.e., the connectivity anisotropy) has so far not been investigated.

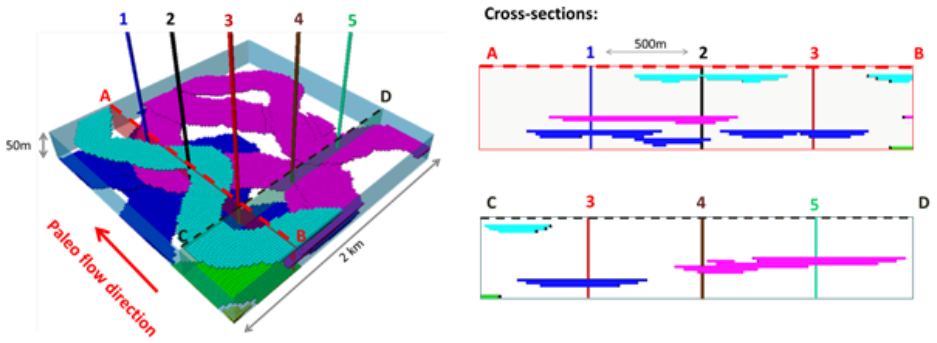

Figure 3.2: Conceptual fluvial reservoir model with 5 wells. Floodplain fines are transparent; sandstone bodies have the same colour if they are connected.

The West Netherlands Basin (WNB) is an example of an area with fluvial HSA exploitation. Nine doublets currently produce from the fluvial Nieuwerkerk Formation (chapter 1).The orientation of these doublets with respect to the paleoflow trend varies. Productivity and injectivity vary considerably in the WNB (Wees et al., 2012). The reduction in injectivity could be related to well layout but also to other factors such as scaling or skin formation. Wees et al. (2012) pointed out that unfortunately it is not possible to identify a single cause of this variability because of limited available data. The uncertainty in injectivity and productivity, limits the growth of HSA

development. In the Netherlands this is reflected by the fact that approximately 100 exploration licences are granted, while only fifteen doublets have been actually realised in the past ten years. Such a gap between HSA potential and actual exploitation exists worldwide (Boxem et al., 2011). Other examples of sedimentary basins with large HSA potential but limited exploitation are the Perth Basin, Australia (Pujol et al., 2015), and the Idaho thrust belt (Welhan, 2016). A better understanding of connectivity anisotropy could reduce the risk associated with HSA exploitation and hence support its growth. Therefore, the first goal of this paper is to evaluate connectivity anisotropy and its dependence on N/G. Secondly, the possible effect of this anisotropy on doublet performance is evaluated. The results should contribute to fluvial HSA development strategies that increase the efficiency and decrease the risks of exploitation. For this purpose, hundreds of detailed facies architecture realisations have been generated. This stochastic approach, in which reservoir heterogeneities are taken into account, is standard in hydrocarbon exploitation (e.g. Keogh et al., 2007). In contrast, geothermal reservoirs are often modelled as homogeneous layers (Mottaghy et al., 2011). The realisations are based on a geological dataset of the Lower Cretaceous Nieuwerkerk Formation (DeVault and Jeremiah, 2002). Sediments in this interval were deposited by a syn-rift, meandering fluvial system. Extensional faulting in the Late Jurassic created half-graben structures between southeast to northwest trending faults. These structures guided the paleo-flow direction of the fluvial system. Intervals with different N/G trends are recognized (Devault and Jeremiah, 2002). N/G trends are determined by the sediment aggradation rate (Shanley and Mccabe, 1994; Posamentier and Morris, 2000). As a result of low aggradation rates meander loops have more time to develop. While they migrate laterally, floodplain fines are eroded and a high N/G interval is generated with wide, thick, amalgamated sandstone complexes. In contrast, low N/G intervals with more narrow and isolated sandstone bodies are created as a result of fast aggradation rates. This is caused by frequent flooding and deposition of fine sediments on the floodplain. The varying N/G trends in the Nieuwerkerk Formation create uncertainty about connectivity of the sandstone bodies between the doublet wells. In our study, the facies realisations are generated with a process-based approach (Karssenberg et al., 2001; Cojan et al., 2005; Karssenberg and Bridge, 2008; Lopez et al., 2010; Grappe et al., 2012). This is different from previous connectivity analyses that used a more standard object-based facies modelling approach (e.g. Keogh et al., 2007). As the facies modelling approach influences both the spatial distribution and the shape of the bodies, it could have an effect on a connectivity analysis (Villamizar et al., 2015). In object-based modelling, the spatial distribution of the sandstone bodies in the model is random. In contrast, in a process-based modelling approach the spatial distribution of sandstone bodies is governed by the simulated sedimentary processes. This creates a more realistic and sedimentologically-based spatial distribution of facies bodies. Another characteristic of the process-based modelling approach is that the geometry of the facies bodies and N/G are related (e.g. Bridge, 2006; Cojan et al., 2005). Previous connectivity studies, however, used an object-based approach where N/G and sediment geometry were varied independently which could affect the results

(e.g. Larue and Hovadik, 2006). With our approach we are able to show that the facies architecture is non-negligible and that detailed geological modelling is required to increase efficiency of HSA exploitation.

3.2. Data and Methods

Hundreds of facies realisations were generated that vary in N/G. The realisations were analysed in three steps. Firstly, the relation between sandstone body clustering and N/G was determined by a connectivity analysis. Secondly, the connectivity anisotropy was analysed by deriving the equivalent permeability in three directions, parallel, perpendicular and vertical to the paleoflow direction. Finally, well pairs were placed parallel and perpendicular to the paleoflow in the realisations and equivalent permeability and pump energy losses were calculated in steady state production simulations.

3.2.1. Geological dataset

The geological modelling in this study is based on a subsurface dataset of the fluvial Nieuwerkerk Formation in the WNB. The dataset was used to derive a realistic range of heterogeneities to constrain the set of facies realisations. The dataset consists of Gamma-Ray (GR) logs and cores from deep wells, their locations are indicated in Figure 3.3. The core study provided thickness ranges of facies bodies which were used as input for the facies modelling. In approximately 75 m of core in MKP-11 and 25m in Q13-09, five different types of facies bodies were recognized: floodplain fines, crevasse splays, single-storey channel bodies and amalgamated sandstone complexes. The thickness of individual sandstone bodies is approximately 4 m (Figure 3.4). Based on the bank-full flow depth, the bank-full flow width was estimated at 40 m (Williams, 1986). Crevasse splay thickness in the cores varied between 0.2 to 0.6 m. (Figure 3.4). Furthermore, cores provide porosity-permeability relations for the reservoir property modelling. The gamma ray logs are used to derive N/G ranges of the Nieuwerkerk Formation. GR logs in the WNB show that N/G varies from approximately 10 to 90% (Figure 3.3).

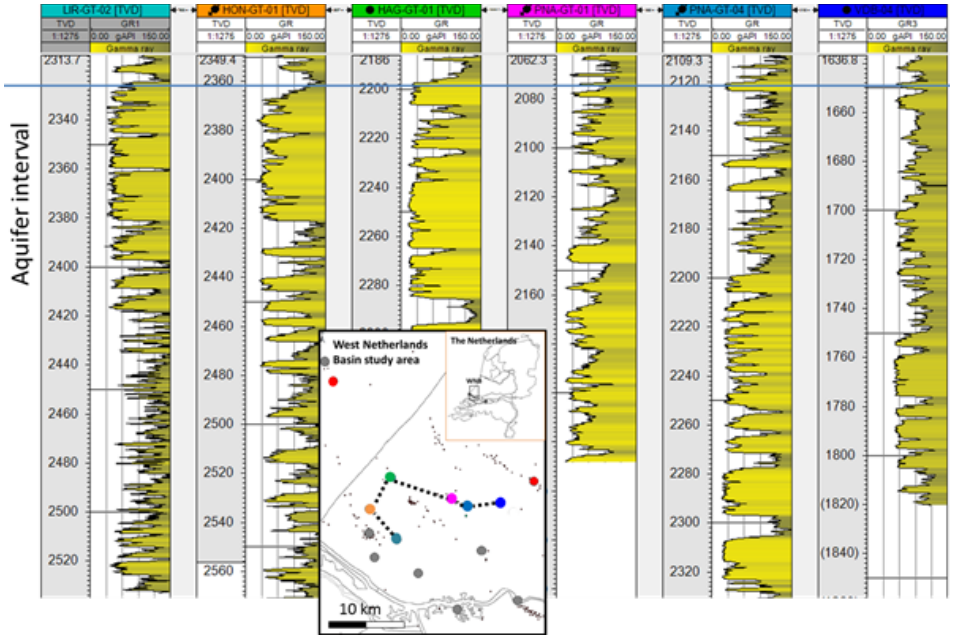

Figure 3.3: Gamma-ray (GR) logs from WNB geothermal doublets. Low GR readings indicate sandstone (yellow); high GR reading indicate finer grained sediments such as silt and clay. TVD is True Vertical Depth. Well locations are indicated by the coloured dots on the map. Red dots indicate hydrocarbon wells with cores, small black dots indicate all hydrocarbon wells in the study area.

3.2.2. Process-based facies modelling

Input parameters for the process-based facies modelling software, Flumy, were (1) channel width and depth, (2) avulsion frequency, (3) flood frequency, (4) maximum overbank flood deposit thickness (H_{th}) and (5) floodplain topography parameter (henceforth: FT-factor). The thickness of floodplain deposit decreases away from the channel (Figure 3.5). The distance at which the thickness decreased exponentially is the FT-factor. A high FT-factor means that the flood deposit is wide and thick which increases the sediment aggradation rate and decreases the N/G of the realisation. Paleo channel depth and width were derived from the core analysis and analogues, respectively. The other parameters cannot be derived directly from subsurface data. Therefore large ranges of values were used to capture the uncertainty. Avulsion frequency was varied between 200 and 1600 years. This parameter could not be derived from the dataset and hence a large range around a 800 to 1000 year (Törnqvist and Bridge, 2002) mean was used. Avulsion frequency mainly affects the sandstone body width. Flood frequency, H_{th} and the FT-factor were the primary controls on N/G. To obtain realisations with N/G values between 10% and 90%, overbank flood frequency was varied between 20 to 200 years, H_{th} between 0.2 to 0.6 m and the FT-factor between 300 to 900 m. During every simulated flood, sediments were deposited on the floodplain with a maximum thickness H_{th} near the channel. In the simulations, sedimentary processes distributed and

shaped different facies bodies such as channel lags, point-bars, crevasse splays, mud plugs and floodplain fines. The process-based method implemented in Flumy software is explained in more detail in Cojan et al. (2005); Grappe et al. (2012).

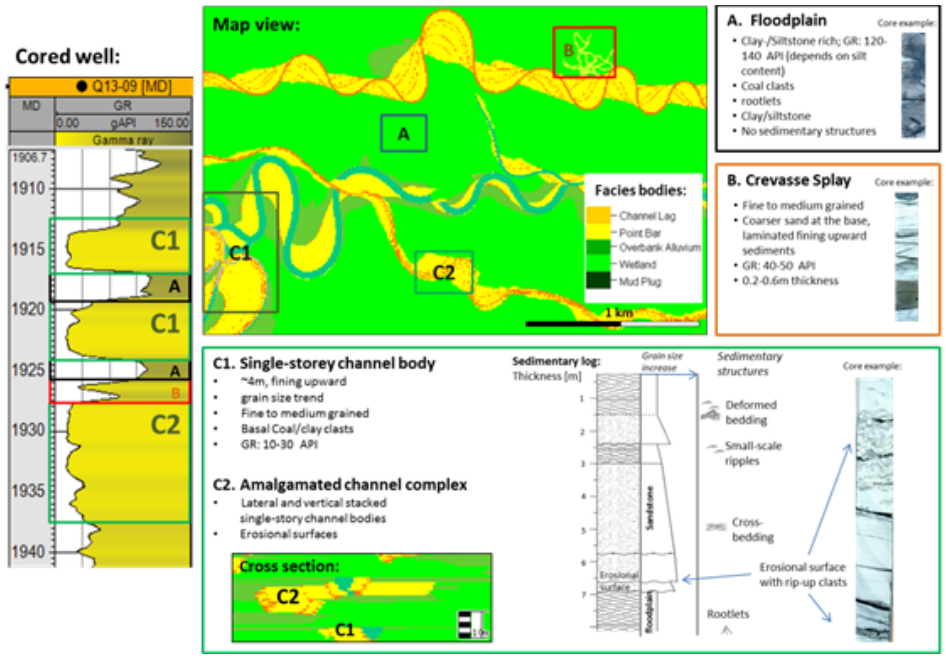

Figure 3.4: GQ13-09 GR log and cored interval on the left. In a map view of a conceptual meandering fluvial system, with the different facies bodies which are encountered in the core. Characteristics of several facies bodies are emphasized.

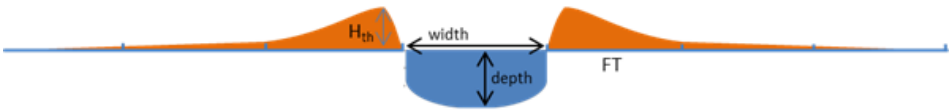

Figure 3.5: Several process-based input parameters related to a river cross section.

3.2.3. Facies realisations

Six types of facies bodies were distributed in the realisations. The set of realisations were divided in two groups. In realisation Group 1, the paleoflow direction was parallel to the long edge and in Group 2, the paleoflow direction was perpendicular to the long edge of the model (Figure 3.6). Our facies realisations have dimensions of 1kmx2kmx50m which relate to a typical area of influence of a HSA geothermal doublet (e.g. Lopez et al., 2010). Grid block size varies from 10 cm near the well bore region to 20mx20mx2.5m at 100 m away from the wells. By utilising this resolution, grid blocks are smaller than the assumed geometries of sandstone bodies

(Zhang and Montgomery, 1994; Loughnane et al., 2014). Synthetic GR logs were made by extraction of a facies column from realisations. GR values were assigned to different facies in these columns: Channel Lag 15, Point-Bar 20, Mud Plug 120, Crevasse splay 50, Overbank alluvium 140. These values were derived from the core analysis (Figure 3.4).

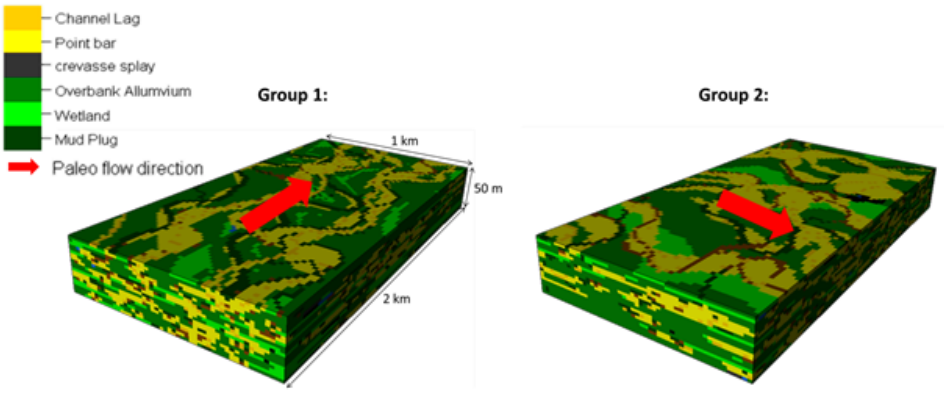

Figure 3.6: paleoflow direction in realisations of Group 1 and in Group 2.

3.2.4. Porosity and permeability modelling

The facies body types that result from the process-based modelling were divided into two classes, reservoir and non-reservoir. The non-reservoir class includes fine grained facies such as crevasse splays, overbank alluvium and mud plugs. Their assumed permeability and porosity are 5 mD and 10%, respectively. Sandy facies bodies such as point-bars and channel lags were all assumed to be reservoir grid blocks. Porosity values were assigned to these blocks based on the core plug porosity data. From this data, a beta distribution correlation function was derived. The distribution characteristics including: mean, standard deviation, skew and kurtosis are equal to 0.28, 0.075, 0.35 and 2.3, respectively. Secondly, the permeability of each grid block was determined by a porosity-permeability relation obtained from petrophysical data of well MKP-11 (TNO, 1977): $k = 0.0633\ e^{29.507\varphi}$, where k is the permeability [mD] and φ is the porosity [-]. Because of this specific porosity distribution, the arithmetic average sandstone permeability is approximately 1000 mD.

3.2.5. Analysis methods

The set of facies realisations were analysed in three ways. First, the clustering of sandstone bodies was evaluated in a connectivity analysis. Secondly, the equivalent permeability in different directions and between the wells was calculated in steady-state, finite-element, isothermal production simulations. For this purpose, a pressure difference was applied to opposite model boundaries parallel, perpendicular and vertical to the paleoflow direction. The resulting average Darcy flow

velocity was calculated and related to equivalent permeability in all three dimensions. Finally, the formation of flow paths between doublet wells was evaluated in a similar way. More than 2000 doublets wells were placed in the facies realisations. Equivalent permeability between doublet wells was compared for parallel and perpendicular doublet layout.

3.2.6. Connectivity analysis

In all realisations, sandstone body clustering was evaluated as a function of N/G. The connectivity (C) was defined such that it is equal to the ratio of the largest sandstone cluster volume and the total sandstone volume (Figure 3.7):

$$C = \frac{V_{\text{sandstone cluster}}}{V_{\text{sandstone total}}} \tag{3.1}$$

In this work, three definitions for connectivity between grid blocks were compared to obtain more information on how sandstone grid blocks are distributed in the realisations. A first option is to consider two blocks as 'connected' only if they have an adjacent face (Figure 3.8A-1). Secondly, two blocks could be connected if they share an edge (Figure 3.8A-2). In this way, not only six but eighteen connections can be formed. Finally, two grid blocks can be considered as connected if they share a corner (Figure 3.8A-3) which results in 26 possible connections. In summary, connectivity was calculated for three connectivity definitions defined as 6-, 18- and 26-point connectivity.

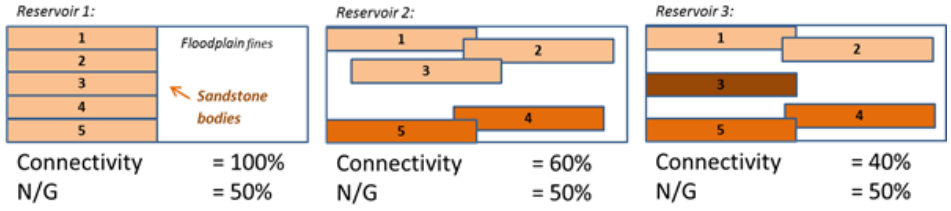

Figure 3.7: Three 2D geobody connectivity examples. The coloured rectangles are schematic sandstone bodies embedded in non-reservoir floodplain fines (in white). Bodies with the same colour are connected.

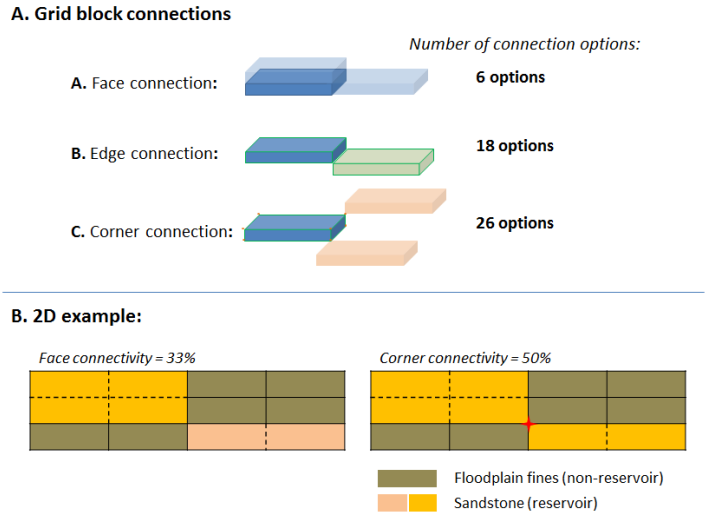

Figure 3.8: (A) Examples of grid block connectivity definitions. (B) 2D example of how these different options affect sandstone connectivity in the same reservoir model.

3.2.7. Equivalent Permeability on realisation scale and in well pairs

In steady-state, finite-element production simulations, a 40 bar pressure difference (ΔP) was consecutively applied in three dimensions between opposite realisation boundaries. To determine the fluid pressure field, the single-phase steady-state continuity equation was solved with constant viscosity (μ) using (3.2).

$$\nabla\left(\frac{k_{\text{facies}}}{\mu}\nabla P\right) = 0 \tag{3.2}$$

In this balance, k_{facies} is the permeability field which is assigned to the grid blocks in each realisation and μ is the water viscosity (0,001 Pa.s). The detailed modelling procedure follows the approach by Saeid et al. (2014, 2015). The Darcy flow velocity (v) can be found as,

$$v = \frac{k_{\text{facies}}}{\mu}\nabla P \tag{3.3}$$

Subsequently, by integrating the fluid flux (q) across the model boundaries on which the pressure difference is applied, the equivalent permeability K can be determined parallel, perpendicular and vertical to the paleoflow direction using (3.4) (e.g. Matthäi and Nick, 2009).

$$K_{\text{equivalent}} = \frac{q\mu L}{\Delta P A} \tag{3.4}$$

where A is the cross-sectional area of the flow and L the distance between the boundaries of the realisation on which the pressure difference is applied. The derived equivalent permeability was related to the N/G of the realisation in the analysis of the results. Finally, equivalent permeability was also determined between doublet well pairs. In all realisations, doublet wells were placed at two spacing distances: 800 and 1000 m. For each spacing distance, three different locations were used in each realisation. Well pairs were always placed parallel to the long edge of the models on the central axis. In total, 2100 simulations were carried out. Large numbers of simulations are required to get statistically meaningful results due to the geological uncertainties associated with random well placement. The simulations yielded a required pressure difference between wells for a 100 m^3/h production rate. This pressure difference was used to determine equivalent permeability between wells using (3.2). Subsequently, the associated pump power [W] was estimated by (3.5),

$$E_{\text{pump}} = \frac{Q\Delta P}{\varepsilon} \tag{3.5}$$

where Q is the flow rate and ε the assumed pump efficiency of 60%. The N/G was the main parameter in our analysis and varied between 10% to 90% in the realisations. The equivalent permeability analysis between the well pairs was calculated for different well placement.

3.3. Results

3.3.1. Facies architecture analysis

In low N/G reservoirs, impermeable floodplain fines separate the sandstone bodies and form extensive flow baffles perpendicular to the paleoflow direction (Fig Figure 3.9A). This is evident from the reservoir example of Figure 3.9A with a N/G value below the connectivity threshold (Larue and Hovadik, 2006). Because of this low N/G value, many isolated single story sandstone bodies occur. At N/G values above the N/G threshold (Figure 3.9B), the sandstone bodies amalgamate, increase in width and form one big cluster with more flow paths. However, still more flow baffles perpendicular to the paleoflow direction can be recognized. Also vertical flow baffles are maintained as indicated by the synthetic GR log. These baffles decrease vertical permeability and permeability perpendicular to the paleoflow direction. The effect of these baffles on connectivity and equivalent permeability is discussed below.

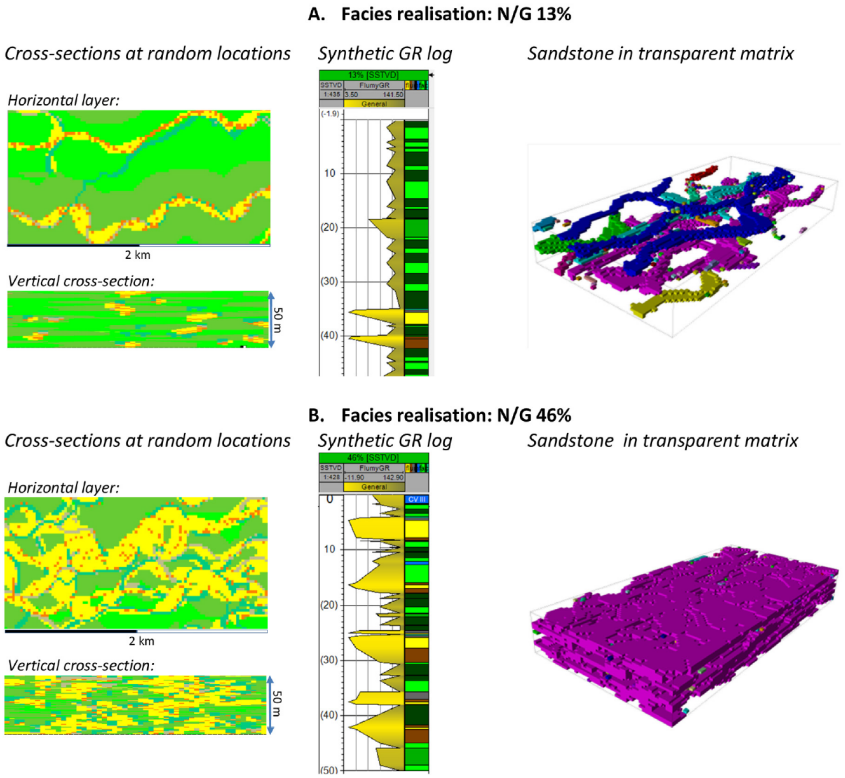

Figure 3.9: (A) Example of a reservoir realisation with 13% N/G, from of Group 1. Facies colours as explained in figure 5. In the 3D reservoir sketch, sandstone bodies have a different colour if they are not connected (B) Examples a reservoir realisation with 46% N/G, from of Group 2. Synthetic GR log are derived from facies column at random location in the realisation.

3.3.2. Connectivity

Results of the connectivity analysis show differences between the three definitions of connectivity (Figure 3.10). For the 18-point connectivity and 26-point connectivity definitions results are similar. 6-point connectivity results in approximately 10% lower connectivity value in the same realisation. The difference between 6-point and 18-point connectivity indicates that grid blocks are often close but do not share a face. This will influence production simulations because flow can only occur through grid block faces. A N/G threshold is recognized at 30% N/G. The use of 18- and 26-point connectivity results in a slight shift of this threshold to approximately 25% N/G.

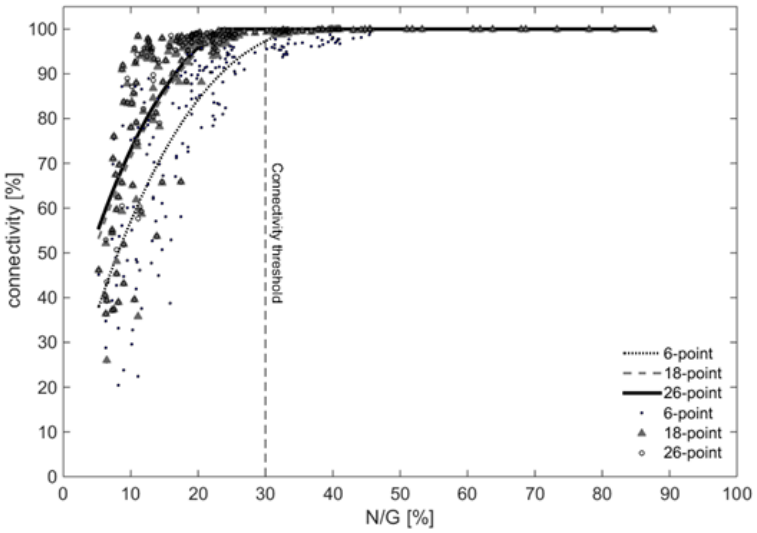

Figure 3.10: Relation of connectivity to N/G for Group 1 realisations.

Below 30% N/G, the connectivity to N/G relation has a large standard deviation (Figure 3.11A). Due to this uncertainty in the connectivity, more realisations are required in the low N/G region to determine a stable average (Figure 3.11B). When the N/G is below 10%, more than 25 realisations are required. In the second N/G range from 12 to 15, the required number of realisations decreases to 15 realisations. Finally, if the N/G is more than 15%, 10 realisations are sufficient.

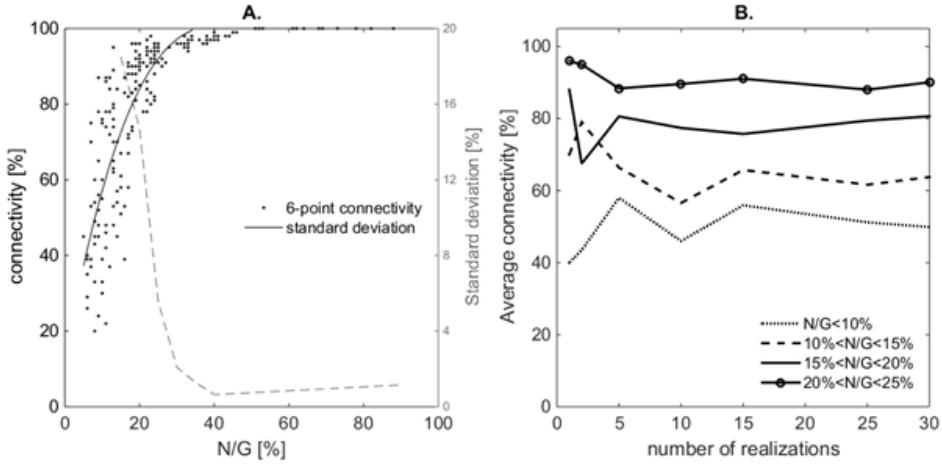

Figure 3.11: Statistical analysis of connectivity in realisation Group 1. (A) Connectivity of Group 1 and its standard deviation as a function of N/G. (B) Average connectivity in 4 N/G bins, with 30 realisations in each bin. The average value is determined with a random pick of an increasing number of realisations per bin. The average is stable when the value no longer depends on the number of realisations.

3.3.3. Equivalent permeability between opposite model boundaries

The relation of equivalent permeability to N/G has a different trend compared to the connectivity analysis (Figure 3.12). Equivalent permeability increases between 5 to 100% N/G to 1000 mD which is the average sandstone permeability. This indicates a dependence of fluid flow behaviour on N/G, also above the connectivity threshold. Below 70% N/G, equivalent permeability is higher in the direction parallel to the paleoflow direction, despite the isotropic properties in each grid block (Figure 3.12). More flow paths are formed parallel to the paleoflow direction compared to perpendicular. This increases the equivalent permeability. The vertical equivalent permeability behaves differently. Below 30% N/G, only very few vertical sandstone grid block connections are formed from top to base in the realisations. Above this N/G value, the vertical equivalent permeability increases but is lower than equivalent permeability in the horizontal directions. The relations of equivalent permeability in the horizontal directions to N/G are in between the harmonic and arithmetic average permeability curves of the realisations. This means that in every realisation connections are formed between the realisation boundaries.

For a more detailed analysis of the anisotropy, the ratio of perpendicular and parallel equivalent permeability (k_{per}/k_{par}) and vertical and parallel (k_{vert}/k_{par}) are determined. These ratios are related to N/G and compared in Figure 3.13. Between 10% and 20% N/G, the equivalent permeability is approximately 40% lower in the direction perpendicular compared to parallel to the paleoflow. This anisotropy decreases towards 70% N/G. Above this threshold, equivalent permeability is equal in both horizontal directions. Vertical permeability increases in this range and is equal to the permeability in horizontal direction at 100% N/G.

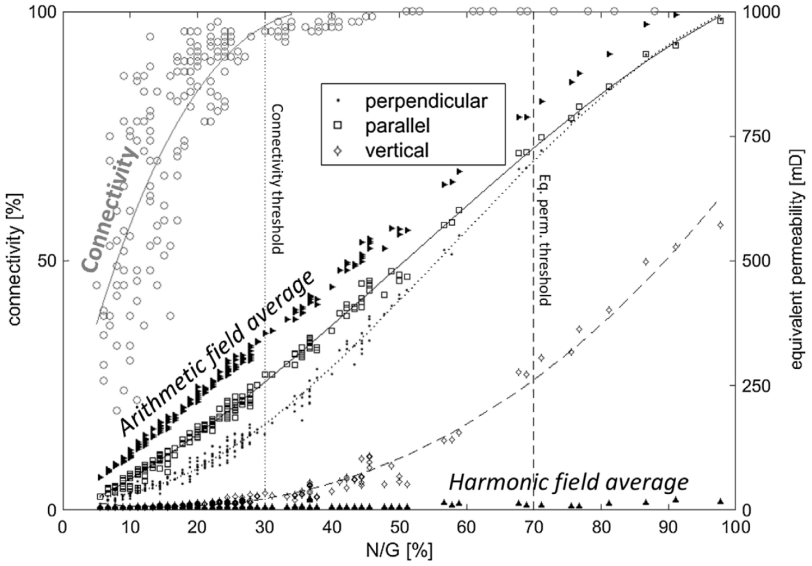

Figure 3.12: Combination of equivalent permeability between opposite model boundaries, connectivity and harmonic and arithmetic average permeability of realisations of Group 1.

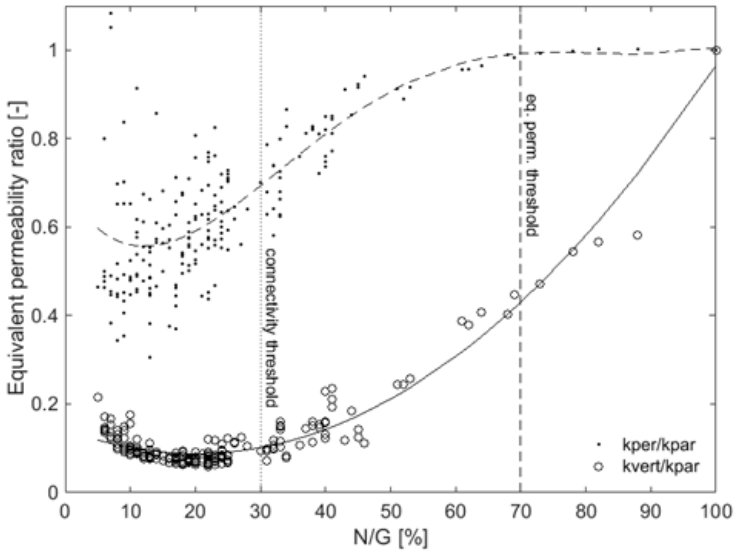

Figure 3.13: Equivalent permeability ratios related to N/G. At the equivalent permeability threshold (70% N/G) perpendicular and parallel equivalent permeability are equal.

To determine whether sufficient realisations are used, equivalent permeability values are grouped in 5% N/G bins. The minimal number of realisations for a stable average is five facies realisations per N/G bin (Figure 3.14), as the average does not change with inceasing realisation numer. The variance in the equivalent permeability to N/G relation is significantly lower than the connectivity to N/G relation (Figure 3.11).

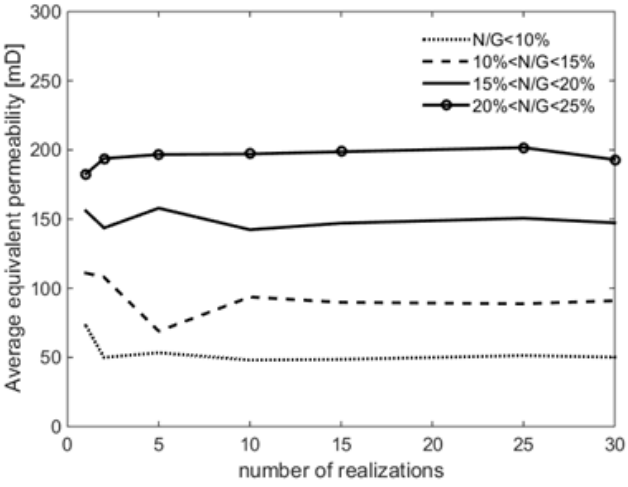

Figure 3.14: Average equivalent permeability in four N/G ranges as a function of number of realisations per range. The average are determined for four N/G bins, with 30 realisations per bin. The average value is determined with a random pick of an increasing number of realisations per bin.

3.3.4. Equivalent permeability between doublet wells

Comparing equivalent permeability calculations between opposite realisation boundaries and between well pairs, three observations can be made. Firstly, equivalent permeability between doublet wells (Figure 3.15A) shows a smaller anisotropy compared to equivalent permeability between realisation boundaries (Figure 3.12). Secondly, the equivalent permeability as a function of N/G is lower. Thirdly, the scatter of the results is larger. These observations result from the random well placement. In our simulations, it is possible that both wells intersect different numbers of sandstone grid blocks or no sandstone grid blocks at all. This would result in unexpected low equivalent permeability, even at high N/G values. When the results are expressed in pump energy losses, the anisotropy is more clearly recognized (Figure 3.15B). Because of the inverse relation between the pressure difference and permeability (3.4), the effect of doublet layout with respect to the paleoflow trend is more clearly expressed in pump energy losses that relate proportionally to pressure (3.5). Nevertheless, our results show that pump losses are approximately 0.1 to 0.2 MW higher with a perpendicular doublet layout for N/G values below 60%. This is approximately 10% of the capacity of a typical WNB doublet.

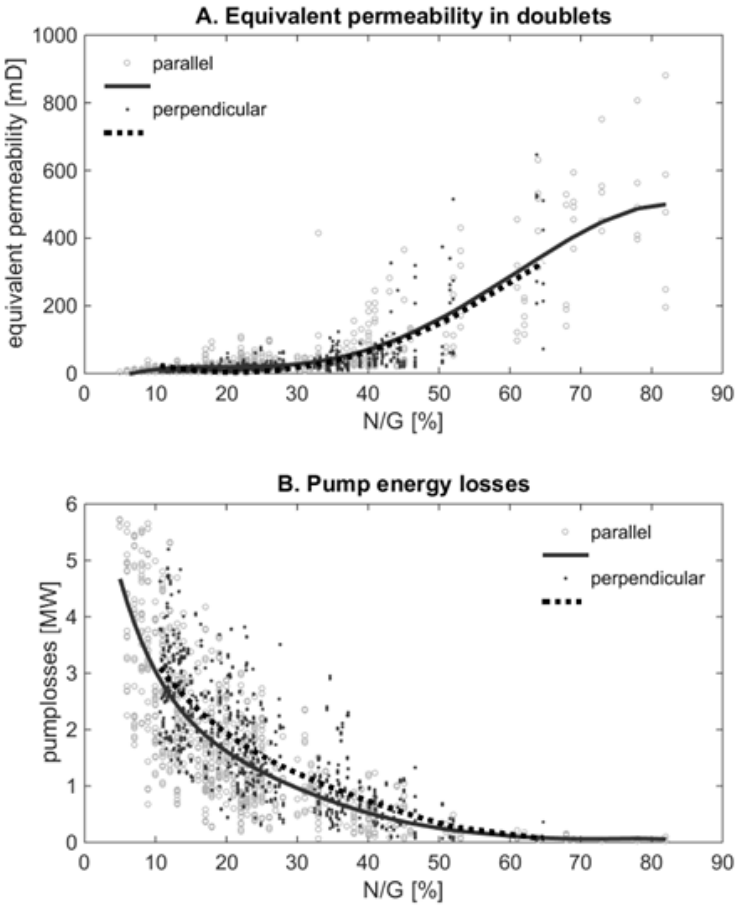

Figure 3.15: (A) Equivalent permeability from the doublet simulations with perpendicular and parallel layout. (B) Pump energy loss estimate based on the same doublet production simulations as in (A).

3.4. Discussion

Connectivity

Our connectivity analysis showed a difference between the use of 6- and 18-point connectivity, especially in lower N/G realisations. It is uncertain to which extend this is a resolution effect. One could imagine that two adjacent grid blocks that connect through an edge are in reality part of a single sandstone body. Higher resolution realisations are required to accurately capture connections in lower N/G reservoirs. In lower N/G reservoirs amalgamation is less frequent and therefore the average surface of connections between sandstone bodies decreases (Bridge, 2006). Smaller objects need higher resolution grid blocks (e.g. Loughnane et al.,

2014). This is however not evaluated in this study. The choice for one of the three connectivity definitions depends on the purpose of the study. If models are generated for production simulations, 6-point connectivity relates more to the simulations because flow only occurs through grid block faces. If the realisations are generated for volumetric analyses, the comparison of the three definitions gives information on how the reservoir grid blocks are distributed. This could be used to evaluate the facies modelling. Despite our process-based facies modelling approach, the connectivity to N/G relation is not significantly different from previous work (e.g. Larue and Hovadik, 2006; Pranter and Sommer, 2011). Therefore, our results do not confirm the expectation of Villamizar et al. (2015) that object-based modelling could result in overestimation of connectivity. The discrepancy between the expectation of Villamizar et al. (2015) and our results could be a consequence of the size of the realisations relative to the size of the individual sandstone bodies. In our 1 km wide models, we describe connectivity of sandstone bodies on a channel belt scale (Donselaar and Overeem, 2008). Villamizar et al. (2015) based their suggestion on studies of Hajek et al. (2010) and Flood and Hampson (2015). These studies recognized autogenic sandstone body clustering in outcrops that are approximately one order of magnitude larger than the channel belt width. Therefore, larger realisations should be used to test this expectation. Connectivity on this larger scale applies to risk assessment of interference between adjacent doublets. Our results apply to connectivity within a single doublet. For evaluation of connectivity on a doublet scale, both facies modelling methods are adequate.

Equivalent Permeability on realisation scale

Comparison of our connectivity and equivalent permeability analyses indicates that the connectivity analysis alone is insufficient to determine doublet layout strategies. This analysis is not able to differentiate the potential of HSA reservoirs with different N/G above the connectivity threshold. However, Crooijmans et al. (2016) showed that also above this threshold, doublet life time depends on N/G. In contrast, the equivalent permeability has an increasing trend over the complete N/G range. This shows that on average an increasing number of flow paths is formed when the N/G increases. Furthermore, the equivalent permeability analysis provides directional information on connectivity. Connectivity is the main factor that influences hydrocarbon recovery (Larue and Hovadik, 2008), for heat recovery however additional analyses are required to assess the potential. To apply the results of our study, three main factors must be taken into account. First, the N/G threshold values and equivalent permeability ratios relate to this specific set of reservoir realisations. They might vary for fluvial reservoirs with different sinuosity, range in paleoflow direction or width to thickness ratio of the sandstone bodies. These are the main parameters that affect connectivity (Larue and Hovadik, 2006). The same workflow but different geological parameters could be applied to assess connectivity anisotropy in other HSA basins. Secondly, the results are affected by simplification of the geological modelling in our study. For example, small-scale internal sandstone body heterogeneities which are smaller than the grid block resolution are neglected. Reservoir properties are assumed isotropic in each grid block. In reality, small-scale sedimentary heterogeneities such as shale drapes, accretion

surfaces and bedding planes decrease the permeability perpendicular to the paleoflow direction (e.g. Pranter et al., 2007). This could be accounted for by utilising anisotropic grid block permeability like in Bierkens and Weerts (1994). Thirdly, sandstone porosity is randomly assigned to sandstone grid blocks. In reality, grain size heterogeneity within sandstone bodies depends on paleoflow speed, and the proximity to the channel axis and river bends. As a result, the permeability distribution is not random across sandstone bodies (Willis and Tang, 2010). These factors could influence the magnitude of the anisotropy and the N/G threshold above which the anisotropy vanishes. Finally, these results indicate large risks associated with horizontal wells in contrast to the results of Hamm and Lopez (2012). The low vertical equivalent permeability in our calculations indicate that flow paths are less likely to be formed between horizontal compared to vertical wells. To compensate, horizontal well length should be large which in turn will significantly increase well costs. This is most likely not an attractive strategy because current HSA exploitation with deviated wells is already marginally economic. The vertical equivalent permeability in our results would be higher if the thickness of the realisations was increased. However, it will always remain lower than equivalent permeability in horizontal directions because of frequent vertical flow baffles that are preserved, also in higher N/G aquifers (Figure 3.10).

Equivalent Permeability between two wells

The anisotropy in equivalent permeability between two wells cannot be clearly recognized compared to equivalent permeability between two opposite model boundaries (Figure 3.12). This is a result of geological uncertainty associated with well placement (Figure 3.15A). If in our simulations a constraint had been used for the well location stating that both wells should intersect the same amount of sandstone, the anisotropy in connectivity would have become more clear. However, we chose unconstraint well placement to evaluate the order of magnitude of pump energy losses as a result of realistic well placement. These losses in our calculations are conservative. In reality doublets with high pump energy losses would not be taken into production without any measures to improve injectivity or productivity. Examples of such measures could be (1) continued drilling into a deeper and higher N/G interval, (2) creation of a side-track or (3) hydraulic stimulation of the well. Moreover, reservoirs with a 10 to 20% N/G are not likely to be exploited at all. No WNB doublets installed so far encounter only reservoir intervals with N/G lower than 30%, especially not with a small total thickness of 50m like in our realisations. The present study focused on the risks associated with perpendicular well layout. However, an advantage of a perpendicular layout could be that longer flow paths are formed which may increase the doublet life time (Hamm and Lopez, 2012). This would allow closer well spacing, reducing well path length and hence drilling costs. Next to reservoir architecture the structural setting is also a doublet layout constraint. For example, fault blocks in the WNB dip perpendicular to the paleoflow direction (Devault and Jeremiah, 2002). Therefore, a consideration in doublet orientation could be to target the deeper and hotter part of the fault block by a production well, and the more shallow part with an injection well to take advantage of the hydrostatic head within the reservoir. The balance between advantages

and disadvantages of these constraints should be analysed in further studies with transient production simulations that provide a basis for net energy optimization. Finally, our results underline the importance of detailed geological modelling. Homogeneous models underestimate the risks related to connectivity. A stochastic approach with detailed modelling of reservoir heterogeneities is required to reduce uncertainties and improve efficiency of HSA doublets.

3.5. Conclusions

On the basis of our calculations with detailed model realisations we can conclude that:

- In fluvial HSA with a N/G below 70%, impermeable facies bodies form significant flow baffles, perpendicular to the paleoflow direction.
- Lower pump energy losses can be expected when a well pair is oriented parallel to the paleoflow direction. This applies to reservoirs with N/G values below 70%.
- Equivalent permeability between doublet wells has a smaller anisotropy compared to equivalent permeability opposite model boundaries.
- The acquisition of geological data and the use of detailed facies architecture realisations are not negligible. Homogeneous realisations could significantly underestimate the geological risks of geothermal doublets. This study provides a workflow for reservoir engineers to determine the optimal doublet layout in HSA.

References

Ainsworth, R. B. (2005). Sequence stratigraphic-based analysis of reservoir connectivity: influence of sealing faults - a case study from a marginal marine depositional setting. *Petroleum Geoscience*, 12(2):127–141.

Bailey, W. R., Manzocchi, T., Walsh, J. J., Keogh, K., Hodgetts, D., Rippon, J., Nell, P. a. R., Flint, S., and Strand, J. a. (2002). The effect of faults on the 3D connectivity of reservoir bodies: a case study from the East Pennine Coalfield, UK. *Petroleum Geoscience*, 8:263–277.

Bierkens, M. F. P. and Weerts, H. J. T. (1994). Block hydraulic conductivity of cross-bedded fluvial sediments. *Water Resources Research*, 30(10):2665–2678.

Boxem, T., van Wees, J., Pluymaekers, M., Beekman, F., Batini, F., Bruhn, D., Calcagno, P., Manzella, A., and Schellschmidt, R. (2011). Thermogis world aquifer viewer-an interactive geothermal aquifer resource assessment web-tool. In *1st EAGE Sustainable Earth Sciences (SES) Conference and Exhibition*.

Bridge, J. (2006). Fluvial facies models: Recent developments. In Posamentier, H. and Walker, R., editors, *Facies Models Revised*, pages 85–170. SEPM Special Publication volume 84.

Cojan, I., Fouche, O., Lopez, S., and Rivoirard, J. (2005). Process-based reservoir modelling in the example of meandering channel. In Leuangthong, O., Deutsch, C., and Clayton, V., editors, *Geostatistics Banff 2004*, pages 611–619. Springer Netherlands, Dordrecht.

Crooijmans, R. A., Willems, C. J. L., Nick, H. M., and Bruhn, D. F. (2016). The influence of facies heterogeneity on the doublet performance in low-enthalpy geothermal sedimentary reservoirs. *Geothermics*, 64:209–219.

de Jager, G., Van Doren, J. F. M., Jansen, J. D., and Luthi, S. M. (2009). An evaluation of relevant geological parameters for predicting the flow behaviour of channelized reservoirs. *Petroleum Geoscience*, 15(4):345–354.

Devault, B. and Jeremiah, J. (2002). Tectonostratigraphy of the Nieuwerkerk Formation (Delfland Subgroup) West Netherlands Basin. *AAPG Bulletin*, 86(10):1679–1707.

Donselaar, M. E. and Overeem, I. (2008). Connectivity of fluvial point-bar deposits: An example from the Miocene Huesca fluvial fan, Ebro Basin, Spain. *AAPG Bulletin*, 92(9):1109–1129.

Flood, Y. S. and Hampson, G. J. (2015). Quantitative analysis of the dimensions and distribution of channelized fluvial sandbodies within a large outcrop dataset: Upper Cretaceous Blackhawk Formation, Wasatch plateau, Central Utah, U.S.A. *Journal of Sedimentary Research*, 85:315–336.

Geel, C. R. and Donselaar, M. E. (2007). Reservoir modelling of heterolithic tidal deposits: Sensitivity analysis of an object-based stochastic model. *Netherlands Journal of Geosciences*, 86(4):403–411.

Grappe, B., Cojan, I., Flipo, N., Rivoirard, J., and Vilmin, L. (2012). Developments in dynamic modelling of meandering fluvial systems. In *AAPG 2012 Annual Convention & Exhibition*, page 1236147.

Hajek, E. A., Heller, P. L., and Sheets, B. A. (2010). Significance of channel-belt clustering in alluvial basins. *Geology*, 38(6):535–538.

Hamm, V. and Lopez, S. (2012). Impact of Fluvial Sedimentary Heterogeneities on Heat Transfer at a Geothermal Doublet Scale. In *Thirty-Seventh Workshop on Geothermal Reservoir Engineering*, Stanford, California.

Henares, S., Bloemsma, M. R., Donselaar, M. E., Mijnlieff, H. F., Redjosentono, A. E., Veldkamp, H. G., and Weltje, G. J. (2014). The role of detrital anhydrite in diagenesis of aeolian sandstones (Upper Rotliegend , The Netherlands): Implications for reservoir-quality prediction. *Sedimentary Geology*, 314:60–74.

Issautier, B., Viseur, S., Audigane, P., and le Nindre, Y. M. (2014). Impacts of fluvial reservoir heterogeneity on connectivity: Implications in estimating geological storage capacity for CO2. *International Journal of Greenhouse Gas Control*, 20:333–349.

Jones, A. and Doyle, J. (1995). Which sub-seismic heterogeneities influence waterflood performance ? A case study of a low net-to-gross fluvial reservoir. In De Haan, H., editor, *New Developments in Improved Oil Recovery*, number 84, pages 5–18. Geological Society Special Publication, Bath, 84 edition.

Karssenberg, D., Törnqvist, T. E., and Bridge, J. S. (2001). Conditioning a process-based model of sedimentary architecture to well data. *Journal of Sedimentary Research*, 71(6):868–879.

Karssenberg, D. E. and Bridge, J. S. (2008). A three-dimensional numerical model of sediment transport , erosion and deposition within a network of channel belts , floodplain and hill slope : extrinsic and intrinsic controls on floodplain dynamics and alluvial architecture. *Sedimentology*, 55:1717–1745.

Keogh, K., Martinius, A., and Osland, R. (2007). The development of fluvial stochastic modelling in the Norwegian oil industry : A historical review , subsurface implementation and future directions. *Sedimentary Geology*, 202:249–268.

King, P. R. (1990). The connectivity and conductivity of overlapping sand bodies. In Buller, A., Berg, E., Hjelmeland, O., Kleppe, J., Torsaeter, O., and Aasen, J. O., editors, *North sea oil and gas reservoirs - II*, pages 353–362. Graham and Trotman, London.

Larue, D. K. and Friedmann, F. (2005). The controversy concerning stratigraphic architecture of channelized reservoirs and recovery by waterflooding. *Petroleum Geoscience*, 11(2):131–146.

Larue, D. K. and Hovadik, J. (2006). Connectivity of channelized reservoirs: a modelling approach. *Petroleum Geoscience*, 12(4):291–308.

Larue, D. K. and Hovadik, J. (2008). Why is reservoir architecture an insignificant uncertainty in many appraisal and development studies of clastic channelized reservoirs? *Journal of Petroleum Geology*, 31(4):337–366.

Lopez, S., Hamm, V., Le Brun, M., Schaper, L., Boissier, F., Cotiche, C., and Giuglaris, E. (2010). 40 years of Dogger aquifer management in Ile-de-France, Paris Basin, France. *Geothermics*, 39(4):339–356.

Loughnane, G., Groeber, M., Uchic, M., Shah, M., Srinivasan, R., and Grandhi, R. (2014). Modeling the effect of voxel resolution on the accuracy of phantom grain ensemble statistics. *Materials Characterization*, 90:136–150.

Matthäi, S. K. and Nick, H. M. (2009). Upscaling two-phase flow in naturally fractured reservoirs. *AAPG Bulletin*, 95(11):1621–1632.

Mottaghy, D., Pechnig, R., and Vogt, C. (2011). The geothermal project Den Haag: 3D numerical models for temperature prediction and reservoir simulation. *Geothermics*, 40:199–210.

Posamentier, H. and Morris, W. (2000). Aspects of the stratal architecture of forced regressive deposits. *Geological Society, London, Special Publications*, 172:19–46.

Pranter, M. J., Ellison, A. I., Cole, R. D., and Patterson, P. E. (2007). Analysis and modeling of intermediate-scale reservoir heterogeneity based on a fluvial point-bar outcrop analog , Williams Fork Formation , Piceance Basin , Colorado. *AAPG Bulletin*, 91(7):1025–1051.

Pranter, M. J. and Sommer, N. K. (2011). Static connectivity of fluvial sandstones in a lower coastal-plain setting: An example from the Upper Cretaceous lower Williams Fork Formation, Piceance Basin, Colorado. *AAPG Bulletin*, 95(6):899–923.

Pujol, M., Ricard, L. P., and Bolton, G. (2015). 20 years of exploitation of the Yarragadee aquifer in the Perth Basin of Western Australia for direct-use of geothermal heat. *Geothermics*, 57(2015):39–55.

Saeid, S., Al-Khoury, R., Nick, H. M., and Barends, F. (2014). Experimental-numerical study of heat flow in deep low-enthalpy geothermal conditions. *Renewable Energy*, 62:716–730.

Saeid, S., Al-Khoury, R., Nick, H. M., and Hicks, M. A. (2015). A prototype design model for deep low-enthalpy hydrothermal systems. *Renewable Energy*, 77:408–422.

Shanley, K. W. and Mccabe, P. J. (1994). Perspectives on the Sequence Stratigraphy of Continental Strata 1. *AAPG Bulletin*, 78(4):544–568.

Törnqvist, T. E. and Bridge, J. S. (2002). Spatial variation of overbank aggradation rate and its influence on avulsion frequency. *Sedimentology*, 49:891–905.

Villamizar, C. a., Hampson, G. J., Flood, Y. S., and Fitch, P. J. R. (2015). Object-based modelling of avulsion-generated sandbody distributions and connectivity in a fluvial reservoir analogue of low to moderate net-to-gross ratio. *Petroleum Geoscience*, 21(4):249–270.

Wees, J. V., Kronimus, A., Putten, M. V., Pluymaekers, M. P. D., Mijnlieff, H., Hooff, P. V., Obdam, A., and Kramers, L. (2012). Geothermal aquifer performance assessment for direct heat production – Methodology and application to Rotliegend aquifers. *Netherlands Journal of Geosciences*, 91(4):651–665.

Welhan, J. A. (2016). Gigawatt-Scale Power Potential of a Magma-Supported Geothermal System in the Fold and Thrust Belt of Southeast Idaho. In *41st Workshop on Geothermal Reservoir Engineering*, Stanford, California.

Willis, B. J. and Tang, H. (2010). Three-Dimensional Connectivity of Point-Bar Deposits. *Journal of Sedimentary Research*, 80(5):440–454.

Zhang, W. and Montgomery, D. R. (1994). Digital elevation model grid size, landscape representation, and hydrologic simulations. *Water Resources Research*, 30(4):1019–1028.

4

The influence of facies heterogeneity on the doublet performance in low-enthalpy geothermal sedimentary aquifers

Abstract
A three-dimensional model is used to study the influence of facies heterogeneity on energy production under different operational conditions of low-enthalpy geothermal doublet systems. Process-based facies modelling is utilised to construct realistic aquifer models honouring geological heterogeneity. A finite element based reservoir simulator is used to model the fluid flow and heat transfer over time. A series of simulations is carried out to examine the effects of aquifer heterogeneity on the life time and the energy recovery rate for different discharge rates and the production temperature (T_{min}) above which the doublet is working. With respect to the results, we propose a design model to estimate the life time and energy recovery rate of the geothermal doublet. The life time is estimated as a function of net sandstone volume, T_{min} and discharge rate, while the design model for the energy recovery rate is only a function of net sandstone volume and T_{min}. Both life time and recovery show a positive relation with an increasing net sandstone volume. Further our results suggest that neglecting geological heterogeneity may lead to significant errors in predicting the life time of low-enthalpy geothermal systems for aquifers with a net sandstone volume below 70%.

This chapter is based on: Crooijmans, R.A., Willems, C.J.L., Nick, H.M., Bruhn, D.F., *The influence of facies heterogeneity on the doublet performance in low-enthalpy geothermal sedimentary reservoirs*. Geothermics **64**, 209-219, (2016).

4.1. Introduction

In the geothermal sector, connectivity and facies heterogeneity are not commonly considered in doublet life time and energy recovery predictions. Simplified geological representations are commonly used such as homogeneous models (Saeid et al., 2014) or layer cake models (e.g. Poulsen et al., 2015; Mottaghy et al., 2011; Deo et al., 2014). The study described in chapter 3 as well as hydrocarbon related studies, however, show that geological parameters such as facies heterogeneity and connectivity also have a major impact on the fluid flow patterns (e.g. Donselaar and Overeem, 2008; Willis and Tang, 2010) and the recovery (e.g. Larue and Friedmann, 2005; Larue and Hovadik, 2006, 2008). This is because these parameters have an impact on the net aquifer volume and flow path formation between the wells. In addition, claystone bodies may form flow baffles or barriers that increase flow path length or reduce net aquifer volume, respectively (chapter 3). The net sandstone volume (N/G) and sandstone body geometry control the connectivity in the aquifer (Larue and Hovadik, 2006). The connectivity is defined as the ratio of the volume of the largest connected sandstone body cluster over the sum of the volume of all sandstone bodies (Hovadik and Larue, 2007; Larue and Hovadik, 2006, chapter 3).The lessons learnt in the hydrocarbon sector provide some insight into the importance of the use of detailed aquifer representations in a geothermal system. These lessons however cannot be applied directly to geothermal studies because oil is only extracted from the pore volume, while the heat extracted from geothermal aquifers is obtained from the fluid in the pores and from the rock matrix. The previous chapter of this thesis provided insight into the impact of facies heterogeneity on flow path formation between doublet well pairs. This chapter describes an evaluation of the impact of facies heterogeneity on doublet life time and energy recovery. For this purpose, 48 detailed facies realisations are selected from the set of realisations that were generated in the study described in chapter 3. The use of these process-based facies realisations ensured realistic representations of sedimentary aquifers. The realisations ranged in N/G from 10 to 100%. A finite element method (FEM) is utilized to simulate the fluid flow and heat transfer processes in geothermal doublets. In the first part of this chapter the modelling approach is explained for both the generation of aquifer realisations and the non-isothermal simulations. Next the relation between N/G and the doublet performance parameters (life time and recovery) is discussed, followed by the effect of the discharge rate. Then, the results are combined to obtain a so-called 'design model', which estimates the life time of a doublet systems and the energy recovery. In the end the difference between randomly generated realisations and the aquifer realisations is assessed to highlight the relevance of the facies based aquifer realisation in low-enthalpy geothermal aquifer modelling.

4.2. Methodology

4.2.1. Aquifer Models

Three types of aquifer models were used in this study. Model Type I and II were made utilising a process-based facies modelling (chapter 3). Model Type III realisations were made using a random facies field generator. The difference between Type I and II is the way in which properties were assigned to the sandstone grid blocks within the sandstone bodies. In Type I porosity and permeability were heterogeneously distributed within the sandstone bodies whereas in the Model Type II single average porosity and permeability values were assigned for the sandstone grid blocks in the realisations. The realisations were then employed for conducting dynamic simulations (Figure 4.1). The heat transfer in the aquifer and temperature at the production well were calculated over time by using the software package COMSOL Multiphysics utilising a finite element method. In the base case (initial) scenario the discharge was 100 m^3/h, the initial aquifer temperature was 75°C and for the base case scenario the production stops when the production temperature dropped to 74°C (Minimal production temperature, T_{min}). The decline in the production temperature was related to the arrival time of the cold water front. Flow and heat transfer simulations were conducted employing all the generated aquifer realisations for several scenarios with different discharge rates (80, 100, 120 and 140 m^3/h). Consequently, the life time values and total heat recovery were calculated for different minimal production temperatures (74, 72, 70 and 68°C).

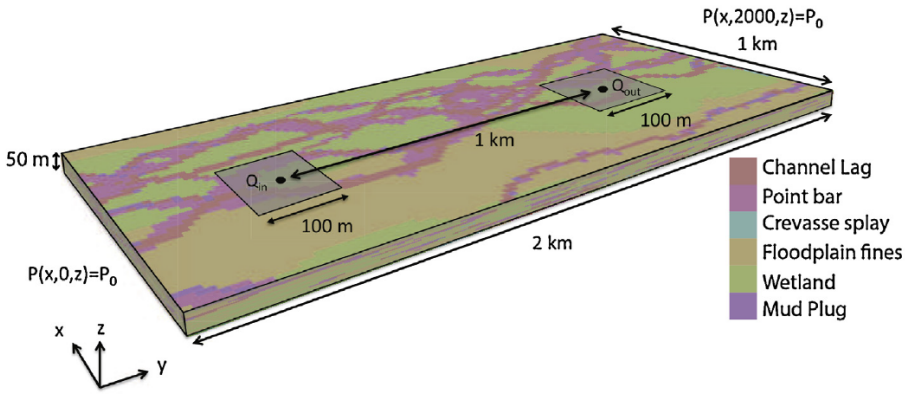

Figure 4.1: Schematic of the model domain and the well locations.

4.2.2. Aquifer model type I, II and III

Process-based facies modelling software Flumy (Grappe et al., 2012) was utilised to generate detailed facies realisations of a 1 km × 2 km × 50 m geothermal aquifer with a resolution of 20 m × 20 m × 2.5 m. For the study described in this chapter, 48 realisations were selected from the total set of realisations that was generated for the study of chapter 3. In this chapter, the paleoflow direction in all realisations

was parallel to the long edge of the aquifer boundary (Figure 4.1). The choice of orienting the paleoflow direction parallel to the long-edge increased the connectivity in the aquifer realisations compared to a paleoflow perpendicular to the long edge (chapter 3). The N/G in the realisations ranged from 10 to 100%. The generation of facies realisations is described in more detail in (section 3.2.3). The process-based facies realisations contained seven types of geobodies; pointbars, sand plugs, channel lag, crevasse splays, levees, overbank floodplain fines and mud plugs. The aquifer models were simplified by dividing the 7 types of geobodies into two groups; sand (channel lag, point bar, sand plug) and shale (crevasse splay, levee, overbank alluvium, mud plug). The sand group was considered as aquifer and the shale group as non-aquifer and the groups were used to calculate the N/G of the realisations. Further, to study the relevance of process-based facies modelling on the estimation of the life time and energy production of the doublets, geo-model realisations (model Type III) were generated with the sandstone and shale grid blocks randomly (uncorrelated) distributed. Model Type III realisations had the same N/G range.

4.2.3. Aquifer property modelling

A beta distribution correlation function was used to generate a heterogeneous porosity field within the sand group of the Type I realisations. This distribution was obtained from petrophysical data of well MKP-11 (TNO, 1977). The distribution characteristics including: mean, standard deviation, skew and kurtosis were equal to 0.28, 0.075, 0.35 and 2.3, respectively. The associated permeability of this group was derived from a porosity-permeability relationship based on the same petrophysical data:

$$k = 0.0633\epsilon^{29.507\phi} \tag{4.1}$$

where k is the permeability [mD] and ϕ is the porosity [–]. The effect of heterogeneity in the thermal rock properties on heat transfer in the geothermal aquifer was insignificant compared to the heterogeneity in the flow properties (Mottaghy et al., 2011). Therefore the thermal rock properties were considered homogeneous and isotropic. The porosity and permeability of the shale group were also assumed to be homogeneous and isotropic (table 4.1). To determine the effect of the heterogeneous porosity of the aquifer bodies, some of the aquifer realisations were rebuilt with a homogeneous sand group and named as model Type II. In this group of realisations the porosity and permeability of the sand group was equal to the averaged porosity and permeability of the sand group in the aquifer realisations of model Type I. The size and distribution of the aquifer bodies were kept the same. The aquifer bodies have a constant porosity of 28% and constant permeability of 1000 mD. All other parameters were kept constant as in the model Type I. The differences in life time and production between a processed-based facies aquifer model (Type I) and a random realisation (Type III) were a measure of the importance of process-based models used in geothermal aquifer simulations.

Parameter	Description	Value	Dimension
α_L	Longitudinal dispersion coefficient	6.5	m
α_T	Transversal dispersion coefficient	2.2	m
k_L	Permeability of the shale bodies	5	mD
λ_L	Conductivity of the pore fluid	0.7	W/m/K
λ_{sand}	Conductivity of the sandstone bodies	2.7	W/m/K
λ_{shale}	Conductivity of shale bodies	2.0	W/m/K
ρ_{sand}	Density of the sandstone bodies	2650	kg/m^3
ρ_{shale}	Density of the shale bodies	2600	kg/m^3
ϕ_{sand}	Average porosity of the sandstone bodies	0.28	-
ϕ_{shale}	Average porosity of the shale bodies	0.1	-
C_f	Specific heat of the pore fluid	4200	J/kg/K
C_{sand}	Specific heat of the sandstone bodies	730	J/kg/K
C_{shale}	Specific heat of the shale bodies	950	J/kg/K
L	well spacing	1000	m
P_0	Initial pressure	200	bar
S	Salinity of the pore fluid	3	ppm/10^6
T_0	Initial temperature	348	K
T_{inj}	Injection temperature	348	K

Table 4.1: List of parameters used in the dynamic model.

4.2.4. Flow and heat transfer model

The generated aquifer realisations (Type I, II and III) were employed for heat transfer and fluid flow modelling. Figure 4.1 illustrates the aquifer and the well locations (well spacing is 1 km). The injection and the production wells had the same discharge rate which remains constant over time. The two outer boundaries at the short edge were assigned a constant pressure, the others were no flow boundaries (Figure 4.1). The N/G at the well positions, in all dynamic models, had to be roughly the same as the N/G of the field, especially for aquifer realisations with low N/G. In some of the aquifer realisations the well may not have been in contact with any sandstone body increasing the well pressure and changing the flow patterns within the realisation. In this work, the maximum allowable difference between N/G at the wells and the aquifer realisation was 2.5%. To achieve this, the doublet wells were placed within a range of 50 m in the x and y direction from the original well locations (Figure 4.1). The orientation of the doublet and the distance between the wells were kept constant in all simulations.

4.2.5. Governing equations

Heat transfer in geothermal systems was described by two main processes: conduction and convection. For a system with a rigid rock, incompressible fluids and local thermal equilibrium between rock and fluid the heat transfer equation reads:

$$\frac{\partial}{\partial t}(\rho C T) = \nabla \cdot (\boldsymbol{\lambda} \nabla T) - \nabla \cdot (\rho_f C_f \mathbf{u} T) + \rho_f C_f q T^* \tag{4.2}$$

where t is time [s], T the temperature [K], λ the total conductivity tensor [W/(kgK)],ρ_f the fluid density [kg/m^3], C_f the fluid specific heat capacity [J/mK], $\boldsymbol{u}$ Darcy velocity vector [m/s], and ρC is the volumetric heat capacity, q is external sinks and sources [1/s], and T^* refers to the temperature at sources. Darcy ve-

locity was calculated as: $\boldsymbol{u} = -(k/\mu)\nabla P$. Where μ is the dynamic viscosity [Pa s] and P is the fluid pressure [Pa]. The fluid pressure field was obtained by solving the continuity equation: $\phi\, \partial\rho_f / \partial t + \nabla \cdot (\rho_f \mathbf{u}) = \rho_f q$. The total thermal conductivity was expressed as: $\lambda = \lambda_{eq}\boldsymbol{I} + \lambda_{dis}$. Where λ_{eq} is the equivalent conductivity of the fluid an the matrix and the λ_{dis} the thermal dispersion tensor. This equivalent conductivity and the volumetric heat capacity were both volume averaged:

$$\begin{aligned} \lambda_{eq} &= (1-\phi)\lambda_s + \phi\lambda_f \\ \rho C &= (1-\phi)\rho_s C_s + \phi\rho_f C_f \end{aligned} \tag{4.3}$$

where the suffixes *s* and *f* stand for solid (shale, sand) and fluid (brine), respectively. Thermal dispersion had influence on the total conductivity. Thermal dispersion was described as a function of the fluid velocity and fluid heat properties. The thermal dispersion tensor which is based on the solute dispersion model (Scheidegger, 1961), reads:

$$\boldsymbol{\lambda} = (\lambda_{eq} + (\alpha_T)|\mathbf{u}|)\mathbf{I} + \rho_f C_f(\alpha_L - \alpha_T)\frac{\mathbf{uu}}{|\mathbf{u}|} \tag{4.4}$$

$|\mathbf{u}|$ was the magnitude of the Darcy velocity vector and α_L and α_T were the thermal dispersion coefficients in the longitudinal and transversal direction, respectively. The brine pore fluid had a constant specific heat capacity, heat conductivity and salinity (Table 4.1. The viscosity of the brine varied with temperature (*T*) and its salinity (*S*) [ppm] (Batzle, 1992):

$$\mu = 0.1 + 0.333S + (1.65 + 91.9S^3)\epsilon^{-[0.42(S^{0.8} - 0.17)^2 + 0.045]T^{0.8}} \tag{4.5}$$

The density of the brine was depended on the temperature, the pressure and the salinity:

$$\rho_f = \rho_w + S(0.668 + 0.44S + 10^{-6}[300P - 2400PS + T(80 + 3T - 3300S^3P + 47PS)] \tag{4.6}$$

where

$$\begin{aligned} \rho_w = 1 + 10^{-6}(&-80T - 3.3T^2 + 0.00175T^3 + 489P - 2TP + \\ &0.016T^2P - 1.3x10^{-5}T^3P - 0.333P^2 - 0.002TP^2) \end{aligned} \tag{4.7}$$

For equation 4.5- 4.7, *T* was in [°C] and *P* in [MPa] (Batzle, 1992). The model domain was discretised by 3D tetrahedral and hexahedral finite elements. In general, discretization errors were the dominant sources of numerical errors in simulations (Matthäi and Nick, 2009). To minimise the discretisation error a maximum finite element mesh size of 20 m × 20 m × 2.5 m was chosen. The minimum finite element mesh size was 0.5 m. The maximum mesh size was the same as the resolution of the realisations. This avoided the necessity of porosity and permeability upscaling (averaging properties due to grid coarsening) of aquifer realisations. Saeid et al. (2015) analysed the discretisation error for a similar dynamic model and found that the chosen mesh size results in a negligible discretisation error for the fluid and heat transfer simulations for the range of studied parameters. In this study, the relative and absolute error tolerances for flow and heat transport simulations were set to 10^{-5} and 10^{-6} respectively.

4.2.6. Life time

The water temperature calculated at the production well was used to obtain the life time of the doublet. The life time of the doublet was determined at the time when the production fluid temperature dropped below the minimal production temperature. The temperature losses in the surface facilities and the wells were neglected. Saeid et al. (2015) illustrated that the temperature losses in the wells have negligible effect on the temperature of the production fluid of a geothermal system.

4.2.7. Recovery and net energy production

The calculated production temperature over time were used to obtain recovery, $R = E_{prod}/E_{Total}$. Where *R* is the recovery of the field [%], E_{prod} the cumulative produced energy [J] and E_{total} the total available energy [J]. The cumulative produced energy was defined as:

$$E_{\text{prod}} = \sum_{i=1}^{n} Q_i \Delta t_i \rho_f C_f (T_{\text{prod,i}} - T_{\text{inj}}), \tag{4.8}$$

and the total available energy as:

$$E_{\text{total}} = \sum_{j=1}^{m} V_j \phi_j \rho_{\text{f,j}} C_{\text{f,j}} (T_0 - T_{\text{inj}}) + V_j (1 - \phi_j) \rho_{\text{s,j}} C_{\text{s,j}} (T_0 - T_{\text{inj}}) \tag{4.9}$$

where t is the time step increment, the subscript *i* the time step, *n* total number of time steps, *Q* the discharge [m_3/s], $T_{prod,i}$, and T_{inj} the temperature [K] of the production fluid and the injection fluid at step *i*, respectively.*m* is the total number of finite elements, V_j the volume of the mesh element *j* and T_0 is the initial temperature [K].The energy production was the produced energy minus the pump energy

that was required to induce a pressure difference between the injection and the production well: $E_{net} = E_{prod} - E_{pump}$. Where E_{pump} was the required pump energy, assuming the efficiency of the pumps was equal to 1:

$$E_{\text{pump}} = \sum_{i=1}^{n} Q\Delta t_i (P_{\text{inj}} - P_{\text{prod}}) \tag{4.10}$$

4.3. Results

4.3.1. Base Case

When applying the base case conditions for the dynamic simulation of different realisations of model Type I the following features were observed: (i) the N/G has noticeable impact on the life time of the doublet especially for low N/G values (Figure 4.2A); (ii) decreasing N/G results in decreasing the life time, which is more pronounced for realisations with N/G smaller than 40%; and (iii) the cumulative energy production shows the same results as the recovery (Figure 4.2A), but the recovery increases slightly faster at N/G values larger than 60%. Since the differences between recovery and the cumulative energy production are negligible only the obtained recovery is discussed in this study. The recovery shows a similar relation with N/G as the life time (Figure 4.2B). Note that 40% N/G is the point where the connectivity starts to decrease with lower N/G values

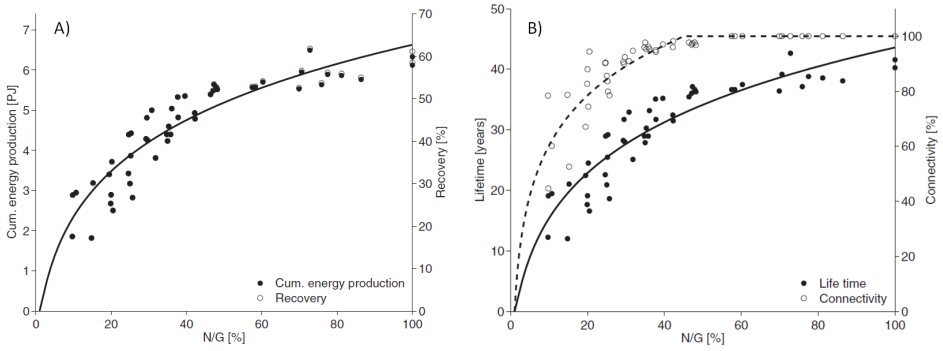

Figure 4.2: (A)Life time of the doublet for Q = 100 m^3/h and T_{min} = 74 °C and connectivity versus N/G, for model Type I realisations. (B) Total energy production and recovery versus N/G for Q = 100 m^3/h and T_{min} = 74 °C and connectivity versus N/G, for model Type I realisations.

The variation in the temperature breakthrough curves obtained at the well production for aquifer realisations (Type I) with similar N/G values increase significantly with a decreasing N/G. For a N/G of around 50% the breakthrough temperatures are almost identical (Figure 4.3C). At a N/G of around 30% the time at which the temperature starts to drop and the gradient at which it drops start to differ among the realisations (Figure 4.3B). The differences are even larger at a N/G around

10% (Figure 4.3A). The variations can also be seen in the required pump energy (Figure 4.4). Higher required pump energy to have the same discharge implies that the sandstone bodies at the injection well are not well connected to the sandstone bodies at the production well. As a result the net energy produced is less scattered than the required pump energy at very low N/G. The difference in the temperature breakthrough curves originates from the difference in the corresponding medium configurations. Aquifer realisations with a N/G of 10% in Figure 4.3A illustrate that the location and geometry of the sandstone bodies determine which part of the aquifer has a high permeability zone. These geometries differ per realisation. Some sandstone bodies go straight, while others are curved and/or split in two, which also results in isolated sandstone bodies in different locations in the domain. When the N/G increases this effect becomes less. At a N/G around 30% there are still some continuous shale bodies separating the sands (Figure 4.3B). The shales form low permeable zones functioning as flow barriers. For realisations around 50% N/G, the sandstone bodies are all connected to each other and cover the whole area, which makes the realisations look more alike (Figure 4.3C).

4.3.2. Impact of discharge and minimal production temperature

As expected, with increased discharge rates, the life time of the doublet decreases (Figure 4.5A). Similarly, with increased discharge, the variance in life time among realisations (Type I) is reduced (Figure 4.5B). This is related to the fast decrease in life time for aquifers with a large N/G. When the discharge rate goes from 60 to 100 m^3/h, the life time decreases with approximately 20 years for Type I realisations with a N/G of 100%, while at a N/G of 10% life time decreases with approximately 10 years. At high discharge rates (Q > 200 m^3/h) an increase in the discharge has rather negligible effect on the life time, while at low discharge rates (Q = 60 m^3/h) small changes have a large impact on the life time, 10 years difference compared with Q = 80 m^3 /h (Figure 4.5B). A decrease in the minimal production temperature results in a longer life time and higher recovery (Figure 4.6). Because the production temperature reduces by only 2 to 5 degree per decade (Figure 4.3), the life time and recovery can be significantly increased if the minimal production temperature is reduced.

4.3.3. Homogeneous versus heterogeneous aquifer bodies

The aquifer realisations with homogeneous sandstone bodies (Type II) have a slightly higher life time, 1.6 years on average with a maximum of 4.2 years, than that of model Type I realisations with heterogeneous sandstone bodies (Figure 4.7). The overestimation falls mostly within the uncertainty level of the calculated life times, which is related to the aquifer heterogeneity.

4.3.4. Random realisations versus aquifer realisations

Utilising the random realisations (Type III) with N/G higher than 70% results in life time values comparable to those calculated for the model Type I realisations (Figure 4.8A). Utilising model Type III realisations in the dynamic model results in

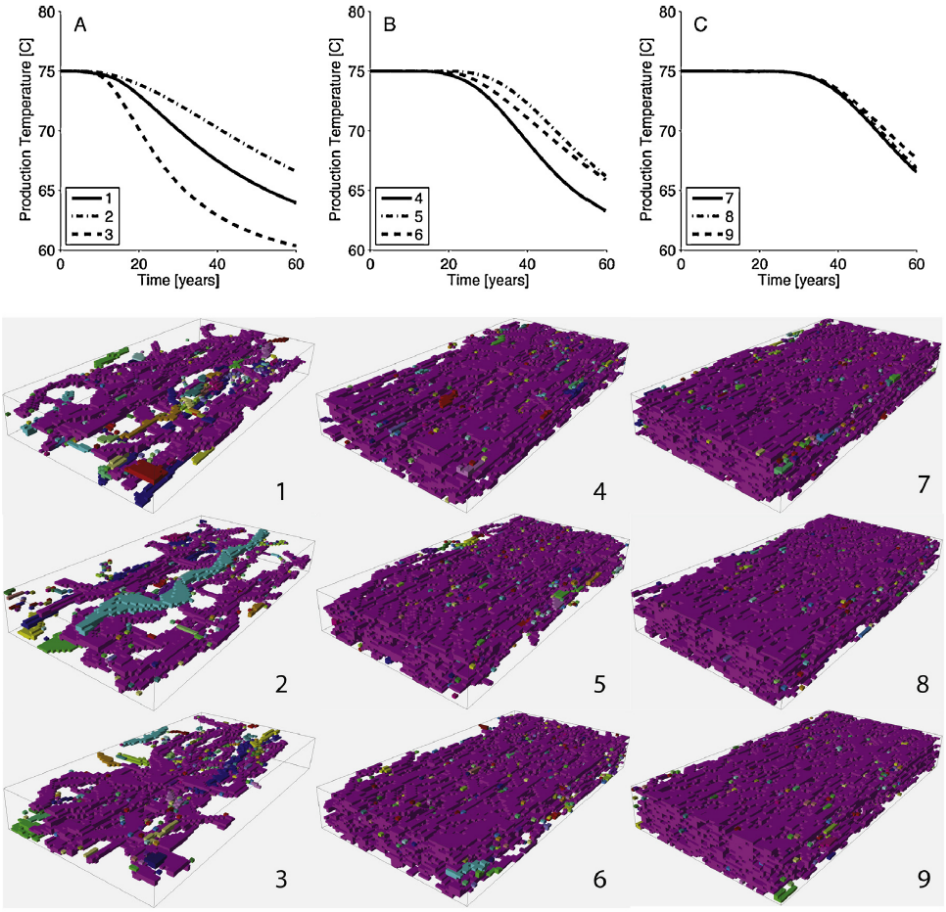

Figure 4.3: Production temperature development for Q = 100 m^3/h, corresponding to different Type I realisations (1–9). Claystone gridblocks are transparent, and connected sandstone bodies have the same colour.

an overestimation of the life time for N/G values between 70% and 40%, where the life time is almost stable. Below 40% N/G the life time starts to drop in case of Type III realisations, but less than that of the Type I realisations. It is found that the connectivity values of the aquifer for Type III realisations drops drastically and reaches zero for Type III realisations with N/G less than 30%, while the Type I realisations have a minimum connectivity of 42% (Figure 4.8B). This means that the random realisations (Type III) have sandstone bodies at the wells which are small and isolated. These realisations do not have a high permeable zone between the wells. And with respect to the boundary conditions, fixed discharge, the pressure difference between the injector and producer increases significantly. The models with the random realisations (Type III) result in a much lower variance in life time for aquifers with the same N/G value when they are compared to the life time values

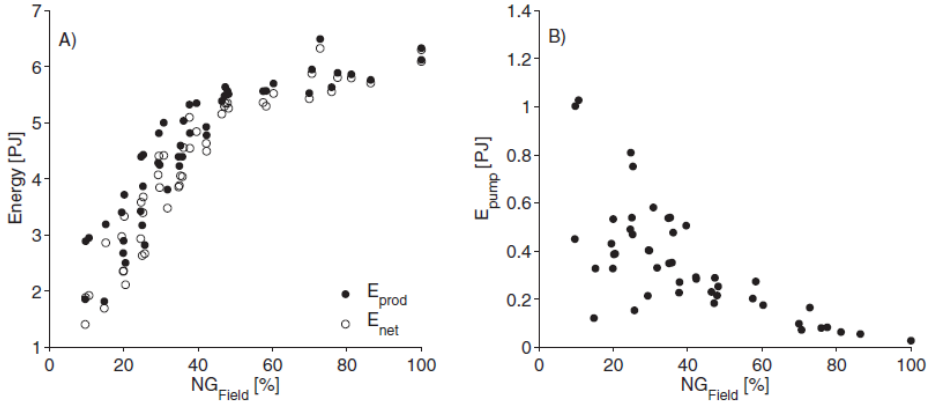

Figure 4.4: (A) The produced energy and the net produced energy versus N/G. (B) Pump energy required to create the pressure difference at the wells versus N/G (4.10)).

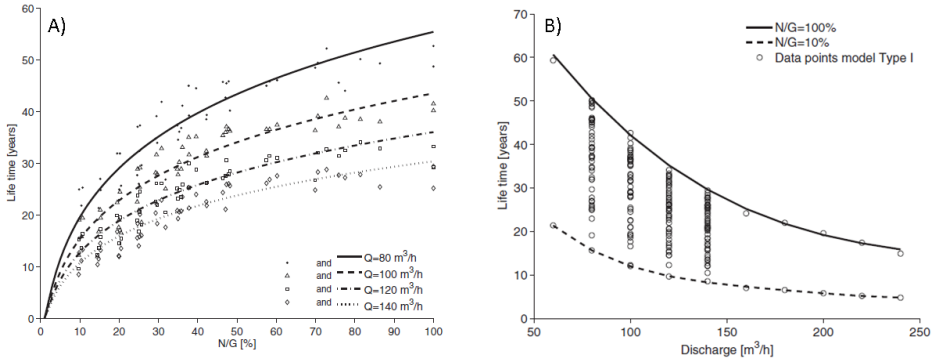

Figure 4.5: (A) Life time versus N/G for different discharge rates (T_{min} = 74 °C). (B) The variance in obtained life time values for N/G at different discharge rates and T_{min} = 74 °C.

obtained for the model Type I realisations (Figure 4.8A).

4.3.5. A Life Time and Recovery design model

In the relations of life time and N/G for various production rates (Figure 4.9) two regions can be recognized. Region 1 has a N/G range from 10 to 45% and Region 2 from 45 to 100% N/G. In Region 1 life time increases logarithmically with increasing N/G. In Region 2 life time increases linearly with N/G.

The design model for life time and recovery are described as equation 4.11 and 4.12:

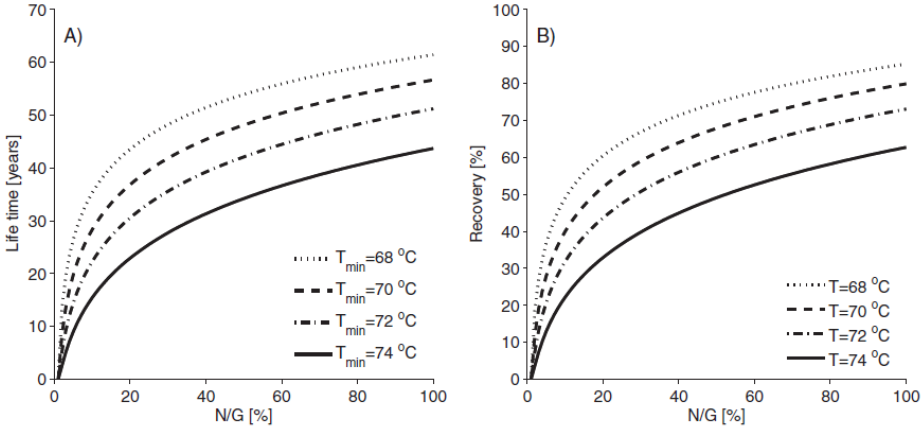

Figure 4.6: (A)The life time and (B) recovery versus N/G of model Type I realisations with a minimal production temperature of 68, 70, 72 and 74 °C for Q = 100 m^3/h.

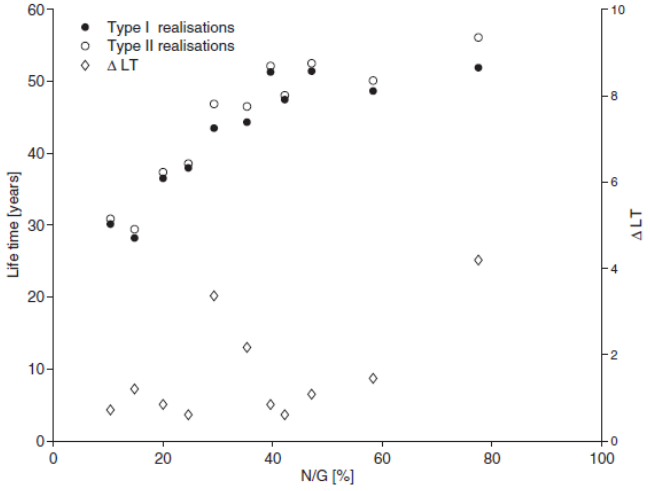

Figure 4.7: Life time versus N/G for aquifer realisations with heterogeneous (Type I) and homogeneous (Type II) sandstone bodies including the difference in life time between them(Δ LT) with Q = 100 m^3/h and T_{min} = 74 °C.

$$LT = \begin{cases} \frac{390+56.9\Delta T}{Q}(ln(N/G))^{1.5} & \text{for } 15 < N/G \leq 45 \\ \frac{390+56.9\Delta T}{Q}(ln(45))^{1.5} + \frac{18.7-2.84\Delta T}{Q}(N/G - 45) & \text{for } 45 < N/G < 100 \end{cases} \quad (4.11)$$

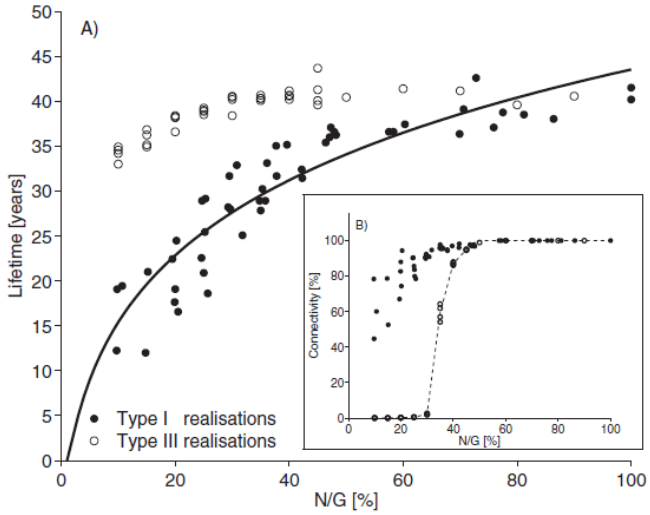

Figure 4.8: Life time versus the N/G of random realisation (Type III) and geological realisation (Type I) with Q = 100 m^3/h and T_{min} = 74 °C.

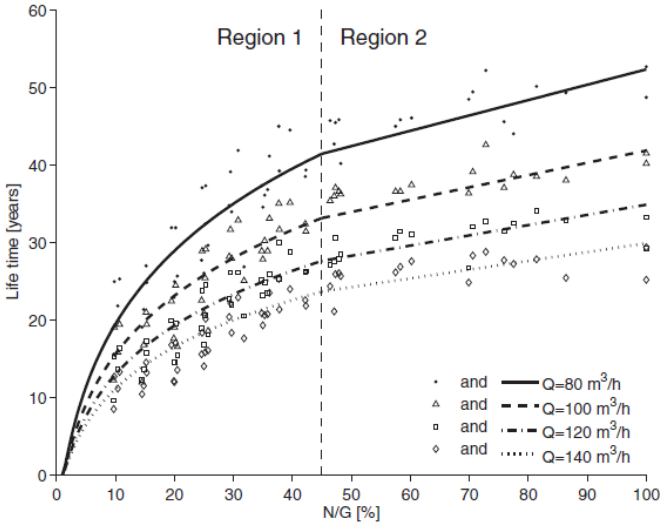

Figure 4.9: Life time versus N/G for different discharges based subdivided into two regions for the design model.

$$R = \begin{cases} (0.75\Delta T + 5.67)(ln(N/G))^{1.5} & \text{for } 15 < N/G \leq 45 \\ (0.75\Delta T + 5.67)(ln(45))^{1.5} + (0.28 - 0.035\Delta)(N/G - 45) & \text{for } 45 < N/G < 100 \end{cases} \quad (4.12)$$

These empirical relations describe the life time as a function of N/G, Q and ΔT, and the recovery as a function of only N/G and ΔT. In Region 1 the geological parameter N/G is the main controlling factor on both life time and recovery. The human controlled parameter Q (discharge rate) is the most influential factor in Region 2 on life time, while the human controlled parameter ΔT is the most influential factor on the recovery. The model is only tested for discharge rates between 80 and 140 m^3/h and minimal production temperature values down to 68°C. More research is required to check if the model is valid for lower minimal production temperatures and higher discharges. This is because below 65°C the production temperature curve is no longer linear (Figure 4.3), which indicates that the effect of ΔT on the life time is non-linear. The predicted life time values are not exactly the same as those obtained from the production simulations (Figure 4.10). This is partly a result of the variance in life time of aquifer models with similar N/G values (Figure 4.8). The effect is found to be the same for the recovery. This figure indicates that the design model works best for N/G from 15 to 100%, but underestimates the life time of aquifers with a N/G around 10% (Figure 4.10).

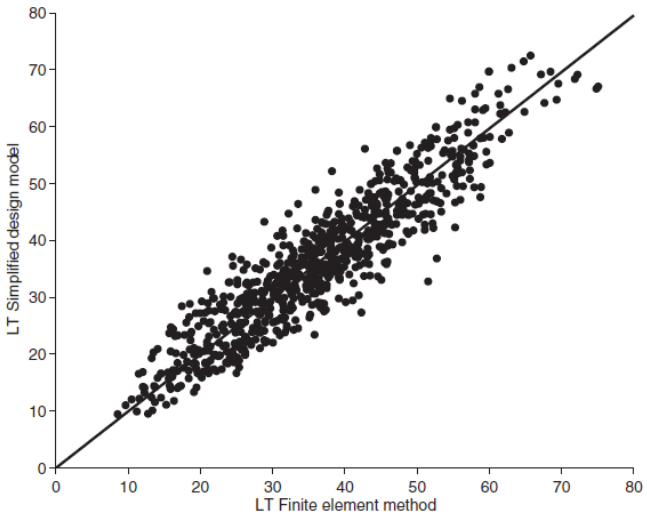

Figure 4.10: Life time obtained with the dynamic model versus the life time obtained with the design model (R^2 = 0.92). The data points of all heat transfer and flow simulations of Type I are used.

4.4. Discussion

Base case - model type I

The effect of N/G on life time and recovery can be described with natural logarithmic relations for N/G values below 45% and with linear relations for N/G values above 45%. In Region 1 the connectivity has a larger variance, precluding accurate prediction of the life time and recovery. The variance in connectivity increases

with decreasing N/G. This could partly be an effect of the chosen resolution of the aquifer realisations (Type I), which result in less accurate connectivity calculations for a N/G below 20%. Hovadik and Larue (2007) showed that increasing the geomodel resolution decreases variance for connectivity and improves connectivity. This in combination with the effect of the facies distribution explains why it is harder to predict doublet performances of low N/G aquifers; more variables play a role. For the linear part the relations are more accurate. The connectivity is 100% for all realisations and has therefore negligible effect on the results. The higher variance in life time for low N/G aquifers indicates that the accuracy of the aquifer model is crucial, which is for high N/G aquifers with lower variances less important, albeit not negligible. The energy recovery shows the same effect as in the oil recovery; once the connectivity starts to drop the recovery drops fast Larue and Hovadik (2008). The absolute values of the recoveries from oil and geothermal energy cannot be compared directly, because the recoveries are defined in a different way. In the oil industry the total amount of oil available is only in the pore of the sandstone bodies, while the total amount of available heat is in the connected pores and the matrix of both the sandstone and non-sandstone bodies. This means the oil can only be produced from the sandstone part, while heat can be produced from the surrounding low permeable layers by conduction. Nonetheless, the heat recoveries obtained in this study have a range from 15 to 65% (Figure 4.2A), which is similar to the oil recoveries reported by Larue and Hovadik (2008). The differences between obtained energy recoveries for realisations with 50 and 100% N/G are small, which indicates that the shales play an important role in geothermal doublet performance for aquifers with N/G lower than 50%. As a result, aquifers with a N/G of roughly 50% are almost as efficient as those with 100% N/G. Notice that the heat capacity and conductivity are similar for sandstone and shale, which makes the differences in heat conduction small.

Discharge

Discharge affects the life time and recovery, but the difference in recovery between a discharge of 80 and 140 m^3/h is small compared to the variance in recovery for production simulations with similar N/G (Figure 4.2A). This means the discharge rate can be adjusted to the yearly energy demand, without influencing the cumulative produced energy significantly during the life time of the doublet. The pressure in the injection well increases with increasing discharge or when the well is only in contact with small isolated sandstone bodies. This pressure cannot be higher than the rock strength, otherwise the aquifer will be fractured. Fractures in the aquifers would change the fluid flow behaviour significantly (e.g. Matthäi and Nick, 2009; Nick et al., 2011) and the stated relations would not be applicable.

Minimal production temperature

Lower minimal production temperatures extend the life time and recovery. When the produced temperature declines the daily energy produced declines as well, because the discharge is constant.If a constant daily energy production is preferred the discharge has to increase to compensate for the produced water with lower

temperatures. This will decrease the life time of the project and speed up the cooling of the production temperature. This loop will accelerate the whole process and the differences in life time will be less than shown in Figure 4.6A. The variance in the obtained life time and recovery increases for decreasing minimal production temperatures (Figure 4.3). This is related to the dispersion effect. The result of this effect is most noticeable after the cold water front has reached the production well. The temperature of the produced water drops more slowly for a system with higher thermal dispersion. This uncertainty in temperature drop makes it harder to predict the life time and recovery for lower minimal production temperatures.

Homogeneous sandstone bodies – model Type II

Aquifer realisations with homogeneous property distribution within the sandstone bodies may overestimate the life time up to 4 years compared to aquifer realisations (Type I) with heterogeneous sandtone properties, but in most cases the overestimation is less than 1 year. The difference in life time between homogeneous and heterogeneous sands is within their uncertainty bounds. Therefore the intra sandstone body heterogeneity could be disregarded for the life time calculation.

Random realisations –model Type III

The simulations with the random realisation result in unrealistic required (well) pressure values and in much higher life times compared to aquifer realisations (Type I) when N/G values are below 70%. These unrealistic pressure values are related to the fixed discharge rate and the shape and connectivity of the sandstone bodies. In the random realisations, hardly any flow paths through only sandstone grid blocks are formed between the wells. As a result very high injection well pressure values are needed to push the water through the shale in between the sands in order to achieve the required discharge rate. A realistic geological model is therefore necessary for N/G values below 40%. Above 40% N/G the connectivity has a smaller impact on life time and recovery, as it is always larger than 95% and well pairs are placed only parallel to the paleoflow direction (e.g., chapter 3. The life time values obtained with the random realisations are overestimated for a N/G between 40 and 60%. For N/G values above 70%, the life time obtained by the random realisations is comparable with the ones obtained with aquifer realisations. Nevertheless, in the random realisations the difference between maximum and minimum possible life times is maximum 5 years, while the results of the aquifer realisation show that the difference can be significantly larger (±10 years), which seems to be the case even for aquifers up to 70% N/G (Figure 4.8A). Therefore production simulations should be employed to calculate the risks of an early cold water breakthrough, especially before drilling. Even though it is hard to make very accurate production simulations before drilling, simulation results will provide a valuable range of expected life times. This means that the geology has a major impact on life time and is as important as the human controlled parameter 'discharge' when estimating the life time of a low-enthalpy geothermal doublet. When layer cake models are used to calculate the life time one major assumption is that the aquifer consits for 100% of permeable sandstone. The comparison of the random realisations with aquifer realisations shows that it is important to know the connectivity of the sandstone

bodies between the injection and production well, not only for the life time, but for well pressure too. This means that if the injector is poorly connected to the producer, higher pressures are needed to keep up the discharge. This pressure varies the most for realisation below 45% N/G, which is the region where the connectivity varies (Figure 4.2A). The pressure increases are probably less noticeable when layer cake models are used.

Design model

The life time and recovery models are only directly applicable for aquifers with roughly the same heat transfer and flow characteristics, well spacing and aquifer thickness as used in this study. The models assume that all aquifers have the same type of non-linear relation, but the fitting parameters are formation specific. Despite the limitations, model can be used for primary calculations for estimating life time and recovery. It must be kept in mind, however, that the results underestimate reality for the lower range of N/G between 35 and 50% and overestimate it for a N/G above 90% (Figure 4.2A). The accuracy of the models is reduced because of the variance in life time and recovery. This variance is especially high. When N/G is below 15%, the models are less accurate because of large variance combined with an underestimation of life time. This is, however, no problem for the targets for low-enthalpy geothermal aquifers in the Netherlands, since the Nieuwerkerk Formation has a N/G between 20 and 50% (Den Hartog Jager, 1996). When applying the model to this Formation the calculated life time can still be between 21 years (N/G = 20%) and 31 years (N/G = 31%) for Q equal to 100 m^3/h and ΔT equal to 1 °C. Inclusion of N/G values measured in nearby fields in the study area can help narrowing this range of N/G and improving the life time prediction. Nevertheless this implies that accurate field data and aquifer realisations are necessary for accurate prediction of the doublets life time and recovery.

4.5. Conclusions

The work combines a process-based model with a flow and heat transfer model. The process-based model is capable of generating aquifer models (Type I and II) utilising core data. We show that the life time can be estimated with the design model for both Region 1 (N/G < 45%) and Region 2 (45%< N/G < 100%) . We have demonstrated that the difference in life time within Region 2 is relatively small and the main controlling factor is the discharge. In Region 1 the dependence of life time on N/G is larger than in Region 2. Therefore small over and underestimation in N/G have a large impact on life time predictions in Region 1. The shale has a positive contribution to the heat transfer in the system, which increases the potential of lower N/G aquifers. When using a geological model with randomly distributed facies, first the life times are overestimated, especially for aquifers in Region 1. Next, the variance in life time for aquifers with the same N/G is less than 5 years for model Type III aquifers, while it is 10 years when process-based facies modelling (Type I) is used. This means a realistic representation of the facies heterogeneity is needed to make more reliable predictions of the life time of a low-enthalpy geothermal doublet.

References

Batzle, M. (1992). Seismic properties of pore fluids. *Geophysics*, 57(11):1396–1408.

Deo, M., Roehner, R., Allis, R., and Moore, J. (2014). Modeling of geothermal energy production from stratigraphic reservoirs in the Great Basin. *Geothermics*, 51:38–45.

Donselaar, M. E. and Overeem, I. (2008). Connectivity of fluvial point-bar deposits: An example from the Miocene Huesca fluvial fan, Ebro Basin, Spain. *AAPG Bulletin*, 92(9):1109–1129.

Grappe, B., Cojan, I., Flipo, N., Rivoirard, J., and Vilmin, L. (2012). Developments in dynamic modelling of meandering fluvial systems. In *AAPG 2012 Annual Convention & Exhibition*, page 1236147.

Hovadik, J. M. and Larue, D. K. (2007). Static characterizations of reservoirs: refining the concepts of connectivity and continuity. *Petroleum Geoscience*, 13:195–211.

Larue, D. K. and Friedmann, F. (2005). The controversy concerning stratigraphic architecture of channelized reservoirs and recovery by waterflooding. *Petroleum Geoscience*, 11(2):131–146.

Larue, D. K. and Hovadik, J. (2006). Connectivity of channelized reservoirs: a modelling approach. *Petroleum Geoscience*, 12(4):291–308.

Larue, D. K. and Hovadik, J. (2008). Why is reservoir architecture an insignificant uncertainty in many appraisal and development studies of clastic channelized reservoirs? *Journal of Petroleum Geology*, 31(4):337–366.

Matthäi, S. K. and Nick, H. M. (2009). Upscaling two-phase flow in naturally fractured reservoirs. *AAPG Bulletin*, 95(11):1621–1632.

Mottaghy, D., Pechnig, R., and Vogt, C. (2011). The geothermal project Den Haag: 3D numerical models for temperature prediction and reservoir simulation. *Geothermics*, 40:199–210.

Nick, H. M., Paluszny, A., Blunt, M. J., and Matthai, S. K. (2011). Role of geomechanically grown fractures on dispersive transport in heterogeneous geological formations. *Physical Review E - Statistical, Nonlinear, and Soft Matter Physics*, 84(5).

Poulsen, S. E., Balling, N., and Nielsen, S. B. (2015). A parametric study of the thermal recharge of low enthalpy geothermal reservoirs. *Geothermics*, 53:464–478.

Saeid, S., Al-Khoury, R., Nick, H. M., and Barends, F. (2014). Experimental-numerical study of heat flow in deep low-enthalpy geothermal conditions. *Renewable Energy*, 62:716–730.

Saeid, S., Al-Khoury, R., Nick, H. M., and Hicks, M. A. (2015). A prototype design model for deep low-enthalpy hydrothermal systems. *Renewable Energy*, 77:408–422.

Scheidegger, A. E. (1961). General Theory of Dispersion in Porous Media. *Journal of Geophysical Research*, 66(10):3273–3278.

TNO (1977). Nl olie- en gasportaal. www.nlog.nl.

Willis, B. J. and Tang, H. (2010). Three-Dimensional Connectivity of Point-Bar Deposits. *Journal of Sedimentary Research*, 80(5):440–454.

5

The impact of reduction of doublet well spacing on the Net Present Value and the life time of fluvial Hot Sedimentary Aquifer doublets

Abstract
This paper evaluates the impact of reduction of doublet well spacing, below the current West Netherlands Basin standard of 1000 to 1500 m, on the Net Present Value (NPV) and the life time of fluvial Hot Sedimentary Aquifer (HSA) doublets. First, a sensitivity analysis is used to show the possible advantage of such reduction on the NPV. The parameter value ranges are derived from West Netherlands Basin HSA doublet examples. The results indicate that a reduction of well spacing from 1400 to 1000 m could already influence NPV by up to 15%. This effect would be larger in more marginally economic HSA doublets compared to the West Netherlands Basin base case scenario. The possibility to reduce well spacing is supported by finite element production simulations, utilising detailed facies architecture models. Furthermore, our results underline the necessity of detailed facies architecture models to assess the potential and risks of HSA doublets. This factor significantly affects doublet life time and net energy production of the doublet.

This chapter is based on: Willems, C.J.L., Nick, H.M., Goense,T., Bruhn, D.F., *The impact of reduction of doublet well spacing on the Net Present Value and the life time of fluvial Hot Sedimentary Aquifer doublets*. Geothermics, **68**, 54-66.

5.1. Introduction

Large potential resources of heat are stored in sedimentary rocks. In the Netherlands alone, the Dutch geological survey estimated the total recoverable heat from this type of resource to be approximately 85,000 PJ (Kramers et al., 2012). Unfortunately, expansion of HSA exploitation is slow, and a large gap currently exists between HSA potential and exploitation (section 1.2). This is a result of a combination of high initial investment costs and large uncertainties in both doublet life time and energy recovery (e.g., chapter 4). Because of these uncertainties, often large well spacing distances are used, ranging from 1000 to 1500 m, to avoid early cold water breakthrough (Mijnlieff and Wees, 2009; Lopez et al., 2010; Mottaghy et al., 2011; Daniilidis and Herber, 2016). Overdesign, however, could lead to unnecessarily long thermal breakthrough time. For example, no thermal breakthrough has yet been reported in the past 40 years of exploitation in the Paris Basin (e.g. Lopez et al., 2010). A reduction of the current well spacing standard could still result in sufficient life time, while improving the financial situation of a doublet in two ways. First, it may reduce the drilling costs by reducing the overall well length, as two wells have to be drilled deviated from the same platform. Secondly, smaller spacing could also reduce the required pump energy due to shorter flow paths between the wells. Another advantage is the decrease of chance on geological flow baffles between the wells, such as sealed sub-seismic faults (e.g. Bailey et al., 2002) or claystone bodies (Larue and Hovadik, 2006; Pranter and Sommer, 2011, chapter 3). Finally, it could increase the possible number of doublets that can be realised in the same area, as suggested by Mijnlieff and Wees (2009). The number of studies on optimisation of geothermal doublet design is limited. These studies often focus on extending life time and maximising energy production (e.g. Sauty et al., 1980; Chandrasiri Ekneligoda and Min, 2014; Adams, 2015). Therefore, in this chapter both the possible financial advantage of well spacing reduction and its impact on doublet life time are evaluated. In the first part, the effect of a variation in well spacing on the Net Present Value (NPV) for a typical WNB doublet is determined. This is derived from a sensitivity analysis in which both production and financial parameters are varied. Parameter ranges are derived from a West Netherlands Basin case study. The analysis is based on finite-element production simulations in homogeneous aquifer models. We evaluate the effect of well spacing reduction on the Net Present Value (NPV) of a HSA doublet. Also, we discuss the effect such a reduction would have on the life time of a doublet. In a second part, the impact of fluvial aquifer architecture on doublet life time is evaluated. For this purpose detailed fluvial facies architecture realisations are used. This is required, because the spatial distribution of permeable and impermeable facies bodies in the aquifer could significantly affect doublet life time and capacity (e.g. Pranter et al., 2007; Hamm and Lopez, 2012; Poulsen et al., 2015; Crooijmans et al., 2016). Homogeneous aquifer models do not capture this uncertainty. Like in chapter 3 and 4, detailed fluvial facies architecture realisations are generated utilising a process-based facies modelling approach (Cojan et al., 2005; Grappe et al., 2012; Hamm and Lopez, 2012) based on a WNB geological dataset. Minimum well spacing is analysed in terms of life time and NPV. The results of this study could be used as an incentive for

re-evaluation of HSA well spacing standards. Utilising detailed facies architecture models, more profound estimates of doublet life time and capacity can be made. This should prevent overdesign and thereby improve the competitiveness of HSA exploitation.

5.2. Data and aquifer modelling

5.2.1. Data

The aquifer models that were used for the study described in this chapter were based on a geological dataset of the fluvial Lower Cretaceous Nieuwerkerk Formation in the West Netherlands Basin (Devault and Jeremiah, 2002; Jeremiah et al., 2010; Donselaar et al., 2015), presented in chapters 2 and 3 of this thesis. The dataset comprises Gamma-Ray (GR) logs of geothermal and hydrocarbon wells and cores of hydrocarbon wells in the WNB. This dataset was used to derive a realistic range of heterogeneities to constraint the set of facies realisations. The core study provided thickness ranges of facies bodies which were used as input for the facies modelling. Based on analogue studies, assumptions are made on the associated width of these bodies (e.g. Williams, 1986; Törnqvist and Bridge, 2002; Gibling, 2006). The GR logs provided a range of N/G of the geothermal aquifers.

5.2.2. Aquifer modelling

Two types of aquifer models were used in this study: (1) detailed facies architecture realisations and (2) homogeneous models. The first type of models were generated with a process-based approach. For the study in this chapter, a selection of 15 realisations was made from the set of realisations that were used in chapter 4. The dimensions of these realisations were 1km x 2km x 50m, the paleoflow direction was parallel to the long edge and the N/G ranged from 15 to 70% N/G. In the process-based realisations, sedimentary processes distribute and shape different facies bodies such as channel lags, point-bars, crevasse splays, mud plugs and floodplain fines. The same aquifer property modelling approach was used as described in chapter 3. Facies grid blocks in the realisations were divided into two classes, aquifer and non-aquifer. The non-aquifer class included fine grained facies such as crevasse splays, overbank alluvium and mud plugs. These bodies were all assumed to be relatively impermeable. Their assumed permeability was 5 mD and porosity 10%. Sandy facies bodies such as point-bars and channel lags were all assumed to be aquifer grid blocks. Porosity values were assigned to these blocks based on the core plug porosity data. From this data, a beta distribution correlation function was derived. The distribution characteristics including: mean, standard deviation, skew and kurtosis were equal to 0.28, 0.075, 0.35 and 2.3, respectively. Secondly, the permeability of each grid block was determined by a porosity-permeability relation obtained from petrophysical data of well MKP-11 (TNO, 1977): $k = 0.0633\, e^{29.5\,\phi}$. In this equation, k is the permeability [mD] and ϕ is the porosity [-]. For the NPV sensitivity analysis, homogeneous aquifer models were created based on the same geological dataset. These models had an average porosity of 28% and permeability between 250 and 2000 mD . This permeability range was derived from WNB HSA

well tests (Lingen, 2014) and core plug measurements (TNO, 1977). The thickness of the homogeneous models in the sensitivity analysis varied between 50 and 120 m.

5.3. Numerical production simulations

The numerical modelling procedure follows the approach as explained in chapter 4. Differently in this chapter, the aquifer was confined between two 50 m thick impermeable over- and underburden layers that provide thermal recharge. The energy balance was solved for a rigid medium fully saturated with water, in which thermal equilibrium was assumed between the fluid and solid phases:

$$\rho C \frac{\partial}{\partial t} T + \rho_{\mathrm{w}} C_{\mathrm{w}} \nabla \cdot (\mathbf{q} T) - \nabla \cdot (\lambda \mathbf{I} \nabla T) = 0 \tag{5.1}$$

In this balance, t (s) is time, T [K] is the temperature, ρ is the mass density [kg/m^3), C_w [J/kgK] is the specific heat capacity, λ [W/mK] is the thermal conductivity, I the identity matrix, and $\boldsymbol{q}$ [m/s] is the Darcy velocity vector. The suffix w refers to the pore fluid and s to the solid matrix. The heat capacity, density and conductivity values for aquifer grid blocks are 730 J/kgK, 2650 kg/m^3 and 2.7 W/mK respectively. For the non-aquifer blocks these values are 950 J/kgK, 2600 kg/m^3 and 2.0 W/mK. The thermal conductivity and the volumetric heat capacity are described in terms of a local volume average. Heat conductivity, density and heat capacity are assumed to be independent of temperature for simplicity and described by: $\lambda = (1-\phi)\lambda_s + \phi\lambda_w$ and: $\rho C = (1-\phi)\rho C_s + \phi\rho_w C_w$, in which ϕ is the porosity. This Darcy flow velocity vector can be determined by: $q = (k\nabla P)/\mu$, where is k [m^2] the intrinsic permeability, μ the temperature and salinity dependent viscosity explained in chapter 4, and P [Pa] the pressure. The pressure field is obtained through solving the continuity equation: $\phi(\partial \rho_w)/\partial t + \nabla\cdot(\rho_w q) = \rho_w S$, where S [1/s] is external sinks and sources. The production simulations yield a production temperature development over time and the required injection and production pressure for the defined production rate. The difference between these pressures for each time step i (ΔP_i) was used to estimate pump energy losses ($E_{pump,i}$) as indicated in equation 5.2 (e.g Willems et al., 2017), where Q is the production rate and ε the pump efficiency. The produced energy ($E_{prod,i}$) was estimated by equation 5.3 on each time step i (e.g Willems et al., 2017) in which ρ_w is the water density of 1050 kg/m^3 and ΔT_i the difference between injection and production temperature on each time step i. The net energy production, or the doublet capacity was determined by the sum of the produced power and the pump power losses.

$$E_{\mathrm{pump,i}} = \frac{Q \Delta P_i}{\epsilon} \tag{5.2}$$

$$E_{\mathrm{prod,i}} = Q \rho_{\mathrm{w}} C_{\mathrm{w}} \Delta T_i \tag{5.3}$$

5.4. Net Present Value model

A NPV model developed by Van Wees et al. (2010) was utilized to relate production simulations to NPV. Input for the NPV calculations were net energy production in Watt and the economic parameters listed in Table 5.1. In our study, additional separator costs were included, because in many WNB doublets natural gas co-production occurs. The NPV is the depreciated, discounted, net-cumulative income after 15 years. This period was chosen, because it is the maximum duration of the Dutch feed-in tariff scheme (SDE+) for geothermal energy (Van Heekeren and Bakema, 2013, 2015). 0.25 M€ pump work-over costs were taken into account every five years, which is equal to half of the estimated pump costs. 40% down-time was assumed for maintenance throughout the year.

Base case economic parameters		
Heat price	6	€/GJ
Electricity price for operations	22.22	€/GJ
Discount rate	7	%
CAPEX		%
Well costs	1.5	M€/ km
Pump	0.5	M€
Separator	0.1	M€
Contigency costs (10%)	0.89	M€
SEI (insurance)	0.69	M€
OPEX	5	% of CAPEX/year
Tax	25.5	% of taxable income
Depreciation period	10	years
Feed-in tariff (SDE+)		
Base energy price (2015)	0.052	€/kWh
correction price (2015)	0.019	€/kWh
contribution SDE+	9.17	€/GJ

Table 5.1: Base case economic parameters for the NPV realisation based on Van Wees et al. (2010)

Because doublet wells are drilled from one surface location, doublet well spacing influences the well length (Figure 5.1). In this study, the length of a single well (*WL*) was approximated by the sum of a vertical (D_{vert}) and a deviated section (D_{dev}), $WL=D_{vert}+D_{dev}$. The vertical section was assumed to be 1500 m. The length of the deviated section, was approximated by:

$$D_{\text{dev}} = \sqrt{(TVD - D_{\text{vert}})^2 + (\frac{1}{2})^2} \tag{5.4}$$

In equation 5.4, *TVD* is True Vertical Depth which is 2.2 km and *L* is the doublet well spacing. Using this equation, a reduction of the well spacing from 1000 m to 800 m could result in a reduction of the total well length by 2% and drilling costs could reduce accordingly. As drilling costs of a 2.2 km deep doublet are approximately 7.2 M€ (Van Wees et al., 2010; Nielson and Garg, 2016), a reduction in spacing from 1000 to 800 m could lead to up to 0.14 M€lower investment. A reduction from the 1500 m standard to 800 m would decrease the total well length by approximately 9% and the associated well costs by approximately 0.65 M€.

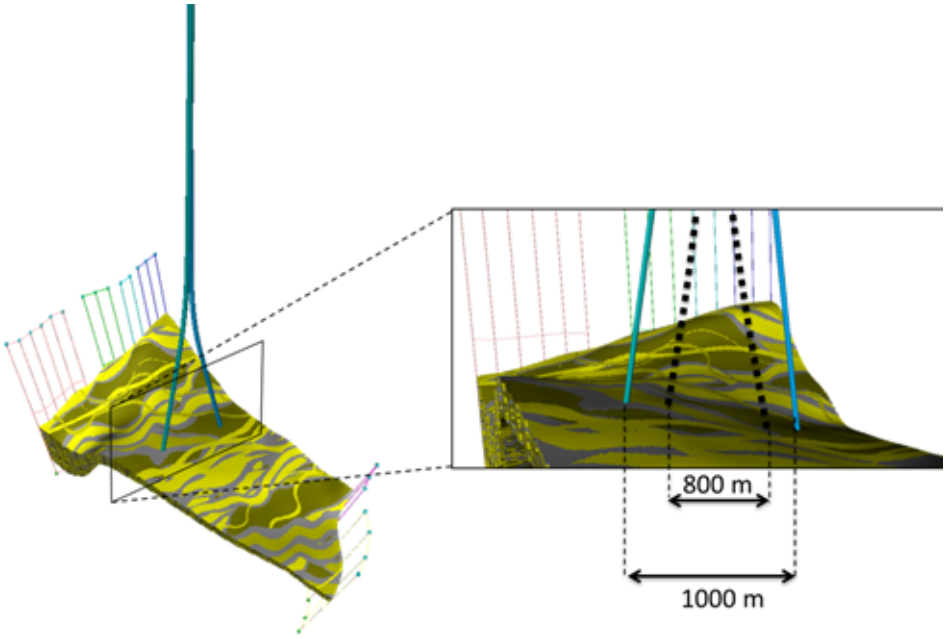

Figure 5.1: Well lay-out example of a conceptual doublet in the WNB. The black dotted lines indicate how a well spacing reduction influences the total doublet well length. The wells target a fluvial sandstone fault aquifer bounded by faults drilled deviated from one surface location. Yellow colours indicate sandstone and greenish and grey colours indicate impermeable floodplain fines.

5.5. Analyses

5.5.1. NPV sensitivity analysis

In the sensitivity analysis, the effect of a 100 m and 400 m well spacing variation from a 1000 m base case scenario on the NPV was evaluated. This was compared to the relative impact of other parameters. In this analysis, homogeneous aquifer models were utilized. Two categories of parameters were compared, financial and production related parameters. The financial parameters were varied by ±10% of the base case value. Production related parameter ranges were derived from the geological data and currently active WNB doublets. The parameter ranges are listed in Figure 5.3. In the analysis, each parameter was varied individually, while keeping the others at the base case value.

5.5.2. Impact of fluvial facies architecture on life time

In the second part of this paper, the effect of aquifer architecture on the advantage of reduction in well spacing was evaluated. In this part, production simulations were carried out utilizing detailed fluvial facies architecture realisations. In the set of realisations, N/G varied between 15 to 70% N/G. Doublet wells were placed at 400, 600, 800 and 1000 m (Figure 5.2A) under the condition that both wells intersect the same amount of sandstone grid blocks, like in chapter 4. Doublet well pairs were

placed parallel to the paleo flow direction as this reduces the required pump energy losses (chapter 3). For comparison, two homogeneous models were generated in which the thickness was adjusted by 15 and 70% respectively (Figure 5.2B and C). In this way, both model types had the same net-aquifer volume range. Two life time scenarios were considered. In the first scenario A, the life time was reached after the production temperature decreased by 10% of its initial value. In the second scenario B, the life time was reached when the temperature decreased by 1°C.

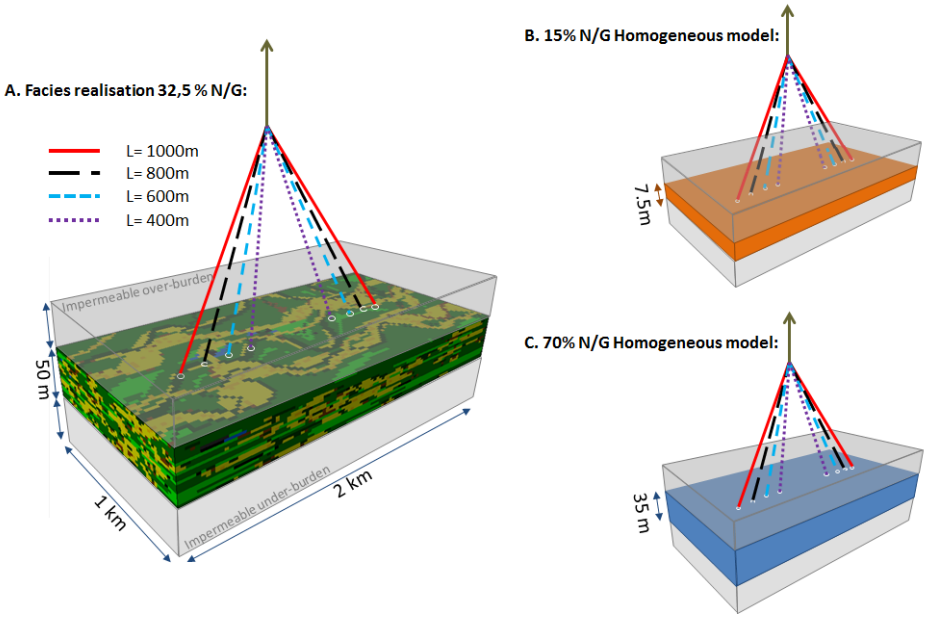

Figure 5.2: (A) Example of a facies realisation used in a production simulation with four well spacing distances. Homogeneous models with adjusted height to compensate for the uncertainty in net aquifer volume for (B) 15% and (C) 70% N/G.

5.6. Results

5.6.1. Base case scenario

The thermal capacity of our base case doublet is 4.1 MW (equation 5.2 and 5.3). The associated discounted cumulative cash flow and the net annual income are presented in Figure 5.3A. For the base case scenario the NPV is approximately 3.7 M€and represents the cumulative discounted cash flow after 15 years. The associated Internal Rate of Return on Investments (IRR) would be approximately 8 years. The thermal breakthrough moment happens after more than 60 years, even if aquifer thickness is reduced to 50 m (Figure 5.3B). After this thermal breakthrough the production temperature only decreases by approximately 1 to 2 °C per decade.

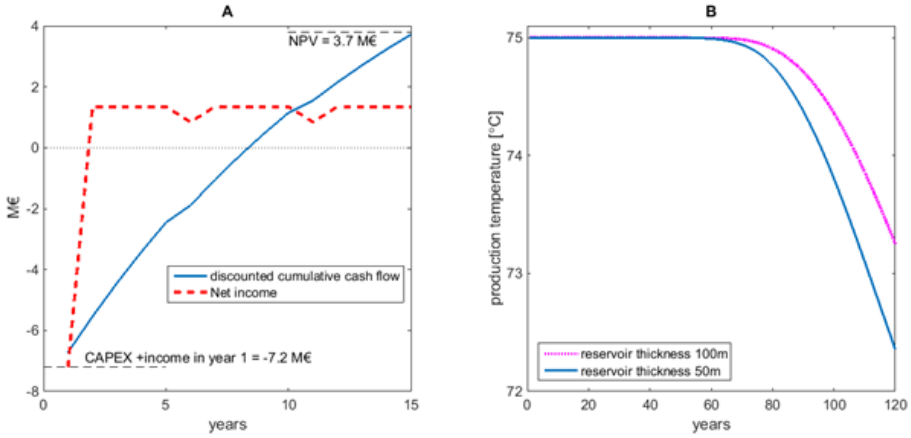

Figure 5.3: (A) Base case scenario cumulative discounted cash flow and net annual income. (B) Production temperature development for 1000m wells spacing, 100 m^3/h production rate in the base case scenario and in a 50 m thick aquifer.

5.6.2. NPV sensitivity analysis

The result of the sensitivity analysis is presented in Figure 5.4. A tornado plot shows the change in NPV in percentages (ΔNPV), as a result of the variation of a single parameter. This change is defined as: $(NPV_{BC} - NPV_x)/NPV_{BC}$ *100%*. NPV_{BC} is the base case NPV, and NPV_x is the NPV as a result of adjustment of a parameter in the sensitivity analysis. The parameter ranges are presented on the right side of the tornado plot. These analysis indicates that variation of the temperature difference between injection and production water (ΔT) has the most significant impact on a HSA doublet NPV. A five degree Celsius variation could change the NPV by approximately 50%. A 10 m^3/h variation of the production rate could vary the NPV by up to 40%. Reducing the well spacing from 1400 to 1000 m could improve the NPV up to 15%. Because well length is estimated by equation 4, the well length decreases by 5.5% if the well is reduced from 1400 to 1000 m. An additional reduction from 1000 to 600 changes well length by 4.2%. Therefore the tornado plot shows a slight asymmetrical result. An additional well spacing

reduction from 1000 to 600 m increases the NPV by approximately 13%. The 100 meter well spacing variation has smaller impact on the NPV of approximately 4%. Permeability, aquifer thickness and pump efficiency have a limited effect on the NPV. Because of the inverse relation between injection pressure and permeability, the negative effect of a 750 mD permeability reduction on NPV is larger than the positive effect of a 1000 mD permeability increase. Variation of the pump energy efficiency by ±10% (equation 5.2) did not have a significant impact on NPV (less than 1%). Other parameters that have a significant impact on NPV are CAPEX and the height of the feed-in tariff subsidy. 10% variation of discount rate, heat price and OPEX affect the NPV by approximately 10%. In our analysis, well spacing is the only independent parameter, which is determined prior to drilling. Production rate and ΔT depend on geological uncertainties, surface facility efficiency and on required heat consumption. Also, all financial parameters depend on economy or government policy. Therefore, these results also indicate the uncertainty in NPV as a result of uncertainty in geological and financial circumstances. Note that these results are based on homogeneous aquifer models, the effect of facies and property heterogeneities are not included.

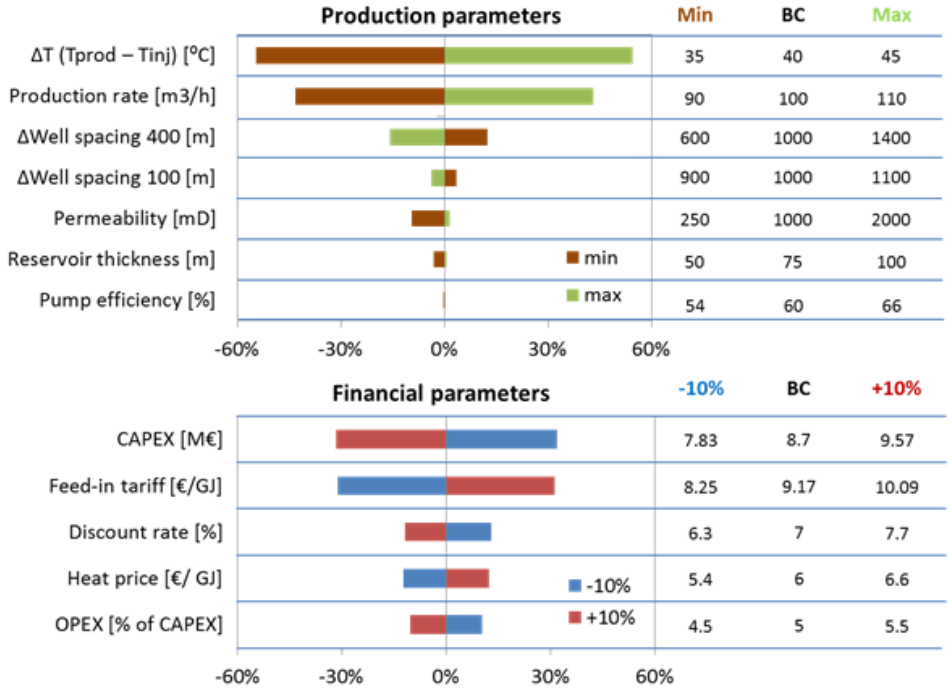

Figure 5.4: Tornado plots illustrating the impact of several parameters on NPV in percentages. The parameter ranges and their base case (BC) values are presented on the right side of the tornado plots.

The parameters in the sensitivity analysis affect the NPV of a doublet because they influence the discounted cumulative cash flow. This is because the initial investment costs are changed or the net income is affected. Examples of discounted cumulative cash flow in three scenarios (A,B and C) from the sensitivity analysis are presented in Figure 5.5. Scenario A is the base case scenario. In scenario B the well spacing is reduced by 400 m from 1000 to 600m while all other parameters are kept at their base case value (Figure 5.4). As a result, the initial investments costs are reduced while the net income is constant. Therefore, the discounted cumulative cash flow curve is shifted upward, increasing the NPV after 15 years (Figure 5.5). In scenario C the production rate is increased from 100 to 110 m^3/h while all other parameters are kept at their base case values. The higher production rate increased the slope of the discounted cumulative cash flow, which also increases NPV (Figure 5.5).

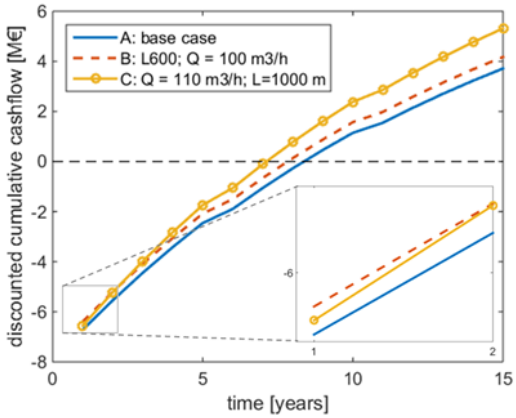

Figure 5.5: Discounted cumulative cash flow for scenario A (base case parameters), B (L=600, Q=100 m^3/h) and C (L=1000 Q= 110 m^3/h) in the sensitivity analysis.

The theoretical advantage of a well spacing reduction on NPV in Figure 5.4, applies to a typical WNB HSA doublet. To evaluate the effect of well spacing variation on NPV in doublets in other basins or countries, the sensitivity analysis is repeated for doublets with different drilling costs, production or reinjection temperatures and production rates. These three parameters are chosen because they have the most significant impact on NPV according to our analysis results in Figure 5.4. In scenario 1 and 2, drilling costs are varied by 0.3 M€/km from the WNB base case (Table 5.1). In scenario 3 the ΔT is 5 degrees higher than in our base case scenario. This could be a result of a higher production temperature or higher heat extraction efficiency and affects the net energy production (equation 5.3). In contrast in scenario 4 the ΔT is 5 degree lower. Finally the production rate is changed by 20 m^3/h in scenario 5 and 6. In these six scenarios only the base case value of the indicated parameter in scenario 1 to 6 is varied while all other values are kept at the same value as in Figure 5.4. For each scenario, a new NPV value is calculated.

Subsequently, the effect of a 100 m well spacing variation from 1000 m on this NPV is calculated. The results are presented in Figure 5.6. The results indicate that well spacing variation has greater impact on NPV in areas with higher drilling costs. If the drilling costs are 0.3 M€/km higher than in the WNB, the 10% well spacing reduction changes NPV by approximately 10% which is approximately 5% more compared to the result in Figure 5.4. If the doublet capacity is lower because of the 5 degree reduction of ΔT, a 10% well spacing reduction could increase the NPV by up to 15%. Well spacing reduction has an even higher impact on NPV in doublet with lower production rates. In a doublet with an 80 m^3/h production rate, a 10% well spacing reduction increased the NPV by approximately 25%. In doublets with lower drilling costs, higher ΔT, or higher production rates compared to the WNB base case, the impact of well spacing reduction on NPV remains a few percentages. These results imply that reducing the well spacing to improve NPV is more relevant for marginally economic doublets.

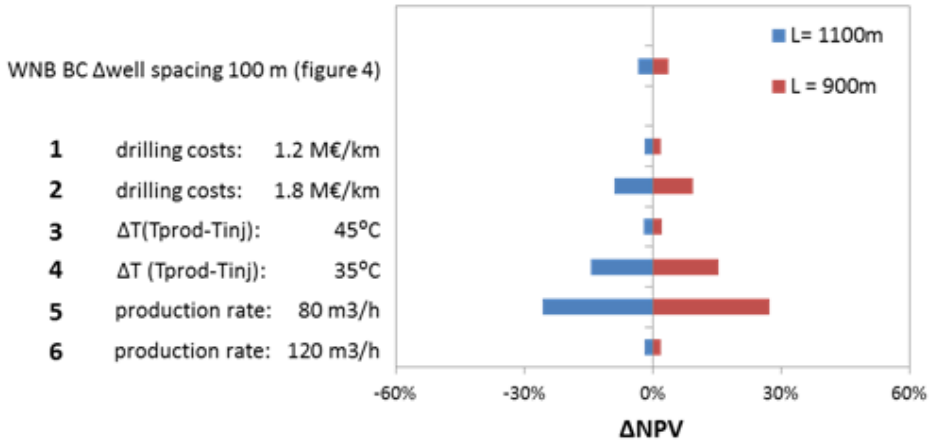

Figure 5.6: Effect of 10% well spacing reduction on NPV from 1000 to 900 m, for different base case scenarios. In scenario 1 to 6 all other parameters are equal to the base case values of Figure 3. ΔT is the difference between injection and production temperatures. For comparison, the effect of 100 m well spacing variation in the base case scenario is presented on top.

5.6.3. Impact of fluvial facies architecture on doublet life time

The production simulations with detailed fluvial facies architecture realisations show that 800 m spacing is sufficient to obtain more than 15 year life time. This is the case when the allowed production temperature drop is 1°C and 7.5°C, with a production rate of 100 m^3/h (Figure 5.7). If the production rate is 150 m^3/h, 800 m spacing is only sufficient when ΔT is 7.5°C. With 600 m spacing the life time exceeds 15 years only with a 100 m^3/h production rate and with ΔT of 7.5°C. The results also indicate an underestimation of the uncertainty in life time by the homogeneous aquifer models. The range of life time results per well spacing distance is larger, when detailed facies architecture realisations are used. This uncertainty increases for larger well spacing distances. In contrast, it is lower for higher production rates. The uncertainty in life time increases slightly for higher allowed production temperature drop (ΔT).

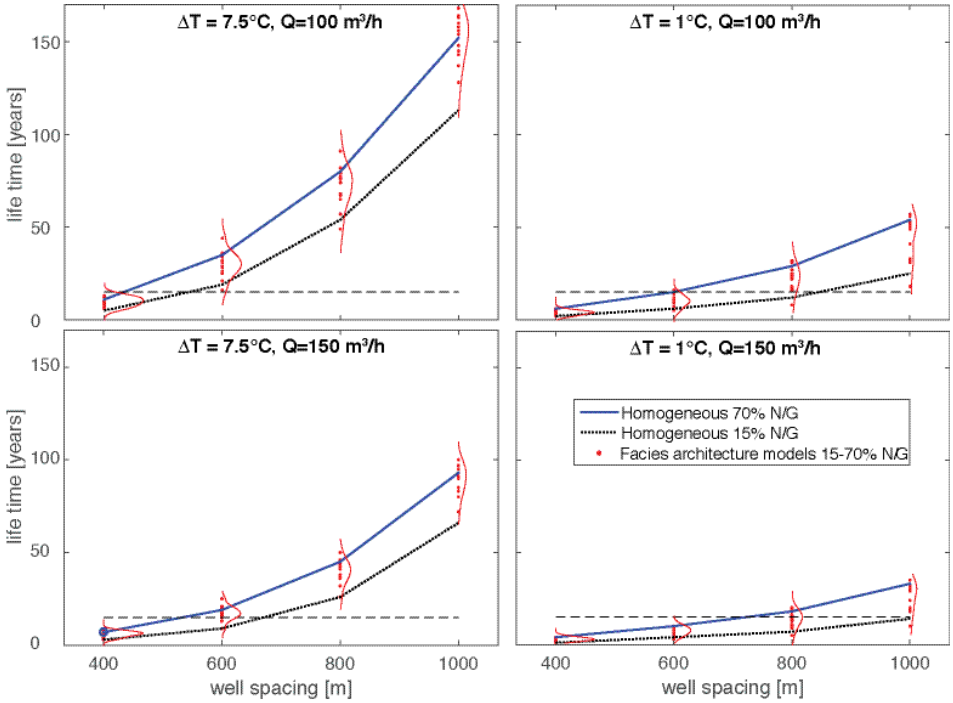

Figure 5.7: Life time for different well spacing in homogeneous models (blue and black line) and facies realisations (red dots) utilising life time scenario of a 7.5°C production temperature drop (left column) of a 1°C drop (right column). The horizontal black dotted line indicates the minimal required 15 year life time for the feed-in tariff scheme. The red line indicates the life time distribution of life time per well spacing for the facies realisations.

5.6.4. Impact of fluvial facies architecture on NPV

Figure 5.8A shows that the fluvial facies architecture could significantly influence the NPV. The NPV to well spacing relation for the 15% homogeneous model is still higher than the average NPV to well spacing relation for all detailed facies realisations. This could be explained by Figure 5.8B. This figure presents the ratio of produced heat (E_{prod}) and pump energy losses (E_{pump}) in each doublet scenario. It shows that in the detailed facies realisations, pump energy losses are significantly higher which decreases the net energy production and hence income. This is a result of the risk of flow path formation between the wells. No clear trend is observed between the energy ratio and well spacing in the facies models in Figure 5.8B. In contrast, a slight reduction of the energy ratio is recognized with increasing well spacing for the 70% N/G homogeneous model. The energy ratio is approximately 5% lower for 400 m spacing compared to 1000 m spacing. For the 15% homogeneous model this reduction is not recognizable in this figure. A similar trend would have been observed for the detailed facies models if sufficient realisations were used. Nevertheless, the effect of well spacing on pump energy losses will not have a significant impact in NPV in this well space range. Note that the ratios in Figure 5.8B apply to a single moment in time as pump energy values are time dependent (Figure 5.8C and D). This is because of the transient pressure stabilisation in the aquifer and because of the temperature dependent viscosity of the brine in our simulations. Pump energy varies more significantly over time in lower N/G realisations (Figure 5.8C) compared to high N/G realisations (Figure 5.8D). Heat production remained constant until thermal breakthrough (Figure 5.8C). The variation in pump energy losses and heat production were, however, small and varied by less than 0.02 MW in 20 years.

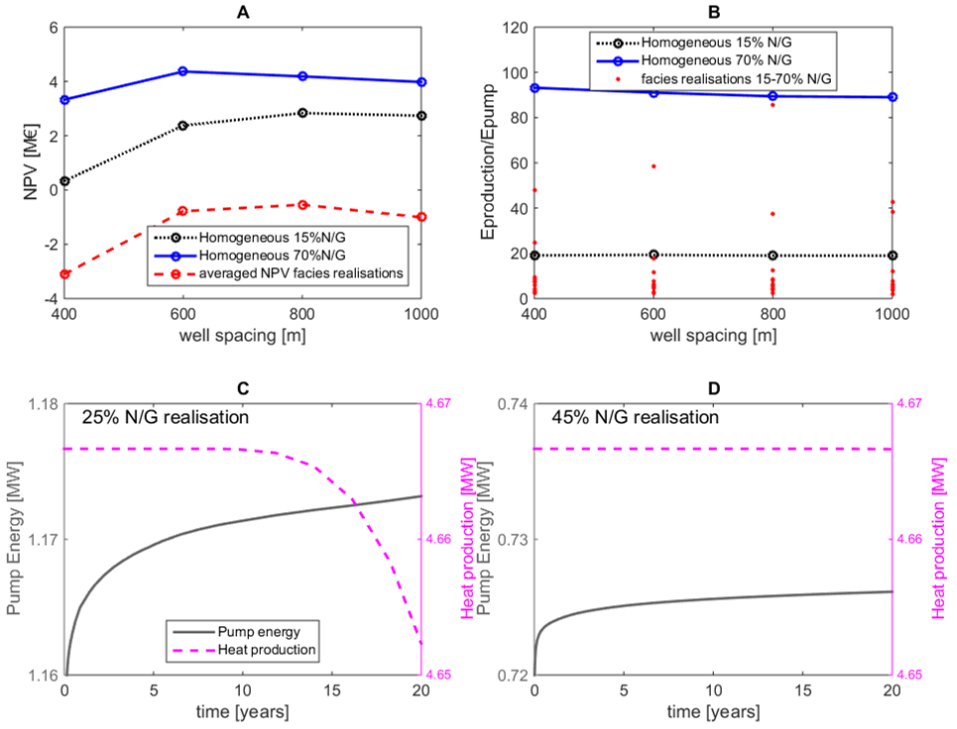

Figure 5.8: (A) NPV related to well spacing. NPV of doublets in facies realisations are averaged per well spacing distance (red dotted line). (B) Ratios of produced energy over pump energy losses after the first year, associated to (A). Red dots indicate the energy ratio of a doublet in a single facies realisations. (C) Pump energy and heat production development over time for 25% N/G and a (D) 45% N/G realisation with 1000 m well spacing and 100 m^3/h production rate. Note the same scale on the vertical axes in C and D while the absolute pump energy values vary.

A consequence of reducing the well spacing is a reduction of the maximal possible amount of recoverable heat (Figure 5.9). In addition, increasing production rate increases NPV but decreases the recoverable energy (Figure 5.9). In contrast larger well spacing increases the recoverable energy as it increases life time. Larger well spacing is therefore favourable in lower N/G aquifers or in doublet with high production rates. The results in Figure 5.9 suggest that a compromise between financial efficiency and recovery efficiency of a doublet could be obtained depending on the expected sandstone volume, required production rate and required life time. Finally, Figure 5.9 confirms that reducing well spacing to improve NPV is more relevant for marginally economic doublets with low production rates. In the 45% and 70% N/G models with 100 m^3/h production rate, an optimum in NPV is most clearly recognized. No peak in the NPV curves is observed when the life time is too low because of high production rate or low sandstone volume.

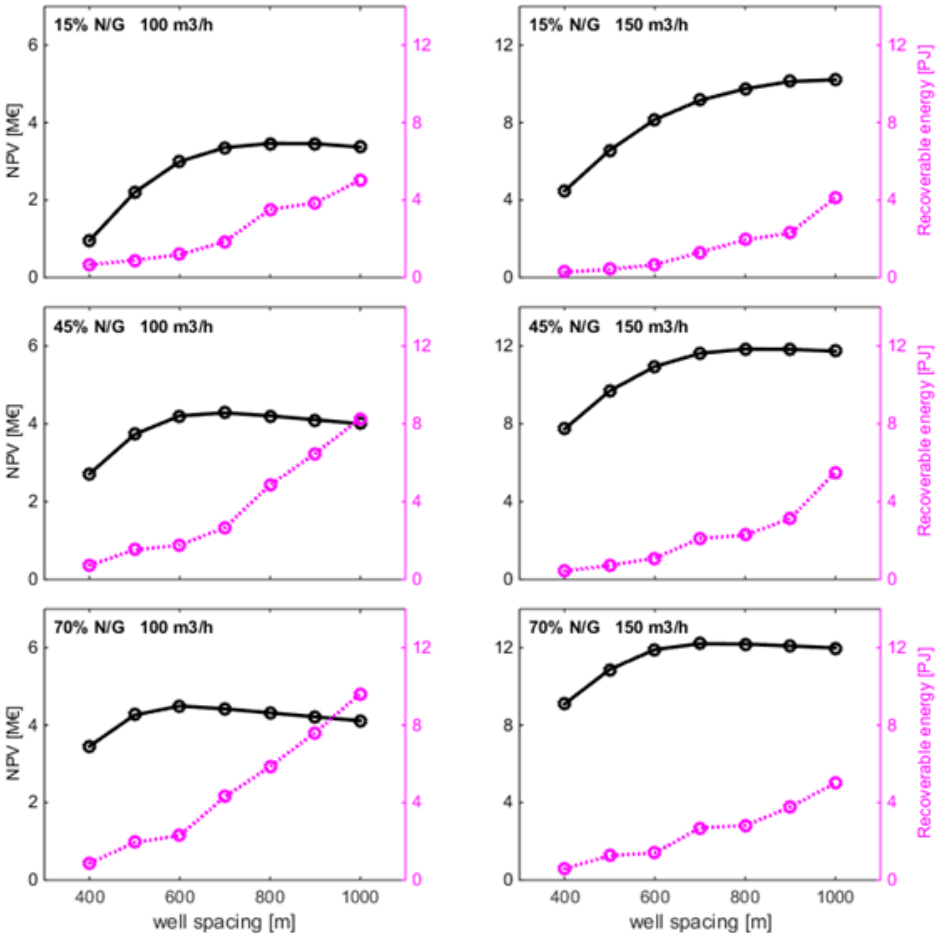

Figure 5.9: Comparison of NPV (blue line) and maximal recoverable energy (pink line) in (A) the 70% N/G and (B) 15% N/G homogeneous models. Note the change in scale of the NPV axis in the two columns.

5.7. Discussion

Well spacing reduction and the advantage on NPV

Our results show a possible improvement of the NPV of approximately 15%, when well spacing was reduced from 1400 to 1000 m. Even a small reduction of 100 m could already improve NPV by up to 4%. The sensitivity analysis indicates that variation of ΔT ($T_{prod} - T_{inj}$) and production rate have a more significant impact on NPV. However, these parameters are to a large extent dependent on (1) geological uncertainties and (2) technological constraints. Geological uncertainties include aquifer temperature of several degrees (Bonté et al., 2012) and aquifer productivity. Also all financial parameters are influenced by external factors such as economy, government policy and regional rates of equipment and technology. Well spacing is one of the parameters in our analysis that could be designed prior to drilling. So far, well spacing is primarily designed to create sufficient life time (e.g. Mottaghy et al., 2011; Daniilidis and Herber, 2016). Therefore our study takes a more comprehensive look at the effect of well spacing. This becomes increasingly important with more widespread deployment of geothermal doublets. The current spacing standard significantly limits the possible number of doublets in the WNB (e.g. Mijnlieff and Wees, 2009). Well spacing reduction would therefore not only improve the financial competitiveness of individual doublets but also enhance exploitation on a regional scale. Furthermore, our results indicate that well spacing reduction has a stronger impact in doublets with a lower productivity or net energy production rate. This is because the NPV results from a combination of initial investment and the height of the net income. These parameters determine the starting point and slope of the discounted cumulative cash flow (Figure 5.2). Optimisation of NPV by reducing well spacing is therefore of particular interest for marginally economic HSA doublets. Our results are based on the assumption that the minimal required life time is 15 years. This applies to HSA doublets in the Netherlands, because this is the maximum duration of the Dutch feed-in tariff scheme. As a result the well spacing for an optimal NPV is the smallest well distance with a minimal production temperature reduction in this period of time. This is of course related to a specific production rate. Most geothermal systems however, are designed to produce for a much longer time such as 30 to 50 years, which requires a larger well spacing. The NPV model by Van Wees et al. (2010) assumes an ideal HSA exploitation scenario. It does not accurately reflect current WNB investment costs and NPV. Firstly, this is a result of neglecting the costs which are associated to years of preparation prior to drilling and consultants. In addition, often unexpected maintenance and workover costs add to the initial investments in the first years. HSA exploitation started approximately 10 years ago in the WNB and currently passes through a learning curve. Therefore, our estimated investment costs apply more to future Dutch doublets that are able to take advantage of the exploitation experience of the first decade of HSA exploitation.

Furthermore, the NPV is increased in the base case scenario of the sensitivity analysis (Figure 5.3A) because of the relatively high porosity and permeability values of 28% and 1000 mD, respectively. In WNB doublets the NPV might be lower because of the impact of geological heterogeneity on net energy production (e.g.,

Figure 5.8A). Nevertheless, well spacing reduction would be especially relevant for more marginally economic doublets as was shown in Figure 5.6.

In our simulations, vertical wells are used. Deviated wells could improve the injectivity and productivity increasing the net energy production and improve NPV. Hence, for optimisation of doublet design, the preferred angle of the deviated well should be determined for a specific aquifer as it depends on the geological model, net sandstone volume and aquifer thickness.

Life time

The main reason for the large current well spacing standard of 1000 to 1500 m is to avoid early cold water breakthrough. However, our production simulations indicate that this spacing might be overcautious. The life time in our production simulations varies between 60 and 100 years in life time scenario A, and 15 to 35 years in life time scenario B both with 150 m^3/h production rate and a 1000 m well spacing (Figure 5.5). This shows that despite our conservative aquifer thickness of 50 m, still a considerable life time could be expected. Most current WNB doublets actually have a larger well spacing. However, well spacing optimisation requires a better understanding of the uncertainties in life time. Doublet life time is significantly affected by facies architecture (Hamm and Lopez, 2012; Crooijmans et al., 2016). Our production simulations with detailed facies architecture realisations indicate that homogeneous models underestimate doublet life time. This is because impermeable claystone bodies provide thermal recharge to the cold water plume and flow baffles increase flow path length between the wells. Secondly, homogeneous models overestimate the net energy production of the doublet (Figure 5.6B) because flow baffles or barriers could decrease injectivity or productivity. Especially in low N/G aquifers, wells might intersect different sandstone bodies that do not form flow paths between the wells which increases the required pump energy losses. Doublet well pairs were oriented parallel to the paleo flow direction and the orientation of the fluvial sandstone bodies. Perpendicular doublet orientation would increase the required pump energy losses (e.g., chapter 3) and therefore reduce NPV. In addition, perpendicular doublet orientation would have increased life time uncertainty. This is a result of a higher probability that impermeable claystone bodies form flow baffles or barriers. Flow-barriers can reduce life time when they cut-off permeable parts of the aquifer reducing the net reservoir volume while the flow baffles increase life time when they increase flow path length (e.g., chapter 4). Our results show that a statistical approach with multiple realisations is required to capture uncertainties in life time and doublet capacity. The large spread in life time (Figure 5.5) indicates that more realisations would be required to accurately capture this uncertainty in life time and capacity as were used in our study. The goal of our study was, however to examine how facies heterogeneities influence the theoretical advantage of well spacing reduction on NPV. Our results support the possibility to reduce the well spacing, especially because the net sandstone volume in our models is very conservative. For example, no WNB doublet only encounters a 15 to 20% N/G aquifer of 50 m thickness. In general, WNB aquifers have a larger thickness and higher N/G percentage. Our conservative sandstone volumes results in low doublet

capacities (Figure 5.6B) and therefore lower NPV compared to the base case scenario. In reality, doublets with very low injectivity or net sandstone volume would not be taken in production without any measures (e.g. Blocher, 2016). Examples of such a measures are to continue drilling into a higher N/G interval or to increase heat exchange surface by hydraulic stimulation. If we would compensate for this, life time and NPV in our results would increase. The detailed facies architecture realisations in this current study are simplified by neglecting small scale permeability heterogeneities and assuming isotropic aquifer properties in grid blocks. Examples of such small scale heterogeneities are shale drapes, accretion surfaces and bedding planes (e.g. Pranter et al., 2007). These features decrease on average the permeability perpendicular to the paleoflow direction. This could be accounted for adjusting the permeability in different directions in each grid block like in Bierkens and Weerts (1994). Furthermore porosity was randomly distributed amongst the sandstone grid blocks. In reality the porosity of channel lags, point-bars and sand plugs varies more systematically across sandstone bodies as a result of sedimentary process (Willis and Tang, 2010), which could influence flow path formation through the sandstone bodies (Larue and Hovadik, 2008). These heterogeneities could further diffuse the cold water plume. Note that in our simulations flow only occurs through the rock matrix and no fractures are present. Fractures, especially parallel to the flow between the doublets could decrease the thermal breakthrough time of the cold water plume. Finally, it could be argued that not only the sandstone volumes in our simulations were conservative, also the assumptions on the minimal production temperature could be considered as such. The minimum required production temperature for economic Dutch HSA exploitation for greenhouse heating is assumed to be 45°C and 65°C for district heating purposes (Pluymaekers et al., 2012). These minimal temperatures are lower than the 67.5°C in our life time scenario A and much lower than the 74°C of scenario B. Furthermore, due to likely technological improvements on insulation and technological efficiency in the next decades, lower production temperatures will most likely be sufficient in the future. Our simulations show that production temperature reduces by 0.5 to 1°C per year, depending on the net sandstone volume and production rate. The speed of production temperature reduction in our simulations is relatively low compared to previous studies (e.g. Mijnlieff and Wees, 2009) because thermal recharge from over and under burden is taken into account (Poulsen et al., 2015). In Figure 5.10 the production temperature development over time in homogeneous aquifer models and detailed aquifer architecture models are compared as an example. Doublets in these simulations have a 600 m well spacing and 100 m^3/h production rate. In the lowest N/G aquifer realisation, the production temperature drops below 60°C after 60 years. In the highest N/G realisation this production temperature is reached after approximately 140 years. Therefore, Figure 5.10 underlines conservative nature of our minimal temperature assumptions.

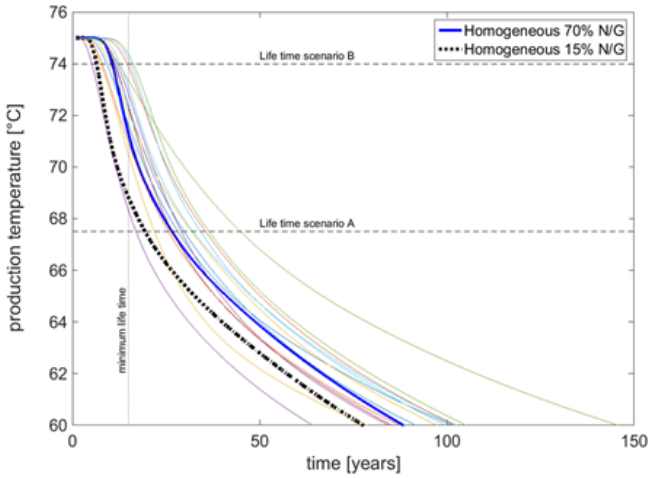

Figure 5.10: Production temperature development over time for a 600 m well spacing for all facies realisations (thin coloured lines) and the two homogeneous models as indicated in the legend.

5.8. Conclusions

This paper presents a modelling based study on the advantages and impacts of a well spacing reduction in HSA doublets. Firstly, our results indicate that a reduction of 400 m well spacing could lead to a NPV improvement of up to 15%. The impact of well spacing reduction on NPV is more significant in marginally economic doublets. Secondly, production simulations with detailed facies aquifer architecture derived from WNB geological data are used to evaluate the impact of smaller well spacing on life time. Our results suggest that sufficient life time could be obtained, if the well spacing is reduced below the current 1000 to 1500 m standard. These current standards aim to avoid early cold water breakthrough. However, our results show potential overdesign of these standards. This results in the negative effect of decreasing the financial competitiveness of geothermal exploitation and reducing the possible number of doublets in a region. Finally, the comparison of production simulations with detailed facies architecture realisations and homogeneous models shows that homogeneous models underestimate the uncertainty in life time and doublet capacity. The aquifer heterogeneities have a significant effect on the flow path formation between the wells. Therefore, a statistical approach with multiple realisation is required to accurately assess HSA potential and to optimise exploitation efficiency.

References

Adams, B. M. (2015). *On the Power Performance and Integration of Carbon-dioxide Plume Geothermal (CPG) Electrical Energy Production*. Phd thesis, University of Minnesota.

Bailey, W. R., Manzocchi, T., Walsh, J. J., Keogh, K., Hodgetts, D., Rippon, J., Nell, P. a. R., Flint, S., and Strand, J. a. (2002). The effect of faults on the 3D connectivity of reservoir bodies: a case study from the East Pennine Coalfield, UK. *Petroleum Geoscience*, 8:263–277.

Bierkens, M. F. P. and Weerts, H. J. T. (1994). Block hydraulic conductivity of cross-bedded fluvial sediments. *Water Resources Research*, 30(10):2665–2678.

Blocher, G. (2016). Hydraulic history and current state of the deep geothermal reservoir Groß Schonebeck. *Geothermics*, 63:27–43.

Bonté, D., Wees, J. V., and Verweij, J. M. (2012). Subsurface temperature of the onshore Netherlands : new temperature dataset and modelling. *Netherlands Journal of Geosciences*, 91(4):491–515.

Chandrasiri Ekneligoda, T. and Min, K. B. (2014). Determination of optimum parameters of doublet system in a horizontally fractured geothermal reservoir. *Renewable Energy*, 65:152–160.

Cojan, I., Fouché, O., Lopéz, S., and Rivoirard, J. (2005). Process-based reservoir modelling in the example of meandering channel. In *Geostatistics Banff 2004*, pages 611–619. Springer.

Crooijmans, R. A., Willems, C. J. L., Nick, H. M., and Bruhn, D. F. (2016). The influence of facies heterogeneity on the doublet performance in low-enthalpy geothermal sedimentary reservoirs. *Geothermics*, 64:209–219.

Daniilidis, A. and Herber, R. (2016). Salt intrusions providing a new geothermal exploration target for higher energy recovery at shallower depths. *Energy*, In press.

Devault, B. and Jeremiah, J. (2002). Tectonostratigraphy of the Nieuwerkerk Formation (Delfland Subgroup) West Netherlands Basin. *AAPG Bulletin*, 86(10):1679–1707.

Donselaar, M. E., Groenenberg, R. M., and Gilding, D. T. (2015). Reservoir Geology and Geothermal Potential of the Delft Sandstone Member in the West Netherlands Basin. In *World Geothermal Congress 2015*, Melbourne, Australia.

Gibling, M. R. (2006). Width and Thickness of Fluvial Channel Bodies and Valley Fills in the Geological Record: A Literature Compilation and Classification. *Journal of Sedimentary Research*, 76:731–770.

Grappe, B., Cojan, I., Flipo, N., Rivoirard, J., and Vilmin, L. (2012). Developments in dynamic modelling of meandering fluvial systems. In *AAPG 2012 Annual Convention & Exhibition*, page 1236147.

Hamm, V. and Lopez, S. (2012). Impact of Fluvial Sedimentary Heterogeneities on Heat Transfer at a Geothermal Doublet Scale. In *Thirty-Seventh Workshop on Geothermal Reservoir Engineering*, Stanford, California.

Jeremiah, J. M., Duxbury, S., Rawson, P., E, S. I., Ashford, N. D., and Tx, H. (2010). Lower Cretaceous of the southern North Sea Basins : reservoir distribution within a sequence stratigraphic framework. *Netherlands Journal of Geosciences*, 89(3/4):203–237.

Kramers, L., Wees, J. V., Pluymaekers, M. P. D., Kronimus, A., and Boxem, T. (2012). Direct heat resource assessment and subsurface information systems for geothermal aquifers ; the Dutch perspective. *Netherlands Journal of Geosciences*, 91(4):637–649.

Larue, D. K. and Hovadik, J. (2006). Connectivity of channelized reservoirs: a modelling approach. *Petroleum Geoscience*, 12(4):291–308.

Larue, D. K. and Hovadik, J. (2008). Why is reservoir architecture an insignificant uncertainty in many appraisal and development studies of clastic channelized reservoirs? *Journal of Petroleum Geology*, 31(4):337–366.

Lingen, P. (2014). LIR-GT-01 – LIR-GT-02 Interference Analysis LIR-GT-01 – LIR-GT-02 Interference Analysis. Technical Report September, PanTerra Geoconsultants B.V., Leiderdorp.

Lopez, S., Hamm, V., Le Brun, M., Schaper, L., Boissier, F., Cotiche, C., and Giuglaris, E. (2010). 40 years of Dogger aquifer management in Ile-de-France, Paris Basin, France. *Geothermics*, 39(4):339–356.

Mijnlieff, H. F. and Wees, J. (2009). Rapportage Ruimtelijke Ordening Geothermie. Technical report, TNO.

Mottaghy, D., Pechnig, R., and Vogt, C. (2011). The geothermal project Den Haag: 3D numerical models for temperature prediction and reservoir simulation. *Geothermics*, 40:199–210.

Nielson, D. L. and Garg, S. K. (2016). Slim Hole Reservoir Characterization for Risk Reduction. In *41st Workshop on Geothermal Reservoir Engineering*, number 2014, pages 1–8, Stanford, California.

Pluymaekers, M. P. D., Kramers, L., Wees, J. V., Kronimus, A., and Nelskamp, S. (2012). Reservoir characterisation of aquifers for direct heat production : Methodology and screening of the potential reservoirs for the Netherlands. *Netherlands Journal of Geosciences*, 91(4):621–636.

Poulsen, S. E., Balling, N., and Nielsen, S. B. (2015). A parametric study of the thermal recharge of low enthalpy geothermal reservoirs. *Geothermics*, 53:464–478.

Pranter, M. J., Ellison, A. I., Cole, R. D., and Patterson, P. E. (2007). Analysis and modeling of intermediate-scale reservoir heterogeneity based on a fluvial point-bar outcrop analog , Williams Fork Formation , Piceance Basin , Colorado. *AAPG Bulletin*, 91(7):1025–1051.

Pranter, M. J. and Sommer, N. K. (2011). Static connectivity of fluvial sandstones in a lower coastal-plain setting: An example from the Upper Cretaceous lower Williams Fork Formation, Piceance Basin, Colorado. *AAPG Bulletin*, 95(6):899–923.

Sauty, J., Gringarten, A., Landel, P., and Menjoz, A. (1980). Lifetime optimization of low enthalpy geothermal doublets. In *Advances in European geothermal research*, pages 706–719. Springer.

TNO (1977). Nl olie- en gasportaal. www.nlog.nl.

Törnqvist, T. E. and Bridge, J. S. (2002). Spatial variation of overbank aggradation rate and its influence on avulsion frequency. *Sedimentology*, 49:891–905.

Van Heekeren, V. and Bakema, G. (2013). Geothermal Energy Use, Country Update forthe Netherlands. In *European Geothermal Congress*, pages 2013–2016, Pisa.

Van Heekeren, V. and Bakema, G. (2015). The Netherlands Country Update on Geothermal Energy. In *World Geothermal Congress 2015*, volume 2013, pages 2–7, Melbourne.

Van Wees, J., Kramers, L., Kronimus, R., Pluymaekers, M., MijnLieff, H., and Vis, G. (2010). ThermoGISTM V1.0 Part II : Methodology. Technical report, TNO, Utrecht.

Willems, C. J. L., Nick, H. M., Donselaar, M. E., Jan, G., and Bruhn, D. F. (2017). Geothermics On the connectivity anisotropy in fluvial Hot Sedimentary Aquifers and its influence on geothermal doublet performance. *Geothermics*, 65:222–233.

Williams, G. (1986). River meanders and channel size. *Hydrology*, 88:147–164.

Willis, B. J. and Tang, H. (2010). Three-Dimensional Connectivity of Point-Bar Deposits. *Journal of Sedimentary Research*, 80(5):440–454.

6

An evaluation of interferences in heat production from low enthalpy geothermal doublets systems

Abstract
Required distance between doublet systems in low enthalpy geothermal heat exploitation is often not fully elucidated. The required distance aims to prevent negative interference influencing the utilisation efficiency of neighbouring doublet systems. Currently production licence areas are often issued based on the expected extent of the reinjected cold water plume on the moment of thermal breakthrough. The production temperature, however, may not immediately drop to non-economic values after this moment. Consequently, the heat production could continue and the cold water plume in the geothermal aquifer could grow further sweeping a larger area. Furthermore, the reservoir pressure influenced by the injection and production spreads beyond the cold water plume extent, influencing not only the productivity of the adjacent doublet systems but also the shape of cold water plumes. This affects doublet life time, especially if adjacent doublets have different production rates. In this modelling based study a multi parameter analysis is carried out to derive dimensionless relations between basic doublet design parameters and required doublet distance. These parameters include the spacing between injector and producer of the same doublet, different production rates, reservoir thickness and minimal required production temperature. The results of this study can be used to optimize positive interference or minimise negative interference aiming at improving geothermal doublet deployment efficiency.

This chapter is based on: Willems, C.J.L., Nick, H.M., Weltje, G.J., Bruhn, D.F., *An evaluation of interferences in heat production from low enthalpy geothermal doublets systems*, ***Submitted***.

6.1. Introduction

Low enthalpy Hot Sedimentary Aquifers (HSA) are often exploited by multiple individual geothermal operators with a single or a few doublet systems. An example of this type of geothermal exploitation can be found in the West Netherlands Basin (WNB) (e.g. Van Heekeren and Bakema, 2015). Different geothermal operators may have different business cases with associated requirements for minimal production temperature, life time and heat production rate. In the WNB a geothermal production licence typically has an area which is equal to a rectangle with a size of $L \times 2L$, in which L is the injector to producer well spacing (e.g. TNO, 1977; Mijnlieff and Wees, 2009). This area should capture the extent of the cold water plume at the moment of thermal breakthrough. After this moment, however, the production temperature may not necessarily drop immediately below non-economic values (e.g. Hamm and Lopez, 2012; Crooijmans et al., 2016; Willems et al., 2016). In the WNB the production temperatures range from 70°C to 90°C, while the minimal required production temperature for economical HSA exploitation is 40°C according to Pluymaekers et al. (2012). Obviously, continued production increases the extent of the cold water plume and thereby the area of influence of a doublet. Hence, the current licencing strategy may limit the recovery efficiency since the heat production could continue after the thermal breakthrough moment. In addition, doublet exploitation affects aquifer pressure distributions over much larger areas than the production licence (e.g. Mijnlieff and Wees, 2009). This could disturb injectivity and productivity of adjacent doublets. Moreover, it could influence the shape of the cold water plumes of adjacent doublets, thus, affecting their life time. This kind of interference becomes more pronounced when an adjacent doublet has a significantly higher production rate. In the Netherlands for example, current production rates vary from 100 m^3/h to 300 m^3/h (e.g. Mottaghy et al., 2011; Pluymaekers et al., 2012; Daniilidis and Herber, 2016) which may require a larger space between the doublets. The current WNB licencing strategy may underestimate the required doublet distance which could eventually lead to an inefficient recovery and a negative interference. The challenges of preventing interferences in a Common-Pool Resource (CPR) are well known in exploitation of other types of geothermal resources than HSA. An example is shallow geothermal systems for Aquifer Thermal Energy Storage (ATES). However, these resources have different characteristics that influence interference. Unlike in HSA exploitation ATES systems operate periodically (and injection and production can be reversed). Therefore exploitation could be optimised in cycles based on experience from a previous cycle (e.g. Sommer et al., 2015). In addition wells can easily be shut in and replaced by new ones on different locations to optimise exploitation due to significantly lower costs (e.g. Jaxa-rozen et al., 2015). A similarity between ATES and HSA exploitation is that doublet systems are often overdesigned and sub optimal use of the heat source is imminent (Sommer et al., 2015; Willems et al., 2016). In contrast, high enthalpy geothermal resources face a different challenge of over-exploitation. In this type of exploitation reinjection is not standard and hence pressure depletion plays a major role in interference (e.g. Malafeh and Sharp, 2014; Tureyen et al., 2015). Compared to other types of geothermal resources, HSA are still a less established type of geother-

mal resource (e.g. Boxem et al., 2011), albeit with a growing interest for heating purposes, not only in the Netherlands. To improve the potential of this type of resource it is of particular importance to reduce risks of negative interference and enhance potential recovery by optimising the layout and licensing of these type of systems. The goal of this study is to better understand the required doublet distance as function of basic doublet design parameters. These parameters include injector to producer spacing, production flow rate, reservoir thickness and minimal required production temperature. The relation between these parameters and required doublet distance could be used to prevent negative interference, but also to optimise doublet deployment. This study is based on a case study of the West Netherlands Basin (WNB) where 15 doublets have been realised and 30 additional exploration licences were granted in the past 15 years. A modelling based approach is used in this study to explore the effect of doublet design parameters and doublet distance on interference in HSA exploitation. The design parameters ranges are derived from a WNB case study (e.g. Willems et al., 2017). Relations between doublet performance, doublet distance and the doublet parameters are derived from the multi-parameter analysis. These relations could be used to determine required doublet distance.

Interference and doublet configurations

In this study, two different doublet configurations are considered. If injectors and producers are aligned, this is referred to as the 'tramline configuration'. In contrast, well functions can be alternated creating 'checkboard' pattern, which is referred to as "5-spot well layout" in the hydrocarbon industry. Mijnlieff and Wees (2009) showed that tramline configurations result in negative interferences in terms of life time and net energy production. Injectors increase the ambient aquifer pressure and therefore can reduce the injectivity of other neighbouring injectors. Producers act in the opposite way. As a result, the cold water plumes are narrower and cold water breakthrough occurs earlier. The opposite effect was recognized for checkboard configurations. In this configuration both life time and injectivity were enhanced. However, checkboard configurations could also induce cross flow between adjacent doublets. Figure 6.1 illustrates both types of configurations, well spacing and doublet distance. Mijnlieff and Wees (2009) used only constant production rates in all doublets and the same well spacing and reservoir thickness throughout. However, production rate contrasts are likely to influence the interference. In addition, the interference could be dependent on reservoir thickness and well spacing as these factors influence the net aquifer volume and hence the life time. For this reason, we included different production rates from neighbouring well doublets as well as variations in reservoir thickness and well spacing in our analysis.

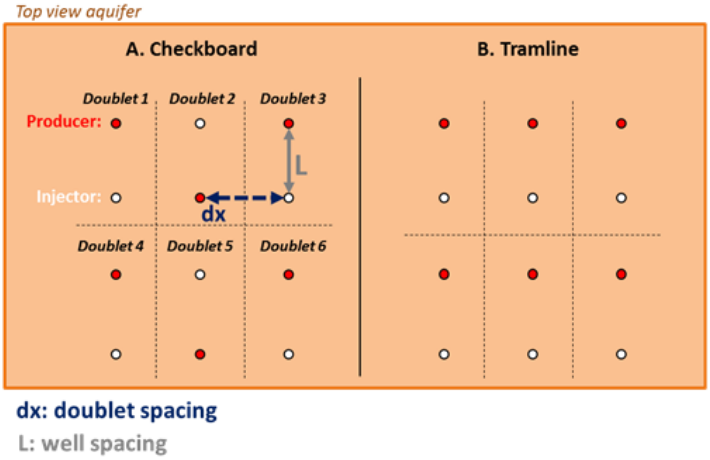

Figure 6.1: Comparison of (A) checkboard configuration in which adjacent wells have oposite functions and (B) tramline configuration where the nearest well of an adjacent doublet has a similar function.

6.2. Method

6.2.1. Overview

A 2D finite element approach was used to conduct a series of simulations for HSA exploitation with two doublets in the same aquifer. In these simulations doublet distance and other basic doublet design parameters were varied. These parameters included well spacing, production rates and reservoir thickness. Here, the distance between wells in the same doublet was referred to as well spacing; the distance between wells of two adjacent doublets was referred to as doublet distance. The multi parameter analysis was carried out for both the checkboard and tramline configurations (Figure 6.1). Based on these simulations the impact of the different parameters on doublet performance was evaluated in terms of life time, net energy production and Net Present Value (NPV). The doublet performance of the two doublets in tramline and the checkboard configurations was compared to production simulations with a single doublet with the same well spacing, aquifer thickness and production rate. Interference was expressed as deviation from the performance of a single doublet as a result of the proximity of another doublet.

6.2.2. Reservoir non-isothermal flow modelling

A 9x9 km 2D, horizontal, homogeneous aquifer model was used for the production simulations. Like in the previous chpaters of this thesis, the aquifer properties were derived from Nieuwerkerk Formation subsurface data (e.g. TNO, 1977; Crooijmans et al., 2016; Willems et al., 2017). These properties are listed in Table 6.1. The aquifer properties were isotropic and only the rock matrix flow was taken into account assuming no presence of fractures.

The numerical modelling procedure followed the same approach as was de-

Parameter	Description	Value	Dimension
k	Permeability	1000	mD
ϕ	Sandstone porosity	0.28	-
λ_s	Sandstone conductivity	2.7	W/m/K
C_{sand}	Sandstone specific heat	730	J/kg/K
C_b	Brine specific heat	4200	J/kg/K
ρ_{sand}	Sandstone density	2650	kg/m^3
ρ_{brine}	Brine density	1050	kg/m^3
T_{res}	Initial reservoir temperature	75	°C
T_{inj}	Re-injection temperature	35	°C

Table 6.1: List of parameters used in the dynamic model.

scribed in section 4.2.5 of this thesis. In this approach, the energy balance was solved for a rigid medium fully saturated with water, in which thermal equilibrium was assumed between the fluid and solid phases: $\rho C\, \partial/\partial t\, T + \rho_w C_w\, \nabla\cdot(\rho T) - \nabla\lambda I\cdot(\nabla T) = 0$. In this balance, t [s] is time, T [K] is the temperature, ρ is the mass density [kg/m^3], C_w [J/(kgK)] is the specific heat capacity, λ [W/(mK)] is the thermal conductivity, I the identity matrix, and q [m/s] is the Darcy velocity vector. The thermal conductivity and the volumetric heat capacity were described in terms of a local volume average. Heat conductivity, density and heat capacity were assumed to be independent of temperature for simplicity and described by: $\lambda = (1-\phi)\lambda_s + \phi\lambda_w$ and $\rho C = (1-\phi)\rho_s C_s + \phi\rho_w C_w$, in which ϕ is the porosity. This Darcy flow velocity vector was determined by: $q = (k\nabla P)/\mu$, where is k [m^2] the intrinsic permeability, μ the temperature and salinity dependent viscosity like in (Crooijmans et al., 2016), and P [Pa] the pressure. The pressure field was obtained through solving the continuity equation: $\phi(\partial\rho_w)/\partial t + \nabla\cdot(\rho_w q) = \rho_w S$, where S [1/s] is external sinks and sources. The suffix w refers to the pore fluid and s to the solid rock matrix. The values of all constant parameters are listed in table 6.1. Triangular elements were used for the spatial discretisation that range in size from 0.2 near the wellbore to 150 m far away from the doublets. The production simulations yielded a production temperature development over time and the required injection and production pressure for the associated production rate and set of parameters. The difference between these pressures (ΔP) was used to estimate pump power losses: $E_{pump} = (Q\, \Delta P)/\epsilon$ (e.g. Willems et al., 2017), where Q is the production rate and ε the pump efficiency of 60%. The produced power (E_{prod}) was estimated by: $E_{prod} = Q\, \rho_b\, C_b\, \Delta T$ (e.g. Willems et al., 2017) in which ΔT is the difference between injection temperature (35°C) and production temperature. The net power production was determined by the sum of the produced energy and the pump energy losses.

6.2.3. Net Present Value model

The results of production simulations were expressed in financial terms utilising the same NPV model as was described in section 5.4 of this thesis. The NPV is the depreciated, discounted, net-cumulative income after 15 years. This period was chosen, because it is the maximum duration of the Dutch feed-in tariff scheme (SDE+) for geothermal energy (Van Heekeren and Bakema, 2013, 2015). Pump work-over costs of 0.25 M€ were taken into account every five years, which is equal to half of the estimated pump costs. A down-time of 40% was assumed for

maintenance throughout the year. The same NPV parameter ranges were used as presented in table 5.1.

6.2.4. Multi parameter analysis

The parameter value ranges were derived from WNB subsurface data and production data from currently active geothermal well doublets in the WNB (TNO, 1977; Van Heekeren and Bakema, 2015; Mijnlieff and Wees, 2009; Willems et al., 2016) and are listed in table 6.2. In the production simulations, different aquifer thicknesses of 25, 50 and 75 m were used. Well spacing was equal in both doublets; four different well spacing distances were used: 600, 800, 1000 and 1500 m. The distance between the two doublets (*dx*) was varied from 4000 m to the well spacing (*L*) minus 100 m in approximately 13 steps. Production rates in the simulations ranged from 50 m^3/h to 300 m^3/h in both doublets. Finally, the multi parameter analysis was carried out for both doublet configurations: checkboard and tramline Figure 6.2). In total some 10,000 simulations were conducted to analyse interference. In addition simulations were carried out with a single doublet with the same parameter value ranges for calibration of doublet performance.

Parameter	Description	Value	Dimension
H	Reservoir thickness	25, 50,75	m
L	Doublet well spacing	600, 800, 1000, 1500	m
dx	Doublet distance	L-100 to 4000	m
Q_1	Production rate doublet 1	50, 100, 150, 200, 250	m^3/h
Q_2	Production rate doublet 2	50, 100, 150, 200, 250,300	m^3/h

Table 6.2: List of parameters used in the dynamic model.

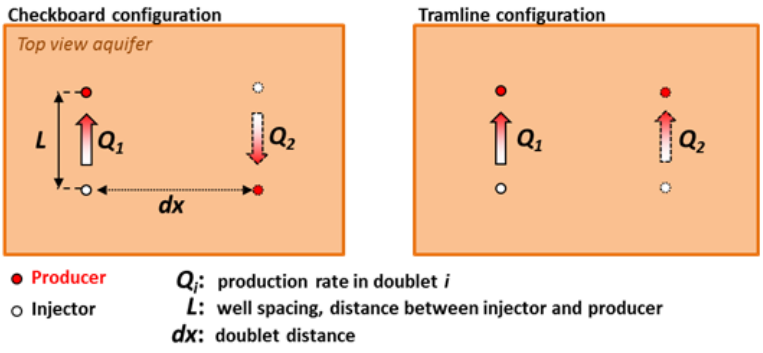

Figure 6.2: Doublet configurations in the production simulations. The arrows indicate the main flow direction of the reinjected cold water towards the production well.

6.2.5. Interference

The doublet performance for each set of parameters was analysed in terms of (A) life time, (B) net energy production, and (C) Net Present Value (NPV). The life time of a doublet was reached when the production temperature decreased to a minimal allowed temperature (T_{min}). Three life time scenarios were compared (I) T_{min} = 72.5°C, (II) T_{min} = 70°C and (III) T_{min} = 67.5°C. Interference was expressed as deviation from the performance of a single doublet. Life time interference (ΔLT) was defined as:

$$\Delta LT = (LT_{\text{dx}} - LT_{\text{s.d.}})LT_{\text{s.d.}}100\% \tag{6.1}$$

in which LT_{dx} is the life time of doublet 1 in a simulation with a certain doublet distance (dx), well spacing (L) and flow rate contrast. $LT_{s.d.}$ is the life time of a single doublet with the same parameter values. Interference in terms of net energy production (ΔEP) is defined in a similar way as:

$$\Delta EP = (EP_{\text{dx}} - EP_{\text{s.d.}})EP_{\text{s.d.}}100\% \tag{6.2}$$

In which EP_{dx} is the net-energy production of doublet 1 width a certain doublet distance (dx) and $EP_{s.d.}$ is the net-energy production of a single doublet. Finally the effect of the interference on NPV of doublet 1 is defined as:

$$\Delta NPV = (NPV_{\text{dx}} - NPV_{\text{s.d.}})NPV_{\text{s.d.}}100\% \tag{6.3}$$

6.3. Results

6.3.1. Area of influence of a single doublet

After thermal breakthrough, production temperature starts to decrease by approximately 2°C per decade (Figure 6.3A). In this example the reservoir thickness is 75 m, the well spacing 1000 m and the production rate 150 m^3/h. For instance, if the minimal production temperature is 70°C, the life time of the doublet is 61 years. The cold water plume has a symmetrical tear-drop shape which is controlled by the streamline pattern. At the moment of cold water breakthrough the cold water plume lies within a rectangle with size 1000 m by 2000 m Figure 6.3B). However, if the life time is 61 years, the cold water plume extends beyond these boundaries (Figure 6.3B). The fluid pressure distribution is constant over time and extends far beyond the rectangle boundaries. The pressure influence on the ambient reservoir pressure is limited. It changes the pressure by less than 1 bar at several hundred meters away from the wells (Figure 6.3C).

6.3.2. Area of influence, Tramline configuration

The impact of doublet distance is quantified for doublets in tramline configurations. In Figure 6.4 production temperature development of one of the two doublets is presented when the doublet distance (*dx*) is 4000, 3000, and 1000 m. The production temperature development in these three scenarios is compared to that of a single doublet with the same well spacing, reservoir thickness and production rate. In this example the reservoir thickness is 75 m and the well spacing of both doublets is 1000 m. The doublets have equal production rates of 150 m^3/h. When the doublet distance (*dx*) is 1000 m the production temperature reduces earlier and faster compared to the scenario with a doublet distance of 3000 m. For two systems with a doublet distance of 4000 m the production temperature development is almost equal to that of a single doublet. These observations can be explained by the temperature- and pressure distribution development around the wells as well as the streamline patterns (Figure 6.5). In tramline configurations, the proximity of the adjacent injector deforms the cold water plume (e.g., Figure 6.5A). The asymmetrical streamlines pattern in this figure confirms that flow velocity is higher in between the two doublets. As a result, the cold water plumes have a narrower tear-drop shape with a smaller doublet distance. In contrast, the cold water plume expands in a more symmetrical way when the doublet distance is 4000 m (Figure 6.5B). Nevertheless, the pressure distribution is still influenced as is reflected by the asymmetrical shape of the contour lines in Figure 6.5B. The production licence area is equal to a rectangle with sides *dx+L* and *dx*, in which *dx* is doublet distance and *L* is well spacing. Comparison of Figure 6.5A and B indicates that with larger doublets distance, a much larger part of the aquifer will be left unswept.

6.3.3. Area of influence: checkboard configurations

The impact of doublet distance is quantified for doublets in checkboard configurations. The results indicate that the thermal breakthrough time is delayed by several years when compared to a single doublet, for a model with the checkboard

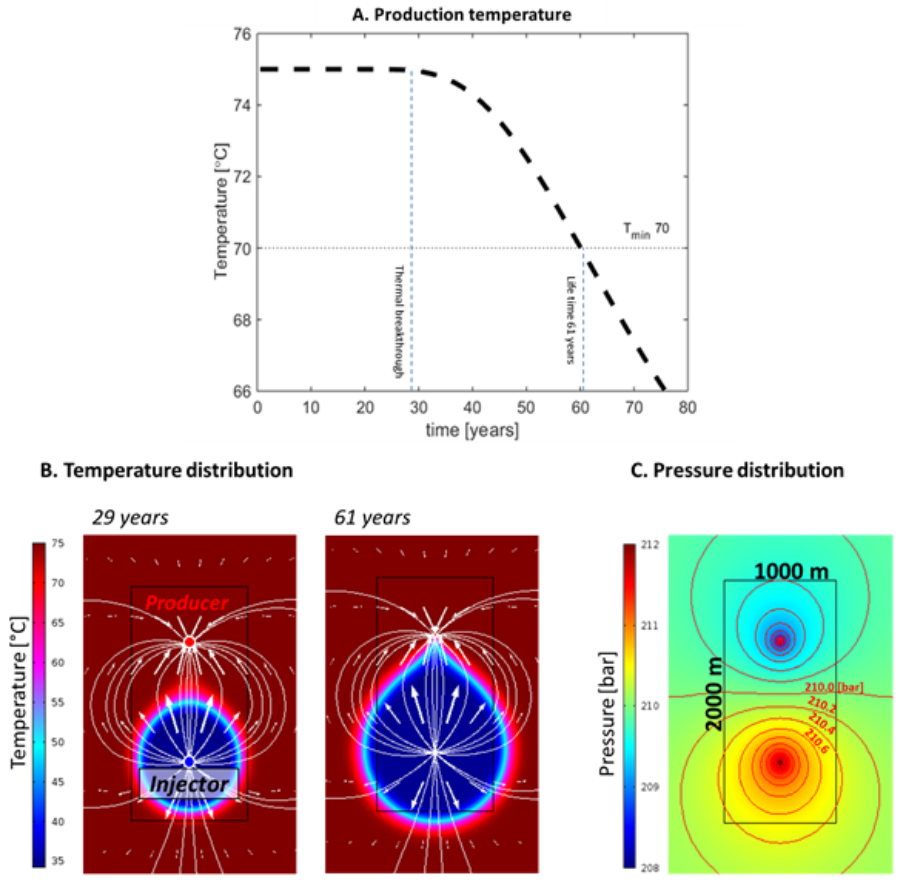

Figure 6.3: (A) Development of production temperature of a single doublet. (B) Temperature distributions, streamlines and velocity vectors in the aquifer after 29 and 61 years. (C) Pressure distribution around the wells. Contour lines indicate a 0.2 bar transition. The black rectangle indicate a standard WNB production licence with the size of *L x 2L*, in which L is the well spacing.

configuration with a doublet equal to the well spacing Figure 6.6). After thermal breakthrough however, temperature reduction is faster compared to that of a single doublet. No noticeable interference occurs if the doublet distance is 4000 m, as the production temperature development is equal to that of a single doublet. When the doublet distance is 1500 m, the delay in thermal breakthrough is even larger. These results indicate that an optimum in life time interference could be found when doublet distance is larger than the well spacing and smaller than 4000 m. In addition, the result in Figure 6.6 indicate that the doublet distance affects the rate of production temperature reduction after the thermal breakthrough moment influencing the doublet life time. Therefore, the life time of a doublet in the checkboard configuration could be lower than that of a single doublet depending on the minimal required production temperature, despite the delay in thermal breakthrough time.

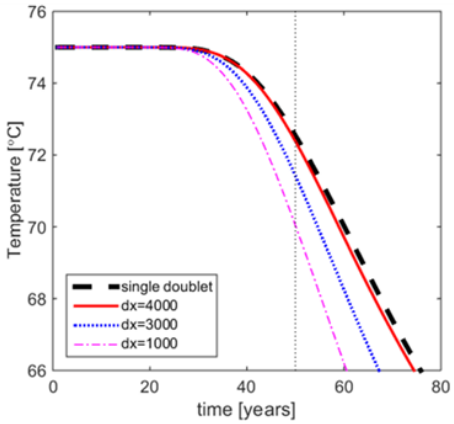

Figure 6.4: A) Development of production temperature of one of the two doublets in the tramline configuration. The well spacing in both doublets is 1000 m and their production rate is 150 m^3/h.

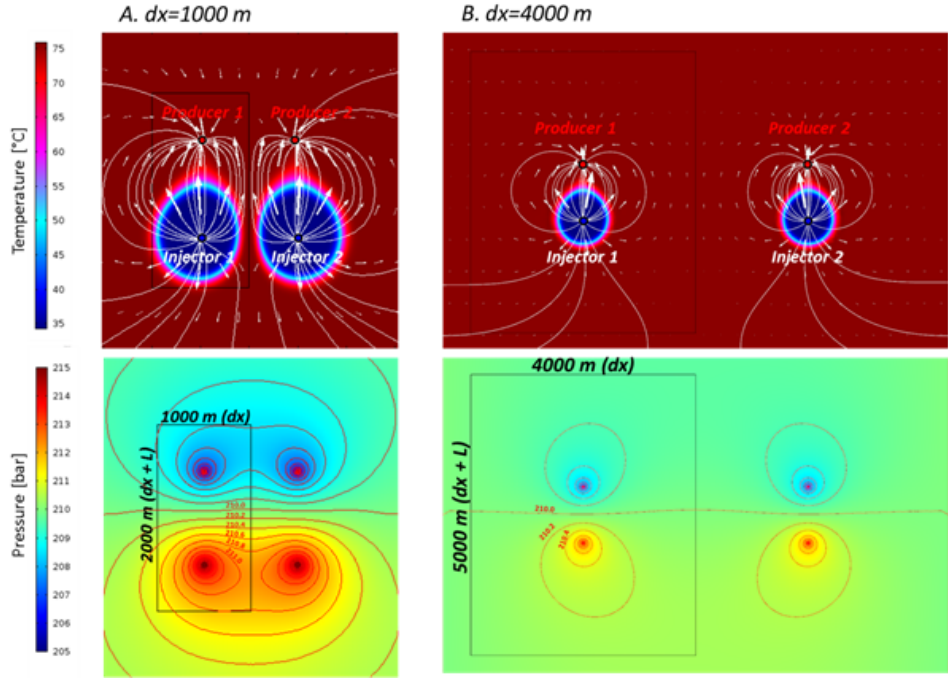

Figure 6.5: Temperature and pressure distribution in the aquifer after 30 years for (A) doublet distance *dx*= 1000 m and (B) doublet distance *dx* =3000 m. Streamlines and velocity vectors are illustrated in the temperature plots. Contour lines indicate a 0.2 bar transition in the pressure distribution plots. The black rectangle indicates the production licences in both scenarios A and B. The reservoir thickness is 75 m, the well spacing (*L*) in both doublets is 1000 m and their production rate is 150 m^3/h.

For example, in case of a minimum production temperature of 70°C, the life time of a single doublet is larger than the life time of a doublet in the checkboard configuration and a doublet distance of 1000 m. Figure 6.7 illustrates that checkboard configurations result in wider cold water plumes compared to tramline configurations (Figure 6.5B). Streamlines are less dense indicating that reinjected water flows less fast towards the producers. This prolongs the thermal breakthrough time. For the case of the doublet distance equal to 1000 m, the cold water plumes cross the production licence boundaries after 30 years. With this doublet distance, the reinjected water flows to both adjacent production wells with the same rate. As a result of this cross flow between the doublets, the production temperature reduces faster after the thermal breakthrough moment. If the doublet distance is larger than the well spacing, e.g. 1500 m Figure 6.7B), the cold water plumes do not cross the production licence boundaries before the thermal breakthrough moment.

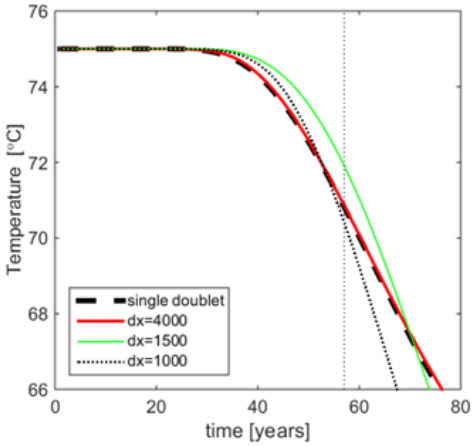

Figure 6.6: Production temperature development of one of the two doublets in the checkboard configuration. The reservoir thickness is 75 m, the well spacing in both doublets is 1000 m and their production rate is 150 m^3/h.

6.3.4. Interference as a function of doublet distance

Interference is evaluated in terms of life time, net energy production and NPV as functions of doublet distance (Figure 6.8). Interference is expressed as deviation of doublet performance from that of a single doublet. If ΔLT, ΔEP or ΔNPV is 0, no interference occurs. Figure 6.8A to C relate to interference in tramline configurations, and Figure 6.8D to F relate to interference in checkboard configurations. The results show that interference is always negative in tramline configurations unless the doublet distance is 4000 m or more, which is 4 times the well spacing in this example. Furthermore, Figure 6.8 indicates that interference is most significant in terms of life time. ΔEP and ΔNPV in these results were smaller than 0.1% while ΔLT varies more significantly from 0 to 30% depending on the doublet distance and doublet configuration. The minimal production temperature has a small effect of

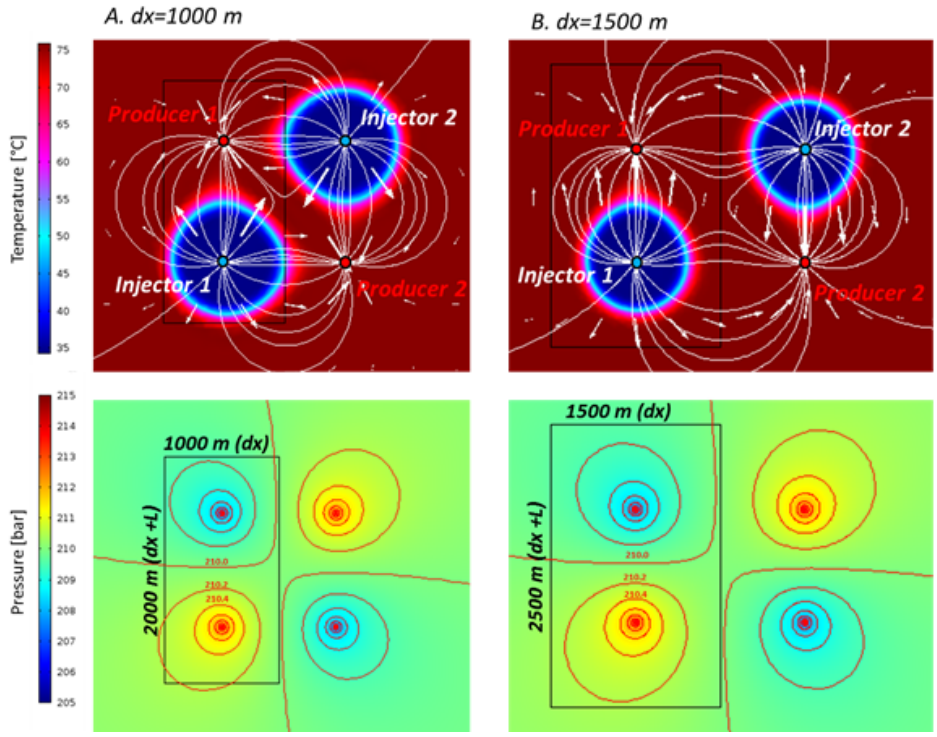

Figure 6.7: Temperature and pressure distribution in the aquifer after 30 years for (A) doublet distance *dx*= 1000 m and (B) doublet distance *dx* =3000 m. Streamlines and velocity vectors are illustrated in the temperature plots. Contour lines indicate a 0.2 bar transition in the pressure distribution plots. The black rectangle indicates the production licences in both scenarios A and B. The reservoir thickness is 75 m, the well spacing (*L*) in both doublets is 1000 m and their production rate is 150 m^3/h.

several percentages on the life time. ΔLT is larger if T_{min} is lower in the tramline configuration. In the checkboard configuration, an optimum in positive interference is recognised. This optimum shifts to higher doublet distance for lower T_{min}.

6.3.5. Interference and production rate contrast - Tramline

A difference in production rate between doublet 1 and 2, henceforth referred to as production rate contrasts, increases interference and the required doublet distance in tramline configurations. This is derived fromFigure 6.9A to C. In this figure the relation of ΔLT and doublet distance is presented for different production rate contrasts. A dimensionless production rate contrast (dQ) is defined as: $dQ=(Q_2- Q_1)/(Q_2+Q_1)$. The interference is more significant in the doublet with the lower production rate. This can be seen inFigure 6.9B and C where ΔLT is larger for doublet 1 which has a lower flow rate than doublet 2. Therefore the required doublet distance should be determined from the perspective of the doublet with the lowest production rate. In tramline configurations interference will always reduce life time unless

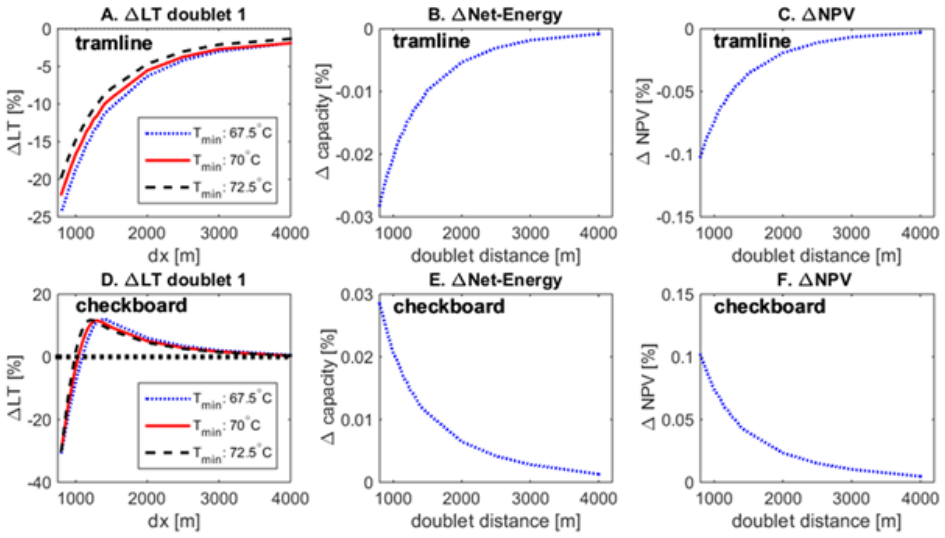

Figure 6.8: Comparison of the performance of a single doublet to a doublet in the tramline configuration (A,B,C) and the checkboard configuration (D,E,F). In A and D the interference is expressed in terms of life time (ΔLT) for three different minimal production temperatures. In B and E interference is expressed in terms of net-energy production (ΔEP) and C and F show interference in terms of net present value (ΔNPV).

very large doublet distance of approximately four times the well spacing or more is considered (Figure 6.6 and 6.8). In Figure 6.9C two examples of determination of minimal doublet distance are shown when the production rates in doublet 1 and 2 are 50 m^3/h and 200 m^3/h, respectively. If the accepted life time reduction is 15% the minimal distance is approximately 1950 m. In case the accepted life time reduction is only 5%, the required doublet distance is 3600 m.

6.3.6. Minimal doublet distance - Tramline

Following the example in (Figure 6.9C, the minimal doublet distance for doublets in tramline configurations is determined for all well spacing, production rate contrasts, reservoir thickness scenarios and for ΔLT of -5% and -15%. Figure 6.10 presents the resulting relations between the minimal doublet distance and dimensionless production rate contrast dQ. In this figure the minimal production temperature (T_{min}) is 70°C. In (Figure 6.10A the accepted ΔLT is 15% and in Figure 10-B accepted ΔLT is 5%. It can be seen that dx_{min} increases for increasing production rate contrasts. Furthermore dx_{min} is larger for doublets with larger well spacing. In Figure 6.10C and D, the minimal distance is normalised by division of dx_{min} by the associated well spacing. The normalised relation between doublet distance and production rate contrast shows that dx_{min}/L is independent of the reservoir thickness. The minimal distance is significantly higher when the allowed negative interference is smaller, i.e. when ΔLT is 5% instead of 15% (Figure 6.10A and B). For example, when the

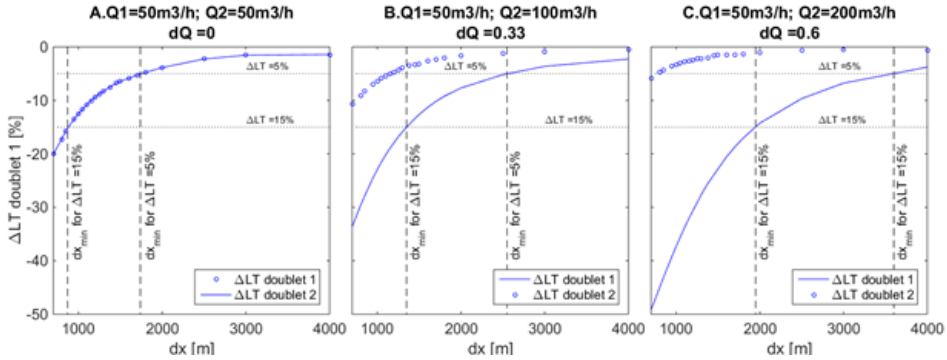

Figure 6.9: Life time interference of doublet 1 and 2 in the tramline configuration, for different production rate contrasts as function of doublet distance. Minimal production temperature is 70°C in this example. In A the production rate is equal in both doublets. In B the production rate contrast is 50 m^3/h, and in C the production rate contrast is 150 m^3/h. In these examples, the reservoir height was 75 m and the well spacing 800 m.

allowed accepted ΔLT is 15% and two doublets in the tramline configuration have an equal production rate ($dQ=0$), the required doublet distance is approximately 1.15 times the well spacing (Figure 6.10C). This increases to 2.1 when the allowed life time reduction is only 5% (Figure 6.10D). Note that maximum production rate contrast with a well spacing of 1500 m is only displayed for values of dQ up to 0.3. This is because the maximum and minimum production rates are 300 m^3/h and 150 m^3/h, respectively. For lower production rates below 150 m^3/h that would result in larger contrasts, the life time of the doublet were longer, longer than 250 years, especially for T_{min} of 67.5°C and 70°C.

Subsequently the normalised relation of doublet distance and dQ is determined for three different minimal production temperature scenarios: (A) T_{min} is 67.5°C, (B) T_{min} is 70°C and (C) T_{min} is 72.5°C. The results in Figure 6.11 show that if T_{min} is lower, dx_{min}/L increases. Required doublet distance is therefore dependent on T_{min}. This is a result of impact of doublet distance on the rate of the production temperature reduction as shown in Figure 6.4. This figure shows that doublet distance influences the rate of production temperature reduction after thermal breakthrough. Because of this effect and because interference is calibrated on the performance of a single doublet in our study, a larger doublet distance is required to compensate when the minimal production temperature is lower.

6.3.7. Interference and production rate contrast - Checkboard

Production rate contrasts influence optima in positive life time interference. This is derived from Figure 6.12. In this figure the relation of ΔLT and doublet distance is presented for doublets in checkboard configurations with different production rate contrasts (dQ). The relations indicate that positive interference is relatively larger in the doublet with the lowest production rate. In addition, the optima of the doublet with the lower production flow rate shift to large dx values if the production rate

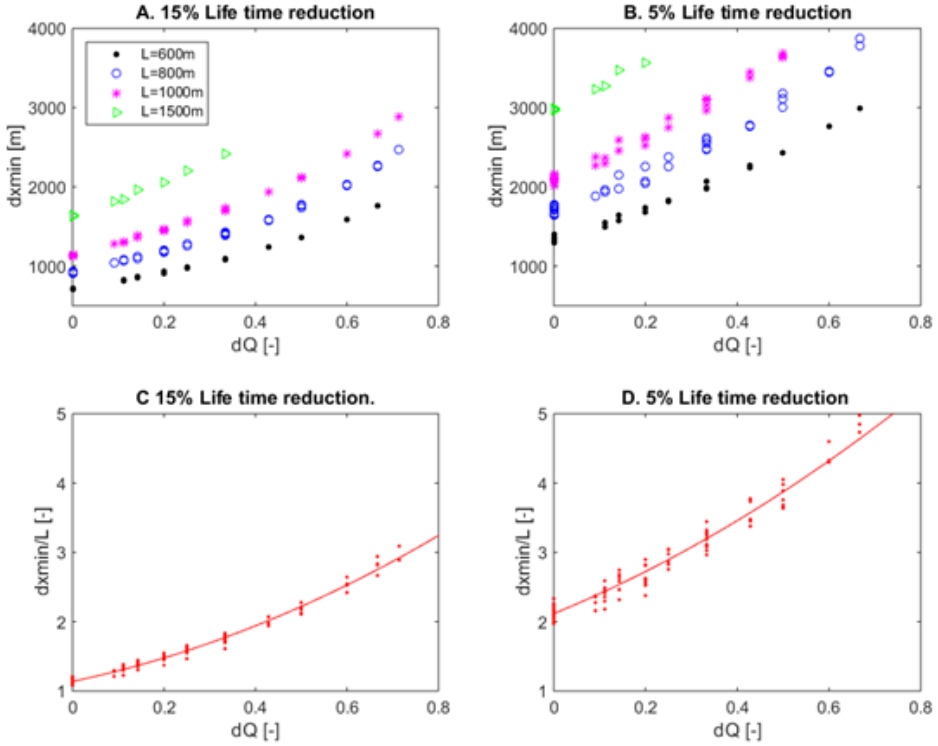

Figure 6.10: (A) Relation of minimal doublet distance and producton rate contrast (dQ) for a 5% life time reduction in the tramline configuration. (B) Relation of minimal doublet distance and producton rate contrast (*dQ*) for a 15% life time reduction in the tramline configuration. (C) Normalised minimal doublet distance of A. (D) Normalised minimal doublet distance of B. For all figures the life time is determined for a minimal production temperature of 70°C.

contrast (*dQ*) increases. Oppositely, the optima for the doublet with the higher production rate shifts to lower *dx* values for higher *dQ* values. The production rate contrast could also result in negative life time interference in the doublet with the lowest production rate, despite the checkboard configuration. An example is presented in Figure 6.12B. In this example, doublet 1 produces at 50 m^3/h and doublet 2 at 100 m^3/h. If the doublet distance is 750 m, an optimum in ΔLT of approximately 5% in doublet 2 is obtained while the ΔLT in doublet 1 is -15%. Doublet distance should be carefully chosen if doublets are placed in checkboard configurations, especially with a production rate contrast. The results in Figure 6.12 illustrate that optimal doublet distance (dx_{opt}) for doublets in checkboard configurations could be chosen from 3 different perspectives. A first option is to choose *dx* to maximise positive interference in the doublet with the lowest production rate. An example is presented in Figure 6.12C. For a doublet distance of 1600 m, the ΔLT in doublet

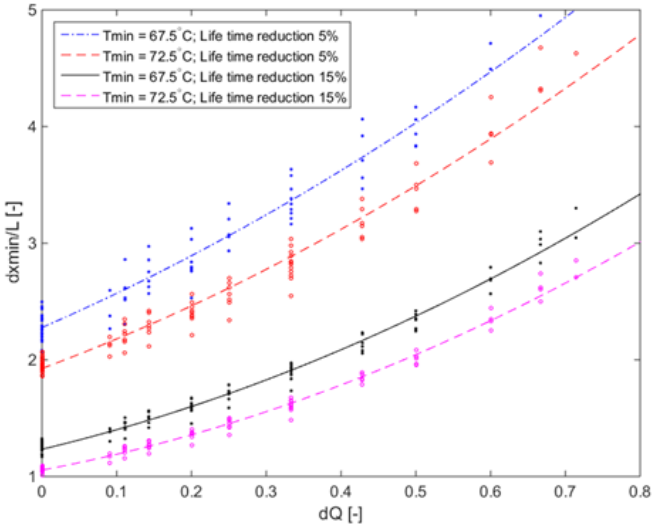

Figure 6.11: Dimensionless relations between minimal doublet distance and flow rate contrast for different minimal production temperature and for a 5% and 15% life time reduction in the tramline configuration.

1 is 30% while the ΔLT in doublet 2 is 0%. In contrast, optimal doublet distance could aim to maximise positive life time interference in the doublet with the highest production rate. An example is presented in Figure 6.12B. For a doublet distance of 900 m, the ΔLT in doublet 2 is 5% while the ΔLT in doublet 1 is -15%. Finally optimal doublet distance could be chosen as a compromise where the ΔLT curves for both doublets intersect. This option is shown in Figure 6.12C by the vertical blue line with a dx = 900 m. In that case ΔLT is approximately 2% in both doublets. In this study, optimal doublet is determined such that interference is optimised for the doublet with the lowest production rate.

6.3.8. Optimal doublet distance - Checkboard

The optimal doublet distance for doublets in checkboard configuration is determined for all well spacing, production rate, and reservoir thickness scenarios (Figure 6.13A). Note that this is optimised with respect to the doublet with the lowest production rate. Like in Figure 6.10C, the dx_{opt} values are normalised by division of d_{opt} by the associated well spacing. The dimensionless relation of the ratio of d_{opt} and well spacing to the dimensionless production rate contrast dQ is shown in Figure 6.13B. This figure indicates that the optimal doublet distance is increased when the T_{min} is lower. For example, for a minimal production temperature of 67.5°C optimal doublet distance is approximately 1.3 times larger than the well spacing. For the higher minimal production temperature of 72.5°C , this factor reduces slightly to 1.2. Therefore, optimisation of interference depends on the minimal allowed

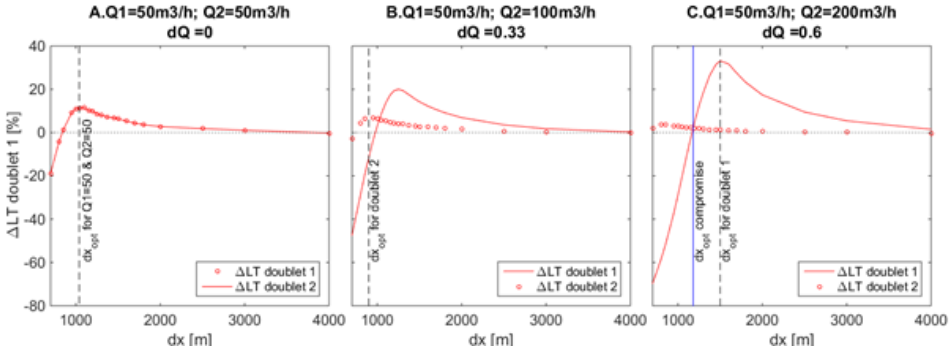

Figure 6.12: Life time interference of doublet 1 and 2 in the checkboard configuration, for different production rate contrasts as function of doublet distance. Minimal production temperature is 70°C in this example. In A the production rate is equal in both doublets. In B the production rate contrast is 50 m^3/h, and in C the production rate contrast is 150 m^3/h. In these examples, the reservoir height was 75 m and the well spacing 800 m.

production temperature and the production rate contrast between both doublets and production rate contrast.

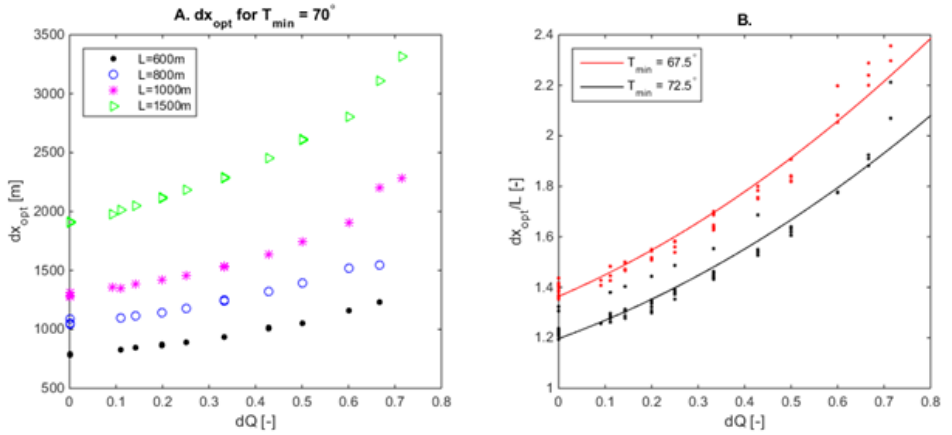

Figure 6.13: (A) Optimal doublet distance for the checkboard configuration as a function the dimensionless flow rate contrast *dQ*. (B) dimensionless ratio of dx_{opt} and well spacing (*L*) as a function the dimensionless flow rate contrast.

6.4. Discussion

Minimum production temperature

Our results indicate that an analysis of the minimal production temperature should be part of a doublet deployment strategy. Firstly, this is because this parameter is related to the life time and the maximum extent of the cold water plume. Our

results underline the possibility for continued production after the thermal breakthrough moment as the production temperature only drops by a few degrees after several decades (Figures 6.4 and 6.6). When thermal recharge from reservoir heterogeneities as well as over- and underburden were taken into account, the rate of production temperature reduction would be even lower (Poulsen et al., 2015; Crooijmans et al., 2016; Willems et al., 2016). In addition, lifetimes could be even longer if we took technical progress into account; lower production temperatures may well be sufficient in the future because heat insulation and heat exchanger efficiency are likely to improve in the next decades. Secondly, the minimal production temperature is related to the required doublet distance as interference could affect the rate of temperature reduction after cold water breakthrough (e.g., Figures 6.4 and 6.6). In our evaluation, interference is calibrated to the performance of a single doublet with the same production rate, well spacing and aquifer thickness. Therefore the dimensionless relations between required doublet distance and production rate contrast that were derived are dependent on minimal production temperature to compensate for interference. Because of the current uncertainty in minimal production temperature for doublet systems, further study is required on this parameter to reduce future interference risks.

Geological heterogeneity

In our study simplified homogeneous models where used to derive the impact of doublet design parameters, such as well spacing production rate and aquifer thickness, on interference. Our results indicate the relative effect of these parameters on required doublet distance. However, geological heterogeneities could affect the resulting relations for required doublet distance. Geological heterogeneities include facies architecture (e.g., chapters 2 and 3), small scale sedimentary features (e.g. Bierkens and Weerts, 1994), faults and fractures (Hardebol et al., 2015; Bisdom et al., 2016) as well as aquifer thickness variation. These heterogeneities affect interference when they affect pressure distribution and aquifer volume around the wells. For example, different types of heterogeneities could either form flow baffles or in contrast form high permeability zones. In both cases they deform the cold water plumes and the pressure distribution around the wells. Their impact on interference depends on the directional trend of the heterogeneities with respect to the location of the adjacent doublet. When the heterogeneities enhance pressure communication between adjacent doublets, larger doublet distance is required compared to when flow baffles decrease pressure communication. In addition, thermal recharge from over- and under-burden was neglected in our analysis. The effect of thermal recharge on doublet life time is dependent on the aquifer thickness and the ratio of flow rate and conduction rate (Poulsen et al., 2015). We expect however, that thermal recharge will not affect our results significantly because interference is calibrated to the performance of a single doublet. The impact will be more significant for lower required production temperatures as thermal recharge affects production temperature reduction. The determination of required doublet distance in specific HSA regions need to include a stochastic approach in which uncertainties in geological heterogeneities as well as thermal recharge from over and under burden is taken into account.

Tramline versus Checkboard configurations

The definition of required doublet distance in this study is dependent on the doublet configuration. A differentiation is made between minimal required doublet distance and optimal doublet distance. Optimal doublet distance is defined as the doublet distance for which an optimum in positive interference is obtained. This is only possible when doublets are placed in the checkboard configuration. In contrast, minimal doublet distance aims to prevent negative interference. For doublets in checkboard configurations this minimal required distance aims to prevent cross flow of reinjected water between adjacent doublets. Cross flow could occur if the doublet distance is smaller than the injector-producer well spacing in checkboard configurations. In addition, it could be induced by production rate contrasts even if the doublet distance is larger than the injector-producer well spacing. When doublets are placed in tramline configurations, minimal doublet distance aims to minimise negative interference. In this configuration reinjected water is forced to flow faster towards the production well of the same doublet. Our results show that this effect cannot be avoided unless doublet distances of at least four times the well spacing are used. This factor could change if geological uncertainties are taken into account as discussed in the previous section. Nevertheless, these results imply that the required distance to avoid negative interference for doublets in tramline configurations significantly limits the possible number of doublets that produce from the same resource. To avoid negative interference, determination of the required doublet distance should be based on the doublet with the lowest production rate Figures 6.9 and 6.12). In that case, after the life time is reached for the doublet with the highest production rate, production could continue in the doublet with the lowest rate and negative impact on exploitation is minimised. In general larger doublet distances are required if the production rate contrast between the doublets increases. This applies to optimal doublet distance in checkboard configurations as well as minimal doublet distance in both configurations. By using tramline and checkboard configurations in our simulations, the two most extreme interference scenarios were compared. In tramline configurations with equal well spacing, negative interference is as large as possible because both the injectors and producers reduce each other's injectivity and productivity negatively. If one of the two doublets had a larger spacing, the negative effect of one of the two wells on the other doublet would be reduced. In contrast, the most positive interference could be achieved in checkboard configurations with equal well spacing. Again, this positive interference would be smaller if one of the two doublets had a larger spacing or a different orientation. Despite these restrictions for specific scenarios, the relations in Figure 6.11 and Figure 6.13 can be used to describe the impact of the parameters in our study on interference. The magnitude of interference would also be larger if the number of doublets increased (Mijnlieff and Wees, 2009). We only used two doublets to analyse interference. For multiple doublets in tramline configurations, minimal doublet distance will increase as less space is available for the cold water plumes. In contrast, the optimal doublet distance will shift to smaller values as thermal breakthrough is delayed longer if a doublet is surrounded by more doublets. After thermal breakthrough, however, the reduction of the production temperature

could also be increased when more doublets are used as cold water fronts from multiple doublets reach production wells.

Regional development

The results of this study underline the importance of a regionally coordinated exploitation strategy. This also has been suggested to benefit ATES as well as high enthalpy geothermal systems (e.g. Malafeh and Sharp, 2014; Jaxa-rozen et al., 2015; Tureyen et al., 2015). A regional doublet deployment approach could aim for positive interference and avoid negative interference resulting from tramline configurations as well as production rate contrasts. These features require larger doublet distances, resulting in lower total installed capacity and lower heat recovery efficiency. In the more advantageous checkboard configuration, a lower injector-producer well spacing can be used while positive interference maintains sufficient life time. This can reduce the required doublet distance even further and increase the possible number of doublets producing from the same resource. Regional doublet deployment will mainly have an impact on life time interference. The results of this study indicate that interference in HSA exploitation is only significant in terms of life time (Figure 6.8). Net energy production and NPV are only affected by less than 1% by the proximity of another doublet. In comparison, the impact of geological uncertainties on net-energy production and NPV are an order of magnitude larger (chapter 5). In our study NPV is determined over a 15 year period because of the Dutch feed-in tariff duration (Van Wees et al., 2010). Interference could affect NPV more significantly when it is determined for a period of time that exceeds the thermal breakthrough time (e.g. Malafeh and Sharp, 2014). In geothermal systems where volumetric reinjection rates are lower than the production rates, interference will affect injectivity and productivity more significantly due to pressure depletion (e.g. Tureyen et al., 2015). Finally it should be mentioned that optimisation of doublet deployment requires a regional geological model including aquifer heterogeneities and their uncertainties. Such a model requires upfront investment for cores, logs and data analysis. However, over a longer time period, the benefits can outweigh investments as negative interference is avoided and doublet placement could be optimised to meet the operator requirements.

6.5. Conclusions

On the basis of our multi parameter analysis we can conclude that:

- The fluid pressure interference in HSA exploitation has a significant impact on doublet life time as it influences cold water plume development. The impact on net energy productivity and NPV is an order of magnitude smaller.
- Optima in positive life time interference are recognized for doublets in checkboard configurations.
- Production rate contrasts between adjacent doublet systems and minimal production temperature influence the required doublet distance.
- Coordinated doublet deployment and smaller well spacing could significantly increase the possible number of doublets.

References

Bierkens, M. F. P. and Weerts, H. J. T. (1994). Block hydraulic conductivity of cross-bedded fluvial sediments. *Water Resources Research*, 30(10):2665–2678.

Bisdom, K., Bertotti, G., and Nick, H. M. (2016). Journal of Geophysical Research : Solid Earth. *Journal of Geophysical Research: Solid Earth RESEARCH*, 121:4045–4063.

Boxem, T., van Wees, J., Pluymaekers, M., Beekman, F., Batini, F., Bruhn, D., Calcagno, P., Manzella, A., and Schellschmidt, R. (2011). Thermogis world aquifer viewer-an interactive geothermal aquifer resource assessment web-tool. In *1st EAGE Sustainable Earth Sciences (SES) Conference and Exhibition*.

Crooijmans, R. A., Willems, C. J. L., Nick, H. M., and Bruhn, D. F. (2016). The influence of facies heterogeneity on the doublet performance in low-enthalpy geothermal sedimentary reservoirs. *Geothermics*, 64:209–219.

Daniilidis, A. and Herber, R. (2016). Salt intrusions providing a new geothermal exploration target for higher energy recovery at shallower depths. *Energy*, In Press.

Hamm, V. and Lopez, S. (2012). Impact of Fluvial Sedimentary Heterogeneities on Heat Transfer at a Geothermal Doublet Scale. In *Thirty-Seventh Workshop on Geothermal Reservoir Engineering*, Stanford, California.

Hardebol, N., Maier, C., Nick, H., Geiger, S., Bertotti, G., and Boro, H. (2015). Multiscale fracture network characterization and impact on flow: A case study on the latemar carbonate platform. *Journal of Geophysical Research: Solid Earth*, 120(12):8197–8222.

Jaxa-rozen, M., Kwakkel, J., and Bloemendal, M. (2015). The Adoption and Diffusion of Common-Pool Resource-Dependent Technologies : The Case of Aquifer Thermal Energy Storage Systems. In *Proceedings of PICMET '15: Management of the Technology Age*, pages 2390–2408, Portland, Oregon.

Malafeh, S. and Sharp, B. (2014). Geothermal Development : Challenges in a Multiple Access Scenario. In *Thirty-Ninth Workshop on Geothermal Reservoir Engineering*, pages 1–11, Stanford, California.

Mijnlieff, H. F. and Wees, J. (2009). Rapportage Ruimtelijke Ordening Geothermie. Technical report, TNO.

Mottaghy, D., Pechnig, R., and Vogt, C. (2011). The geothermal project Den Haag: 3D numerical models for temperature prediction and reservoir simulation. *Geothermics*, 40:199–210.

Pluymaekers, M. P. D., Kramers, L., Wees, J. V., Kronimus, A., and Nelskamp, S. (2012). Reservoir characterisation of aquifers for direct heat production : Methodology and screening of the potential reservoirs for the Netherlands. *Netherlands Journal of Geosciences*, 91(4):621–636.

Poulsen, S. E., Balling, N., and Nielsen, S. B. (2015). A parametric study of the thermal recharge of low enthalpy geothermal reservoirs. *Geothermics*, 53:464–478.

Sommer, W., Valstar, J., Leusbrock, I., Grotenhuis, T., and Rijnaarts, H. (2015). Optimization and spatial pattern of large-scale aquifer thermal energy storage. *Applied Energy*, 137:322–337.

TNO (1977). Nl olie- en gasportaal. www.nlog.nl.

Tureyen, O. I., Sarak, H., Altun, G., and Satman, A. (2015). A modeling analysis of unitized production : Understanding sustainable management of single-phase geothermal resources with multiple lease owners. *Geothermics*, 55:159–170.

Van Heekeren, V. and Bakema, G. (2013). Geothermal Energy Use, Country Update forthe Netherlands. In *European Geothermal Congress*, pages 2013–2016, Pisa.

Van Heekeren, V. and Bakema, G. (2015). The Netherlands Country Update on Geothermal Energy. In *World Geothermal Congress 2015*, volume 2013, pages 2–7, Melbourne.

Van Wees, J., Kramers, L., Kronimus, R., Pluymaekers, M., MijnLieff, H., and Vis, G. (2010). ThermoGISTM V1.0 Part II : Methodology. Technical report, TNO, Utrecht.

Willems, C. J. L., Goense, T., Nick, H. M., and Bruhn, D. F. (2016). The relation between well spacing and Net Present Value in fluvial Hot Sedimentary Aquifer geothermal doublets ; a West Netherlands Basin case study. In *41st Workshop on Geothermal Reservoir Engineering*, pages 1–13, Stanford, California.

Willems, C. J. L., Nick, H. M., Donselaar, M. E., Jan, G., and Bruhn, D. F. (2017). Geothermics On the connectivity anisotropy in fluvial Hot Sedimentary Aquifers and its influence on geothermal doublet performance. *Geothermics*, 65:222–233.

7

General discussion and conclusion

The focus of this thesis is on the investigation of doublet deployment parameters influencing heat exploitation of fluvial HSA. This final chapter combines the results of the previous chapters and shows that a coordinated, geologically based approach to geothermal doublet deployment is a prerequisite for efficient large-scale heat exploitation from fluvial HSA. This is done by comparing the efficiency of heat exploitation of two different deployment strategies; the current WNB 'first come, first served' strategy and an optimised, coordinated deployment strategy. The efficiency of both strategies is compared by simulating their impact on exploitation in an aquifer model of the Pijnacker/Delft fault block in which currently two active doublet systems are realised (Figure 7.1).

7.1. Aquifer model of the Pijnacker/Delft fault block

The model used in the simulations is a simplified homogeneous representation of the aquifer in the Pijnacker/Delft fault block. The model consists of a horizontal 50 m thick homogeneous sandstone layer confined between 300 m impermeable over- and underburden layers providing thermal recharge. Two of the four boundaries of the model are formed by northwest to southeast trending faults. The other two boundaries are placed allowing the model to capture the extent of current exploration licences (Figure 7.1). The permeability of the aquifer layer is assumed isotropic and equal to 1000 mD. The permeability of the over- and underburden is 5 mD. Element size ranges from 0.3 m to 40 m in the aquifer layer and from 40 m to 300 m in the over- and underburden layers. In the production simulations the same numerical approach is used as described in chapter 6.

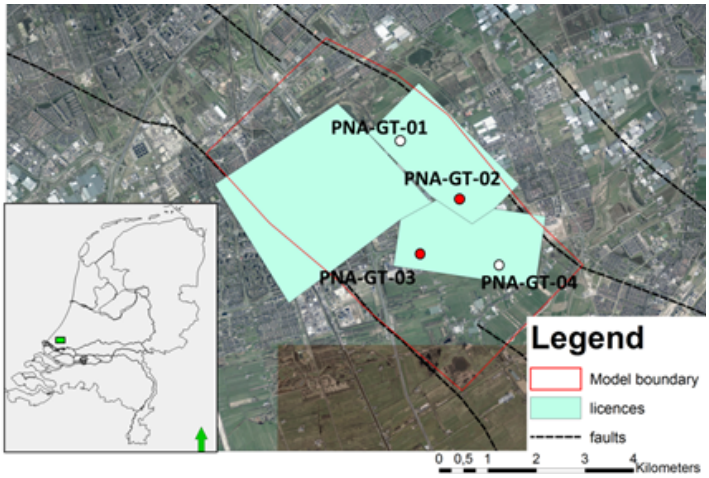

Figure 7.1: Overview of the Pijnacker/Delft fault block, the model outline and the currently active doublets and geothermal licences. Satellite immage: ESRI base-map, licence polygons from www.nlog.nl

7.2. Doublet deployment strategies

In the current 'first come, first served' deployment strategy (Figure 7.2A), a maximum of three doublets can be placed in the model. This is caused by the large well spacing of 1500 m and the irregular doublet orientation. In a second coordinated deployment strategy (Figure 7.2B), the preferred doublet orientation, well spacing (L) and doublet distance (dx) were based on the results of chapters 3 to chapter 6. The preferred doublet orientation with respect to the paleoflow trend was chosen from the southeast to northwest, parallel to the main faults. Utilising a single orientation for all doublets increases the possible number of doublet systems as could be derived from Figure 7.2. Although this orientation would create a lower pump energy loss in heterogeneous models (chapter 3), it will not influence this simulation, because a homogeneous model was used. Well spacing of 800 m in 50 m thick homogeneous aquifers have an expected life time of 30 to 40 years according to our results of chapter 5. We assumed this to be sufficient for direct-use applications in the WNB. The checkboard configuration was chosen to reduce doublet distance and optimise positive interference (chapter 6). The associated distance was 1040 m. This is based on an assumed minimal required production temperature of 67.5°C, which is 90% of the initial aquifer temperature of 75°C. As a result of these deployment parameters, 9 doublets were placed in the aquifer model (Figure 7.2B). In both deployment strategies a constant 200 m^3/h production rate (0.05 m^3/s) was assumed. The simulations provided a production temperature development over time in all doublet systems. The associated energy production (E_{prod} [W]) was estimated by: $E_{net}=Q\ C_p\rho_b\ (T_{prod}-T_{inj})$, in which Q is the production rate of the doublet equal to 0.05 [m^3/s], C_p is the water heat capacity of 4200 [J/(kg°C)], ρ_b is the water density of 1000 [kg/ m^3], T_{prod} is the production temperature that varied in time and T_{inj} the reinjection temperature of 35°C. The total cumulative

energy (E_{cu}) was the sum of the net energy production over the total life time of each doublet system: $E_{cu} = E_{net}\ t$, in which t is production time in seconds. To evaluate interference, the production temperature development of the doublets in both deployment strategies are compared to production temperature development with a single doublet with 1500 m and 800 m respectively. Interference is defined as deviation of the production temperature of a single doublet with a similar well spacing.

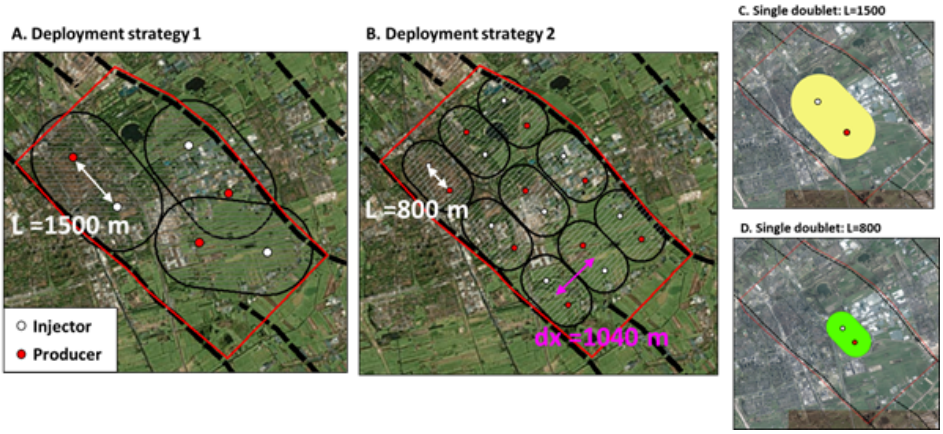

Figure 7.2: Topview of the doublet locations in the current 'first come, first served' deployment 'strategy 1' with 1500 m well spacing (L). (B) Doublet locations in the coordinated deployment 'strategy 2' with doublet distance (dx) of 1040 m and 800 m well spacing. (C) and (D) doublet location in the single doublet reference simulations.Satellite immage: ESRI base-map, well locations from www.nlog.nl

7.3. Results

The 800 m well spacing in the coordinated deployment strategy leads to sufficient life time of approximately 41 years per doublet (Figure 7.3A). The results show that life time is increased as a result of interference in this deployment strategy, because the life time of the single doublet with similar spacing would be 30 years (Figure 7.3A). The life time of the 'first come, first served' deployment (strategy 1) with 1500 m well spacing on the other hand is much longer, ranging from 100 to 200 years (Figure 7.3B). In simulations with this strategy negative interference is recognised as a result of uncoordinated doublet deployment. Two out of three doublets have a lower life time compared to that of a single doublet with similar spacing. The magnitude of interference in the Pijnacker/Delft fault block could not be derived from these simplified simulations. However, the simulations indicate that negative interference is more likely without coordinated doublet deployment in HSA exploitation. The annual heat production rate is 0.83 PJ/year in strategy 1 and 2.5 PJ/year in strategy 2 (Figure 7.3C). This suggests it is possible to increase the heat recovery rate from HSA by using smaller well spacing and coordinated doublet deployment. Based on the result of chapter 5 we can assume that this

will also improve the NPV of each doublet. Both an improved NPV as well as increased heat production rate could enhance HSA exploitation as they make HSA a financially more attractive resource. However, the smaller well spacing in strategy 2 does have a negative impact on the total cumulative recovered energy. The total cumulative recoverable heat in strategy 1 is higher than in strategy 2, because of its longer lifetime. It could have been even higher without the negative interference. By further optimising the doublet deployment parameters also the cumulative recoverable energy of strategy 2 could be increased to match the result of scenario 1, for example by reducing the production rate or increasing the well spacing. The main advantage of coordinated doublet deployment is that heat production rate could be increased through realisation of more doublet systems while the risks for negative interference is reduced. In future optimisation studies for a specific HSA, geological heterogeneities should be taken into account to ensure that life time and net energy production are not overestimated as a result of homogeneous aquifer modelling. Despite the simplifications in aquifer modelling in our final simulations, the results show that coordinated geothermal doublet deployment is a prerequisite for efficient heat exploitation from fluvial HSA. As such it could fill the gap between the current HSA exploitation and the theoretical potential.

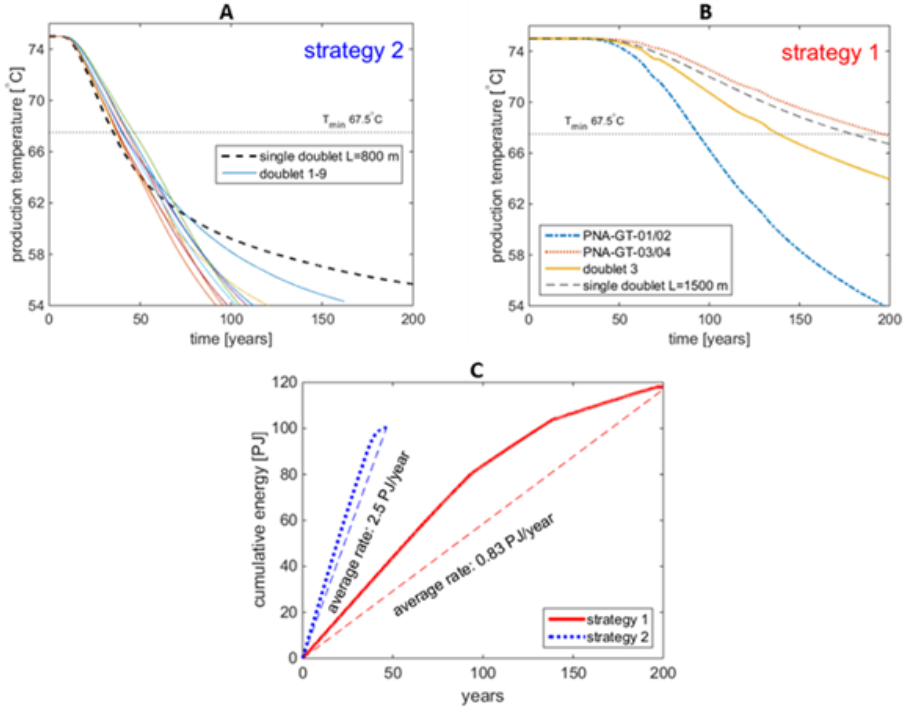

Figure 7.3: Production temperature development in (A) deployment strategy 2 and (B) strategy 1. (C) Cumulative produced heat as function of time for both deployment strategies. The dotted line indicates the associated average yearly heat production rate for both strategies.

7.4. Outlook and recommendations

This thesis provides an example of the potential gain of coordinated doublet deployment and describes a workflow to derive deployment parameters. The results imply a next major challenge for HSA exploitation, which is the generation of a policy driven environment which is in favour of coordinated doublet deployment. The current policy in the Netherlands leads to an individual 'first come, first served' deployment, despite the obvious disadvantages for upscaling exploitation. A coordinated deployment could not only lead to increased heat production, as shown in this thesis, but also be a means to share data and investment costs amongst multiple operators in the same area. Furthermore, it could be a means to mitigate risk resulting from geological uncertainties. Well placement in any type of subsurface resource exploitation has a certain success rate regardless of extent of data acquisition and geological analysis of this data. Exploitation risks as a result of geological uncertainties can be reduced by exploitation of the same resource through multiple doublet systems. Exploitation with multiple doublets also requires further research into design of adequate heating distribution networks. Another related parameter that needs to be evaluated in future studies is the minimal required production temperature. More accurate estimation of this parameter could increase heat use efficiency in a heat distribution network. Furthermore, additional studies are required for actual doublet deployment optimisation for specific HSA. Firstly, the uncertainty of well placement should be evaluated. In chapter 2 it was shown that fluvial reservoirs have an anisotropy in connectivity which leads to higher equivalent permeability in the direction parallel to the paleoflow direction. However, the anisotropy was masked by the impact of geological uncertainty on well placement. This was recognised from the large range of resulting pump energy losses in the well pair production simulations, even in aquifer realisations with high net sandstone content. The success rate of wells could be analysed in numerical studies in which not only well placement but also aquifer thickness and net sandstone volume is varied. Secondly, the uncertainty in heat capacity and heat conductivity modelling is neglected in our study. In our models, heterogeneity of heat capacity and conductivity in neglected. The assumed values for these parameters affect production simulations and therefore requires validation by means of numerical sensitivity analyses. Finally, our reservoir simulations are conducted in horizontal aquifer models with only matrix flow. In reality the structural setting including sealing and non-sealing faults and fractures will have a significant impact on flow and has to be incorporated in determination of deployment strategies.

AppendixA

Age assessment of cutting samples in well PNA-GT-02, HON-GT-01 and VDB-GT-04

PNA-GT-02

Sample/Interval 2120-2175 m: Late Barremian.
The age interpretation is based on:

- LOD *Cassiculosphaeridia magna* at 2120 m
- LOD *Trichodinium speetonensis* at 2120 m

Remarks: isolated occurrence of *Muderongia simplex* subsp. *microperforata* at 2120 m is most likely a result of reworking. Facies: near coastal marine conditions, at the base (2175 m) a more shallow/restricted marine influence. This is explained by a more proximal setting. Marine dinoflagellate cysts are recognised, of which open-marine species prevail (approximately 30% of the total number of dinoflagellate cysts and sporomorphs).

Sample/Interval 2195-2215 m: Late Early Barremian, Elegans Ammonite Zone, or older.
The age interpretation is based on:

- LOD *Kleithriasphaeridium cf. corrugatum* at 2195 m
- LOD *Muderongia crucis/tetracantha* at 2195 m

Remarks: the Early Barremian, Elegans Ammonite Zone top should be below 2175m because the age of this sample is determined as Late Barremian. Facies: lagoonal to restricted shallow marine near coastal conditions. *Subtilisphaera perlucida* is dominant at 2195 m which indicates a lagoonal depositional environment. At 2215 m *Subtilisphaera perlucida* and the open marine species *Spiniferites* spp. are the most abundant dinocysts.

Sample/Interval 2235-2275 m: earliest Barremian, Variabilis Ammonite Zone, or older.
The age interpretation is based on:

- LOD *Chlamydophorella membranoidea* at 2235 m
- LOD *Cribroperidinium confossum* at 2235 m

Remarks: The occurrence of *Cribroperidinium confossum* is generally related to the earliest Barremian variabilis Ammonite Zone (Duxbury 1977, Jeremiah et al., 2010). The LOD of *Chlamydophorella membranoidea* is calibrated in the earliest Barremian, Variabilis Ammonite Zone (Davey, 1979), this is why the sample cannot be younger as indicated.

Sample/Interval 2440-2590 m: Valanginian
The age interpretation is based on:

- LOD *Aequitriradites verrucosum* at 2440 m

Remarks: *Aequitriradites verrucosum* is a good marker for the Ryazanian-Valanginian interval.

Sample/Interval 2600-2850 m: Late Ryazanian (post base *kochi* Ammonite Zone)- Early Valanginian
The age interpretation is based on:

- LOD *Stiphrosphaeridium dictyophorum* at 2600 m
- LOD *CCanningia compta* at 2620 m
- LOD *Hystrichosphaeridium scoriaceum* at 2690 m
- Low numbers of *Classopollis* in all assemblages down to sample depth 2850 m

Remarks: The LOD of *Canningia compta* is an excellent marker for the Early Valanginian (TNO standard zonation scheme for the Late Jurassic to Early Cretaceous). *Hystrichosphaeridium scoriaceum* has a LOD in the Early Valanginian and occurs very rarely in the Late Ryazanian, *stenomphalus-icenii* zones (Heilmann-Clausen, 1987). The "climate shift" in the kochi Ammonite Zone of the Early Ryazanian is not reached. That the sporomorph genus *Classopollis* remains in very low values until end depth of the studied interval confirms this.

HON-GT-01

Sample/Interval: 2320 m: Late Barremian.
The age interpretation is based on:

- LOD *Hystrichodinium ramoides*
- LOD *Muderongia staurota*

Sample/Interval: 2340-2360: early Late Barremian.
The age interpretation is based on:

- LOD *Kleithriasphaeridium fasciatum* 2340 m

Remarks: Costa and Davey (1992) describe a LOD of a non-specified Barremian interval fissicostatum/rude Ammonite Zone. (Heilmann-Clausen, 1987) more specifically indicate a LOD in the earliest Late Barremian brunsvicensis Ammonite Zone.

Sample/Interval: 2380-2420 m: late Early Barremian, Elegans Ammonite Zone, or older.
The age interpretation is based on:

- LOD *Muderongia crucis/tetracantha* at 2380 m
- LOD *Rhynchodiniopsis cf. cladophora* at 2380 m
- LOD *Kleithriasphaeridium corrugatum* at 2400 m
- LOD *Muderongia simplex* subsp. *microperforata* at 2400 m

Sample/Interval: 2560-2730 m: Valangian
The age interpretation is based on:

- LOD *Batioladinium* cf. sp. I (Davey, 1982) at 2560 m
- LOD *Aequitriradites verrucosum* at 2640 m
- LOD *Pareodinia* sp. (Davey, 1982) at 2660 m

Remark: the presence of Batioladinium varigranosum at 2630 m indicates an age of Early Hauterivien or older is consistent with this current age determination.

Sample/Interval: 2740 m: Early Valangian
The age interpretation is based on:

- LOD *Canningia compta*
- LOD *Perisseiasphaeridium insolitum*

Sample/Interval: 2750-2810: Late Ryzanien (post-kochi Ammonite Zone).
The age interpretation is based on:

- LOD *Batioladinium pomum* 2750 m

Remark: the "climate shift" in the kochi Ammonite Zone in the Early Ryazanian is not recognised. The sporomorfengenus *Classopollis* is only sparsely encountered in the deepest samples.

VDB-GT-04

Two additional samples (at depth 1890 m and 1910 m) were taken for palynological re-analysis from well VDB-GT-04. A Late Ryazanian-Early Valanginian age for interval 1740-2006 m was recorded.

Sample/Interval 1890-1910 m: Late Ryazanian-Early Valanginian The age interpretation is based on the presence of *Perisseiasphaeridium insolitum, Stiphrosphaeridium dictyophorum, Canningia compta, Hystrichosphaeridium scoriaceum* and *Oligosphaeridium diluculum*. Dinoflagellate cysts that are limited chronostratigraphically to the Ryazanian are missing. The association has a relatively extended range from Late Ryazanian to Early Valanginian. The flooding at depth 1890 m may most likely be associated with the Paratollia MFS.

Acknowledgements

Working on this PhD thesis was only possible with the help, support and contributions of many people. In this section, I would like express my gratitude because this made the past four years a very pleasant, interesting and a satisfying period.

First of all I would like to thank Hamid Nick, one of the main contributors to this thesis work. With his many ideas and enthusiasm, the thesis was shaped and strengthened. Hamid taught me many things ranging from reservoir engineering related topics to almost getting rid of the fingernail biting habit. This made me progress and I am very grateful for all this.

I would like to thank David Bruhn for his great supervision of the thesis work. I very much appreciate the feed-back, freedom and trust you gave me during the study. Your enthusiasm for geothermal development and extensive knowledge inspired me in the past years and make me want to continue to work on this topic in the future.

The project would not have existed without the efforts of Rick Donselaar and Gert Jan Weltje who created the project proposal. They were also responsible for the essential geological basis of this research. I would like to thank Rick especially for the guidance in writing and his patience with processing drafts. I am very grateful for the trust you gave me when you hired me and for the combined five years of cooperation and guidance that started during my MSc project.

Another prerequisite for this study was the support of the DAP and DAPP subsidiaries and efforts of the DAP board – currently consisting of Mike Woning, Bas Vos, Anne-Martine Dortland and Twan Goense. Especially the years of voluntary support and enthusiasm of Mike and Bas kept the DAP dreams alive. I am very happy that the current and previous DAP board members helped in creating the geothermal research group at our university.

I would like to thank Harmen Mijnlieff for sharing his insights, experience and advise. I really appreciate your willingness to discuss and advice throughout the years of the project. Not only did this improve my work, in addition your efforts and the efforts of TNO AGE, greatly support geothermal development in the Netherlands in general.

While my supervisors and subsidiaries created the starting point and foundation of this research project, the subject and relevance was created by pioneering geothermal operators. The Dutch geothermal operators and organisations such as Veegeo Energy, Hydreco, ECW, Panterra, IF Technology, WEP, Platform Geothermie and DAGO, managed to demonstrate the potential of direct-use geothermal applications, as one of the first in the world. The initiative of the operators in the Netherlands provided a spark for geothermal research, which was a prerequisite for the

existence of this PhD study. I am very grateful for this spark and for the possibility to use data, discuss possible research questions and receive feed-back on my work.

Schlumberger and COMSOL are acknowledged for providing the academic software licences of Petrel and COMSOL Multiphysics. I gratefully made use of the publically available subsurface and licence data from www.nlog.nl for the anlayses and the generation of maps and figures.

PhD studies can be lonely tasks, but because of my colleagues, this felt very different. I would like to thank Koen, Kevin, Remi, Andrea, Helena, Liang, Max, Baptiste, Menno, Quinten, Thais, Navid, Siddarth, Runhai, Zaman, Lisanne, Richard, Nima, Boris, Yohei, Negar, Iris, Ranjani, Reuben, Christian and all others for crucial coffee breaks, reflection on life, jokes, feed-back. I am especially happy that you accepted the fierce geothermal propaganda that I tested on you. Not only PhD colleagues created a very nice working environment, also the Applied Geology Research staff and support were responsible for this. I would like to thank Ralf, Lydia, Marlijn, Claudia, Margot, Anke, Marja, Marijke and Hannie for all their help in the past years. Andrea Vondrak and Dirk Munsterman contributed significantly to the study described in the second chapter. I would like to thank them for the nice and productive collaboration.

I would like to thank my friends for their support and great times we had in the past years. Virtual rocks and geothermal simulations are amazing but they do not actually talk back, dine, sail through canals, drink, drop-in, trip, wipe-out, travel and listen. There is probably never enough Fisherman's Friend to hide my true emotions about this. Henk and Antoinette, thank you for your hospitality and the change to do some serious and real engineering in your yard in the past months.This not only provided for essential distraction and relaxed weekends but also made our next adventure in South America possible. Above all, I want to express most gratitude to my father, mother, Jeanine and Rianne for everything they did, so much, for too short and all the time.

Curriculum Vitæ

Cees WILLEMS

31-03-1988	Birthday, Amsterdam, The Netherlands.

Education

2000–2006	Vossius Gymnasium, Amsterdam
2006–2008	Bachelor Chemistry – University of Amsterdam
2008–2010	Bachelor Molecular Science and Technology (Chemical Engineering) - Delft University of Technology
2010–2012	Master Petroleum Engineering – Delft University of Technology
2013–Present	PhD. Applied Geology Delft University of Technology *Thesis:* Doublet deployment strategies for geothermal Hot Sedimentary Aquifer exploitation: *Application to the Lower Cretaceous Nieuwerkerk Formation, West Netherlands Basin.* *1st Promotor:* Prof. dr. D.F. Bruhn *2nd Promotor:* Prof. dr. G.J. Weltje *Co-promotor:* dr. M.E. Donselaar

List of Publications

Journal Publications

5. **Willems, C.J.L.**, Vondrak, A., Munsterman, D.K., Donselaar, M.E., Mijnlieff, H.F., *Fluvial sequence stratigraphy of Lower Cretaceous geothermal aquifers derived from palynological cuttings analysis*, ***Submitted***.

4. **Willems, C.J.L.**, Nick, H.M., Weltje, G.J., Bruhn, D.F., *An evaluation of interferences in heat production from low enthalpy geothermal doublets systems.*, ***Submitted***.

3. **Willems, C.J.L.**, Nick, H.M., Goense,T., Bruhn, D.F., *The impact of reduction of doublet well spacing on the Net Present Value and the life time of fluvial Hot Sedimentary Aquifer doublets.*, Geothermics, **68**, 54-66.

2. **Willems, C.J.L.**, Nick, H.M., Donselaar, M.E., Weltje, G.J., Bruhn, D.F., *On the connectivity anisotropy in fluvial Hot Sedimentary Aquifersand its influence on geothermal doublet performance.*, Geothermics, **65**, 222-233, (2017).

1. Crooijmans, R.A.,**Willems, C.J.L.**, Nick, H.M., Bruhn, D.F., *The influence of facies heterogeneity on the doublet performance in low-enthalpy geothermal sedimentary reservoirs.*, Geothermics, **64**, 209-219, (2016).

Conference proceedings and conference abstracts

7. **Willems, C.J.L.**, Goense, T., Nick, H.M., Bruhn, D.F., *The relation between well spacing and Net Present Value in fluvial Hot Sedimentary Aquifer geothermal doublets; a West Netherlands Basin case study.*, 41st Workshop on Geothermal Reservoir Engineering, 22-24 Februaryl, Stanford, California, U.S.A. (2016)

6. **Willems, C.J.L.**, Crooijmans, R.A., Nick, H.M., Bruhn, D.F., *The effect of fluvial architecture in Hot Sedimentary Aquifers on the connectivity and life time of a geothermal doublet.*, World Geothermal Congress 2015, 19-25 April, Melbourne, Australia (2015)

5. **Willems, C.J.L.**, Crooijmans, R.A., Nick, H.M., Bruhn, D.F., *Influence of fluvial sandstone architecture on geothermal energy production.*, Presented at: European Geothermal Workshop, 19-20 September, Strassbourg, France (2015)

4. **Willems, C.J.L.**,Donselaar, M.E., Weltje, G.J., Bruhn, D.F., *The influence of fluvial reservoir architecture on geothermal energy production in Hot Sedimentary Aquifers.*, Presented at: Nederlands Aardwetenschappelijk Congres, NAC 12 , 8-9 April, Veldhoven,The Netherlands (2014)

3. **Willems, C.J.L.**, Weltje, G.J., Donselaar, M.E., Bruhn, D.F., *The influence of fluvial reservoir architecture on geothermal energy production in Hot Sedimentary Aquifers.*, Presented at: 5th European Geothermal PhD Day, 31 March - 2 April, Darmstadt, Germany (2014)

2. **Willems, C.J.L.**, Donselaar, M.E., Weltje, G.J., *Reservoir modelling of Lower Cretaceous West Netherland Basin aquifers for geothermal energy production.*, 76th EAGE Conference and Exhibition 2014, 16-19 June, Amsterdam,The Netherlands (2014)

1. **Willems, C.J.L.**, Weltje, G.J., Donselaar, M.E., Bruhn, D.F., *Reservoir Quality of West Netherlands Basin aquifers for geothermal energy.*, Presented at: GEO T Expo, 14 November, Essen, Germany (2013)